Volume Change Behavior of Expansive Clay Stabilized with Bio-based Silica Gel

by

Limon Bogere

A Thesis Presented in Partial Fulfillment
of the Requirements for the Degree of
Master of Science

Approved November 2020 by the
Graduate Supervisory Committee:

Claudia E. Zapata, Chair
Hamed Khodadaditirkolaei
Edward Kavazanjian

ARIZONA STATE UNIVERSITY

December 2020

ABSTRACT

This document presents the assessment of the swelling behavior of expansive clay stabilized with bio-based silica gel and subjected to wetting and drying cycles. The expansive clay used in this research was obtained from Anthem, Arizona. Rice husk is a rich silica by-product of rice production with commercial uses and applications in the industry. Rice husk ash from two different sources -California (named ASU) and India- were subjected to chemical characterization. Fourier Transform Infra-red Spectroscopy was used to verify the functional groups of the gel formed. Results showed differences between the ashes from different sources and confirmed the presence of silica structure bonds. X-Ray Diffraction (XRF) results showed that the ASU ash contained more amorphous silica than the Indian ash.

One dimensional swell and consolidation tests were performed to investigate the volume change behavior of the untreated and silica gel treated remoulded samples. The free swell of the clay decreased from 12.3% (untreated sample) to 7.2% (ASU sample) and 11.4% (Indian sample). The effect of the wet and dry cycles on the swelling and consolidation characteristics of the untreated clay demonstrated that the treatment is irreversible after three cycles. Swelling of clay treated with ASU ash was reduced after the first cycle, while that of the clay treated with Indian ash was reduced after three cycles. This was due to the gelation time difference between treatments. Scanning Electron Microscopy images showed that the structure of the untreated clay was discontinuous, flaky and without aggregations whereas particles in the treated samples were aggregated and new bonds were created, decreasing the surface area. The X-Ray Diffraction (XRF) results showed that the main mineral responsible for expansive

behavior of the clay studied was illite. The d-spacing of the illite decreased from 4.47Å for the untreated clay to 3.33Å for the treated clay. This study demonstrates a promising technique for clay swelling reduction and a more sustainable solution than that available to current practicing engineering.

DEDICATION

I dedicate this thesis to my family who have showed me unswerving support throughout this incredible journey. I dedicate this thesis to my country, Uganda, which birthed me and armored me to explore this world.

ACKNOWLEDGEMENT

First and foremost, I would like to take this chance to thank Dr. Claudia Zapata for giving me the opportunity to work in one of her labs in 2017. This helped me gain experience working in the lab as an undergraduate and it led me to make the choice to go to graduate school. I would also like to appreciate Dr. Edward Kavazanjian for helping be part of the CBBG community and work in research to complete a master's degree. I also thank Dr. Zapata for working tirelessly with me on my research and CBBG projects.

Secondly, I thank Dr. Hamed Khodadadi for helping me in the meetings with geotechnical knowledge and in the labs with several experiments. I also thank Hani Alharbi for mentoring me as an undergraduate student.

Last but not least, I want to cordially thank Mr. Jeffrey Long and Mr. Peter Goguen, who were there for me every single time I needed something to work with, buy, find, or fix in the labs. I want to extend my sincere gratitude to Peter for working endlessly with the software in the basement to ensure I retrieved all my data till the very last days of my research. Mr. Goguen spent endless days fixing the software in the basement as it is very old and many times replaced equipment to ensure I had results. I greatly appreciate your support, Peter and Jeff.

TABLE OF CONTENTS

Page

CHAPTER Page

CHAPTER Page

LIST OF TABLES

Table Page

LIST OF FIGURES

Figure Page

Figure Page

CHAPTER ONE

INTRODUCTION

1.1 Motivation of study/Problem Statement

Expansive soils contain minerals like smectite capable of absorbing water and expanding to several times its initial volume. Expansive clays cause greater financial loss (13 billion dollars of damage annually) to property owners than all the other natural disasters combined (Puppala & Cerato, 2009). The American Society of Civil Engineers states that one in every four homes has damage caused by expansive soils. Lime treatment is the most commonly used technique in practice to mitigate cracks in the infrastructure and damages caused by the high volume change experienced by expansive soils, but this method has disadvantages that include carbonation (formation of carbonates and bicarbonates) and sulfate attack on concrete or cement; both having negative effects on the environment. Silica grouting from bio-sources is a developing technique used to mitigate the infrastructure damages caused by the high volume change experienced by expansive soils technique that improves strength, controls volume change and has little to no harmful environmental effects.

1.2 Background on Soil Improvement

Techniques used today for ground improvement include dynamic compaction, deep soil mixing, grouting and lime treatment, among others. Portland cement is the most common ground improvement technique for granular materials, but it is also used to improve clayey soils. Carbonation is the most popular strategy in recent research studies focused on controlling volume change of problem soils. However, these techniques have their own adversaries. According to the Environmental Protection Agency (EPA),

cementation is the third largest source of environmental pollution, producing up to 829 million tons of carbon dioxide per year and 500,000 tons per year of carbon monoxide, sulphur dioxide, and nitrogen dioxide (Hanle, 2004). Also, lime treatment results in carbonation and concrete sulfate attack, which could be problematic.

Rice husk is a common waste material of the rice harvest industry often put to no use or burnt (Bakar et al., 2016). In 2017, the United States Department of Agriculture estimated that United States produced 178.2 million hundredweight (cwt, 1 cwt =100lb) of rough rice. The USDA estimates that the paddy rice world production is about 700 million tonnes (470 million times of milled rice) with Asia taking up to 90% of the production.

Rice husk consists of the organic matter (cellulose, lignin, protein and vitamins) in the inner epidermis and the inorganic matter is comprised mainly of amorphous silica in the outer epidermis (de Luca, 2017). On combustion, ash is obtained with a silica content of usually over 95% by weight and some impurities (D.D. Bui, 2001; Real et al., 1996; Yalçin and Sevinç 2001; Rivas et al., 2016). Lanning (1963) and Ibrahim (1980) stated that the silicon found in the husk exists on a molecular level in a hydrated form of silica as silica gel or biogenic silica (amorphous silica found in plants). The bulk density of rice husk ranges from 83 to 125 kg/m^3, while its specific gravity is about 0.75 g/cm^3 (de Luca, 2017). Kaupp (1984) stated that grinding to various degrees of fineness increases the unit weight by 2 to 5 times. There are many instances where rice husk has been used as pest control agent, bio-fertilizer additive, heat generator, gas for cook stoves, and electricity generation (Prasad and Pandey, 2012). Some examples of useful products from rice husk include furfural and sodium silicate (de Luca, 2017). Sodium

silicate solution after polymerization is sometimes referred to as colloidal silica or silica gel (Bergna and Roberts, 2005; Luiz Foletto, 2006; De Sousa et al., 2009). Due to its low viscosity, silica solution is ideal for soil stabilization on existing infrastructure, as it requires low pressures for injection purposes (Gallagher et al., 2007).

Recent studies conducted by de Luca (2017) presented a procedure to produce silica gel out of rice husk. The procedure included preliminary analyses on the optimization of factors affecting the rice husk ash, sodium silica and silica gel production. De Luca demonstrated that silica gel treatment reduced free swelling of a highly expansive material by up to 77%.

1.3 Research Objectives

The primary objective of this research study is to devise a bio-based soil stabilization technique for expansive clays using silica gel from rice husk. While this is the main objective of the ASU research group led by Assoc. Professor Zapata, the main goal of this study is to evaluate the effects of wetting and drying cycles on expansive clay materials treated with silica gel and hence, stablish the durability of the treatment. There are three major studies presented in this document: a) the assessment of the chemical differences between ash and silica gels manufactured from rice husk obtained from California, USA and from India; b) the study of volume change behavior of stabilized expansive clay materials; and c) the assessment of the behavior of stabilized expansive clay subjected to wetting and drying cycles. To achieve these goals, lab experiments were carried out to investigate the effect of different input parameters into the process and to determine the optimal conditions for this technique to be applied.

1.4 Plan of Work

The research was organized following the plan of work described in the tasks presented below.

1.4.1 Task 1

The goal of Task 1 is to present the literature review of this document. It will thoroughly detail the different works of several researchers who in the past dedicated their work to volume change behavior of expansive clays and colloidal silica treatment of soils. This work will be presented in Chapter 2 - Literature Review.

1.4.2 Task 2

The goal of Task 2 is to characterize and compare the bio-silica gel produced at Arizona State University laboratories from rice husk produced in California (referred as ASU from herein), and that obtained from rice husk ash shipped from India. The characterization was performed at different stages of the gel production. The studies reported under this task include:

a) Characterization of rice husk ash by XRF and XRD results

b) Characterization of sodium silicate solution by FTIR results

XRD and XRF allowed the determination of the elements in the solution and the ratio between sodium oxides and silicon dioxide, while the FTIR allowed for the determination of the spectrum and the functional groups in the solution. This study aided at establishing optimal conditions for burning rice husk in a furnace and extracting sodium silicate solution from rice husk ash.

1.4.3 Task 3

The goal of Task 3 is to evaluate the effect of sodium silicate gel on the volume change of expansive soils. Silica gel from ASU and from India were used in the testing program and the results were compared. The soil was subjected to several cycles of wetting and drying and the effect of the cycles on free swelling and swelling pressure were evaluated for untreated and treated specimens.

The laboratory program to complete Task 2 comprised:

- Characterization of the clay material used for evaluating the treatment. This characterization included the determination of the grain size distribution, specific gravity, Atterberg limits and compaction soil properties of a local expansive soil from Anthem, Arizona enhanced with bentonite.
- Volume change measurements via oedometer tests on untreated soils and soils treated with silica gel obtained from ASU and India ash sources. The tests were conducted at different curing times and at pH 4.
- Oedometer tests on treated and untreated samples subjected to wetting and drying cycles.

1.5 Thesis Organization

This research paper is organized in the following manner to execute the above plan of work.

- Chapter One (this chapter) comprises the problem statement and motivation behind the study, background on soil improvement techniques, the objectives for the research, the plan of work and the thesis organization.

- Chapter Two contains the literature review of the project. This chapter contains information about past and recent research studies on expansive soils, their characterization and composition, the methodology used for soil improvement, the application techniques used to control volume change behavior of expansive clay and the conclusions drawn from them.
- Chapter Three presents the procedure used to produce sodium silicate solution and silica gel, products to be used for the stabilization of expansive clay. It discusses in detail the extraction of silica gel from ash, from burning to gelification, the silica gelification process and observations made in the laboratory from microscopic characterization of ashes obtained from two locations: California rice husk burned at Arizona State University (ASU) laboratory and Indian ash.
- Chapter Four presents the engineering properties of untreated and treated clay material with silica gel. Results from grain size distribution, Atterberg limits, specific gravity and compaction results are included. The volume change behavior of the untreated and treated expansive clay subjected to wetting and drying cycles are discussed.
- Chapter Five lists conclusions and recommendations of the research project for further use in soil improvement practices.

CHAPTER TWO

LITERATURE REVIEW

2.1 Importance of the Study

The importance of this study was to research and understand the volume change behavior of unsaturated expansive clay specimens when treatment with silica gel via odometer testing. By understanding the volume change behavior of expansive clay, engineers can make appropriate changes to design considerations which in turn will lead to economic advantages. This chapter presents a summary of past literature written about expansive soils, their engineering properties, the volume change behavior incorporated with wetting and drying cycles of expansive soils and the effects of silica gel treatment. The review is divided into sub-sections. The engineering properties of expansive soils will be presented first, then the different practices used to obtain swell pressure, swell potential, and swell index. The review then finally discusses the different research papers on volume change behavior of expansive clays and the different treatment methods currently used.

2.2 Clay Mineralogy

2.2.1 Clay Types and Origins

Most clays are derived from rock through the process of weathering. Weathering can occur by mechanical disintegration or chemical decomposition. Disintegration may be a result of running water, wind abrasion, thawing or freezing. Decomposition, however, is due to oxidation or hydration (Kassif, Livneh and Wiseman, 1969). Clays formed by disintegration and decomposition of the parent bedrock are called residual

soils. They are deep brown to red in color and are highly plastic (Kassif, Livneh and Wiseman, 1969).

2.2.2 Clay Profile

The complete cross section of a soil material from surface to parent rock is called the pedological soil profile. The material in this zone is referred to as the C horizon. There is a deeper leached surface horizon called the alluvial or A horizon and an even deeper zone of accumulation termed as the illuvial or B horizon, sometimes called the hardpan/claypan on which the water table exists (Kassif, Livneh and Wiseman, 1969).

2.2.3 Mineralogy and Chemistry

According to Kassif, Livneh and Wiseman (1969), there are two basic clay structural units: pyramidal or tetrahedral, and octahedral. The tetrahedral unit is made up of four oxygen atoms with a silicon atom at the center. The oxygen atoms at the base of the tetrahedra lie in one plane and each one is shared by two tetrahedra. The apex of the tetrahedron consists of a hydroxyl ion, such that the silicon layer lies between the layer of hydroxyls above and a layer of oxygen below. The tetrahedra combine to form sheets (Kassif, Livneh and Wiseman, 1969). These are the main clay minerals:

- Kaolinite; comprises gibbsite sheets joined to silica sheets (Figure 2.1).
- Halloysite; similar to kaolinite except that the bond between the individual units is due to a molecule of water (Figure 2.2).
- Montmorillonite; most common and most important due to its swelling properties. Structure is made up of gibbsite sheet between two silica sheets (Figure 2.3).
- Illite; similar to montmorillonite in structure but instead of aluminum ion, it has a silicon ion at the center. Due to the high negative charge caused by the silicon, the

clay absorbs potassium ions between layers, as part of a process called as cation exchange capacity (C.E.C) (Kassif, Livneh and Wiseman, 1969).

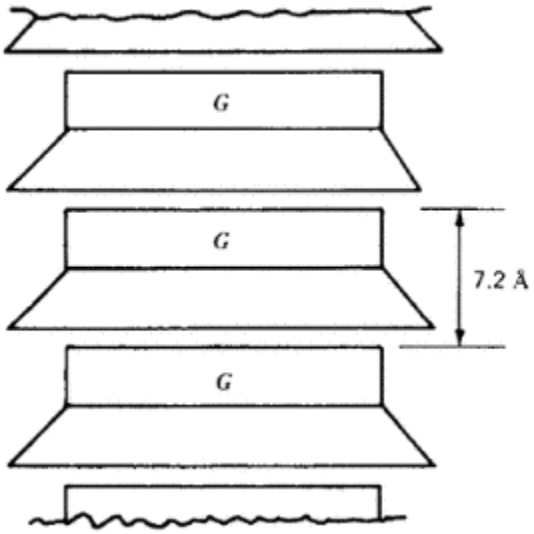

Figure 2.1: Kaolinite (adopted from Mitchell and Soga 2005).

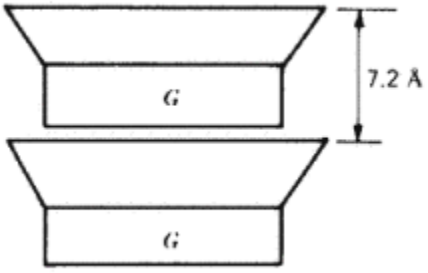

Figure 2.2: Halloysite (adopted from Mitchell and Soga 2005).

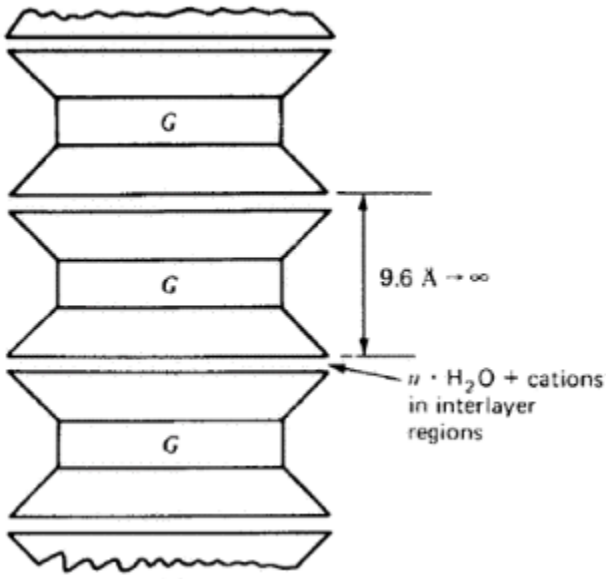

Figure 2.3: Montmorillonite (adopted from Mitchell and Soga 2005).

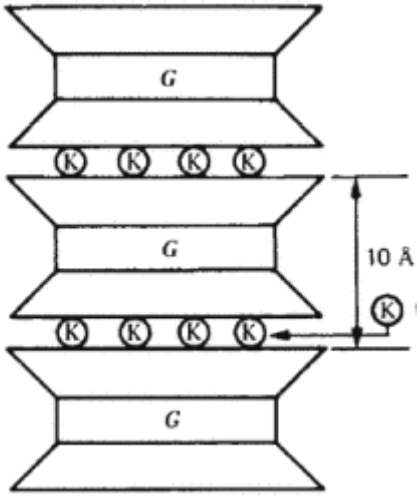

Figure 2.4: Illite (adopted from Mitchell and Soga 2005).

2.2.4 Criteria for Clay Minerals

The different clay minerals are characterized by first order basal reflections at 7, 10, or 14 Å. Positive identification of specific mineral groups ordinarily requires specific pretreatments. Separation of size fractions requires thorough dispersion of the sample.

Detailed procedures for pretreatments useful in X-ray diffraction analysis of clay soils are given by Whittig and Allardice (1986) and Moore and Reynolds (1997).

2.2.5 Clay Minerals

Clay minerals belong to a family called phyllosilicates. This mineral family comprises of other layer silicates such as serpentine, pyrophyllite, talc, mica, and chlorite. Clay minerals occur in small particle sizes, and they have a negative charge in their unit cells balanced out by the adsorption of cations from solution via isomorphic substitution. The structures of the common layer silicates are made up of combinations of two simple structural units, the silicon tetrahedron and the aluminum or magnesium octahedron (Mitchel and Soga 2005).

2.2.5.1 Silica Sheet

In a classic clay mineral structure, four oxygen atoms surrounding a silicon atom forming a tetrahedron which shapes are interconnected in a sheet structure by sharing three of the four oxygens in each tetrahedron to form a hexagonal net (Mitchel and Soga 2005).

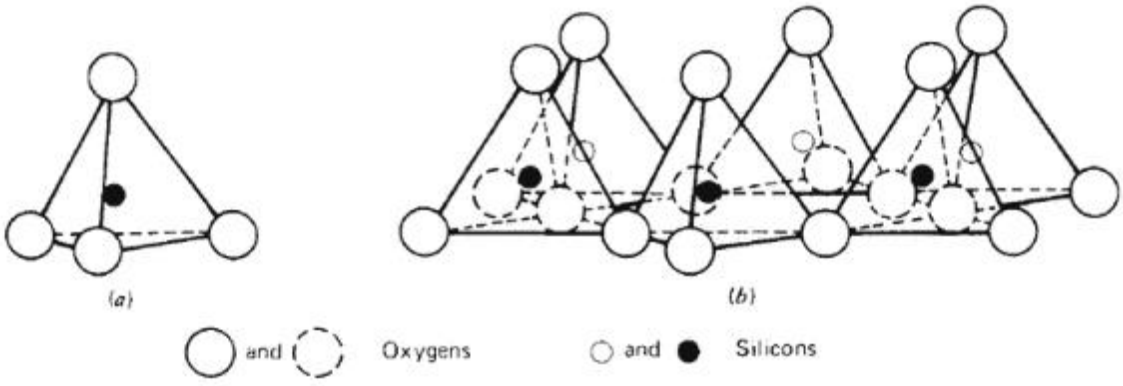

Figure 2.5 Silicon tetrahedron and silica tetrahedra arranged in a hexagonal network (adopted from Mitchell and Soga, 2005).

2.2.5.2 Octahedral Sheet

This sheet structure is composed of magnesium or aluminum in octahedral coordination with oxygens or hydroxyls (Mitchel and Soga, 2005).

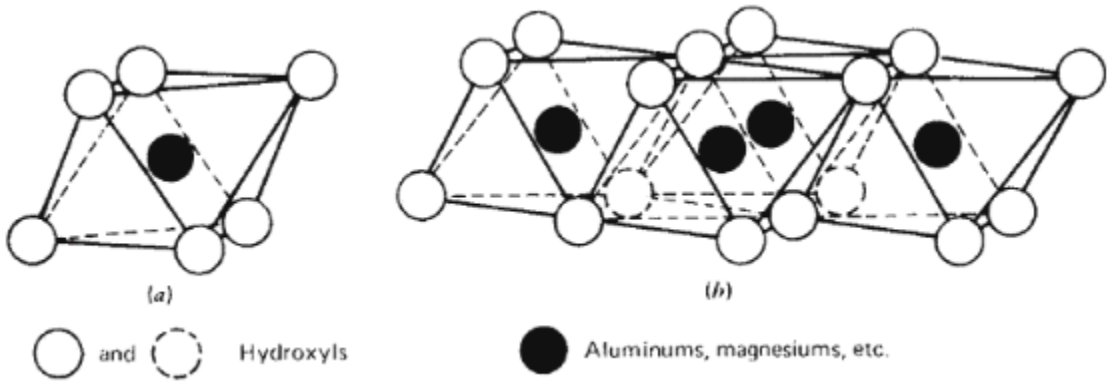

Figure 2.6: Octahedral unit and sheet structure of octahedral units (adopted from Mitchell and Soga, 2005).

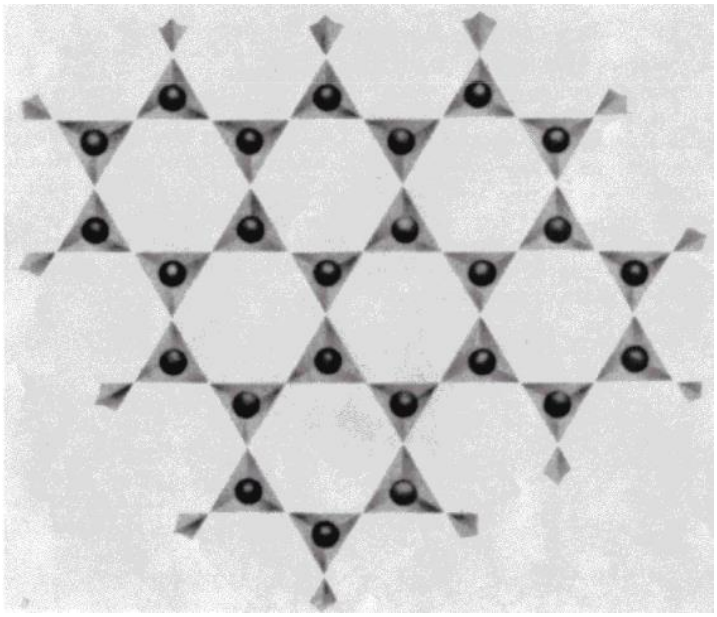

Figure 2.7: Silica sheet in plain view (adopted from Mitchell and Soga, 2005).

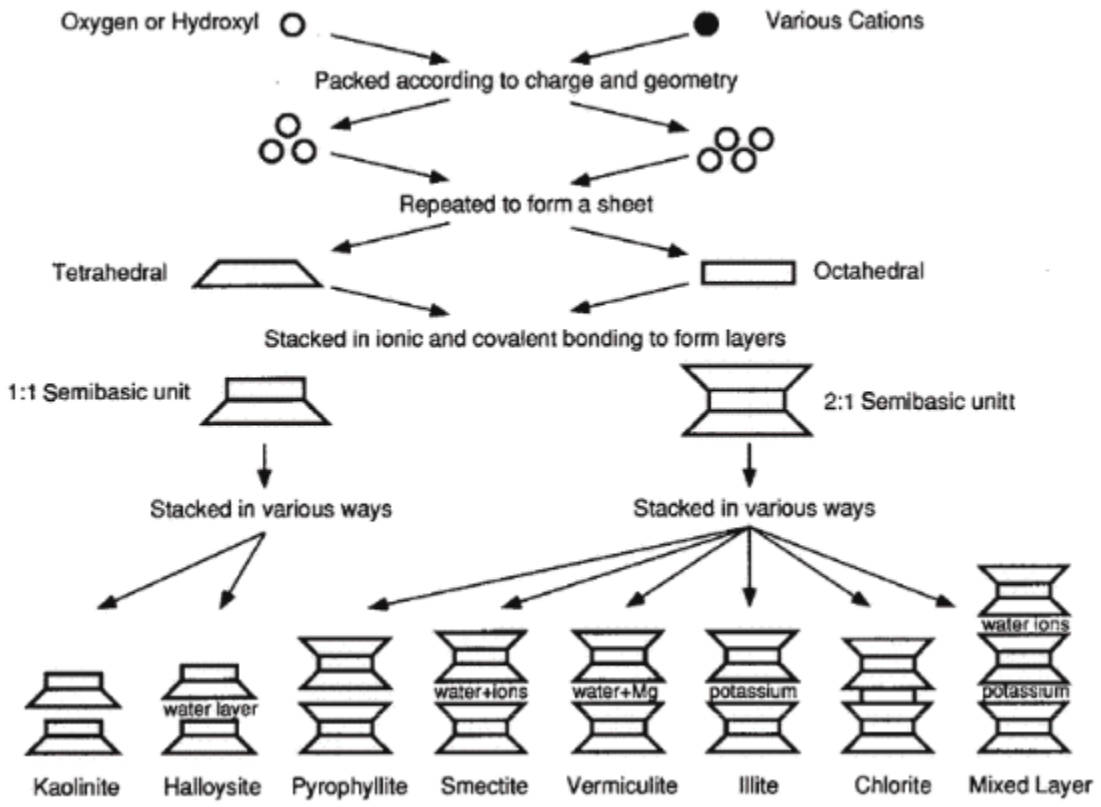

Figure 2.8: Synthesis pattern for the clay minerals (Mitchell and Soga, 2005).

2.2.5.3 Smectite

Smectite and vermiculite particles adsorb water between the unit layers and swell, whereas particles of the non-clay minerals, pyrophyllite and talc, which have comparable structures, do not. There are two possible reasons (van Olphen, 1977):

1. The interlayer cations in smectite hydrate, and the hydration energy overcomes the attractive forces between the unit layers. There are no interlayer cations in pyrophyllite; hence, no swelling.
2. Water does not hydrate the cations but is adsorbed on oxygen surfaces by hydrogen bonds. There is no swelling in pyrophyllite and talc because the surface hydration

energy is too small to overcome the van der Waals forces between layers, which are greater in these minerals because of a smaller interlayer distance.

Whatever the reason, the smectite minerals are the dominant source of swelling in the expansive soils that are so prevalent throughout the world.

2.2.5.4 Bentonite

A very highly plastic, swelling clay material known as bentonite is very widely used for a variety of purposes, ranging from drilling mud and slurry walls to clarification of beer and wine. The bentonite familiar to most geo-engineers is a highly colloidal, expansive alteration product of volcanic ash. It has a liquid limit of 500 percent or more. It is widely used as a backfill during the construction of slurry trench walls, as a soil admixture for construction of seepage barriers, as a grout material, as a sealant for piezometer installations, and for other special applications. When present as a major constituent in soft shale or as a seam in rock formations, bentonite may be a cause of continuing slope stability problems. Slide problems at Portuguese Bend along the Pacific Ocean in southern California, in the Bearpaw shale in Saskatchewan, and in the Pierre shale in South Dakota are in large measure due to the high content of bentonite. Stability problems in underground construction may be caused by the presence of montmorillonite in joints and faults (Brekke and Selmer-Olsen, 1965).

2.3 Engineering Properties of Expansive Soils

For a long time, different researchers have tried to identify the different properties to classify expansive soils. Some of these properties discussed in this review are Atterberg limits, Cation Exchange Capacity (CEC), Specific Surface Area (SSA), Activity, Swell Index, and Clay mineralogy.

2.3.1 Cation Exchange Capacity

According to Mitchel and Soga (2005), the cation exchange capacity (CEC) depends on the isomorphic substitutions that occur within the clay minerals. Isomorphic substitution means that some octahedral and tetrahedral spaces in clay minerals are occupied by cations other than those in the ideal structure (i.e. aluminum in place of silicon, magnesium instead of aluminum, and ferrous iron for magnesium). Isomorphic substitution gives the clay minerals a net negative charge except for the kaolinite group. To maintain electrical equilibrium, cations are attracted and held between the layers, and on the surfaces and edges of the particles. The number of exchangeable cations is what is called cation exchange capacity (CEC) usually expressed in milliequivalents (meq^3) per 100g of dry clay. Table 2.1 shows the values of CEC for some common clay mineral.

Table 2.1: CEC values for Common Clay Minerals (Mitchell and Soga 2005).

Clay mineral	CEC ((meq^3)/100g)
Kaolinite	3
Illite	25
Halloysite	12
Vermiculite	150
Smectite	85
Chlorite	40

2.3.2 Specific Surface Area (SSA)

The Specific Surface Area, SSA is determined by the number of polar molecules retained on the surface of a clay particle under laboratory-controlled conditions and it indicates the main governing clay minerals (Mitchell and Soga, 2005). It is expressed in

square meters per gram. Table 2.2 shows the ranges of SSA for some common clay mineral.

Table 2.2: SSA Values for Common Clay Minerals (Mitchell and Soga 2005).

Clay mineral	**CEC ((meq^3)/100g)**
Kaolinite	10-20
Illite	65-100
Halloysite	35-70
Vermiculite	40-80
Smectite	50-800

2.3.3 Atterberg Limits

Atterberg limits are useful to Geotechnical engineers in that they are the threshold for description, classification, and identification of expansive soils. The idea was first introduced to Geotechnical engineering by Terzaghi in 1925 and later enhanced by Casagrande in 1932. Casagrande devised a unique standard test method to determine the liquid limit (LL), plastic limit (PL) and plasticity index (PI) of the soil. The liquid limit test is a form of dynamic shear test (Mitchel and Soga 2005). Casagrande (1932) deduced that the liquid limit corresponds approximately to the water content at which a soil has an undrained shear strength of about 2.5 kPa. According to Terzaghi (1925), plastic limit is the water content below which the physical properties of water do not correspond to those

of free water. However, it can also be defined as the lowest water content at which the cohesion between particles is low enough to allow movement but significantly high enough to allow particles to maintain the molded positions (Yong and Warkentin, 1966). Later on, in 1948, Casagrande developed a soil classification system which was modified into the Unified Soil Classification System (USCS). Under this system, fines are classified as one of the following: non-plastic (NP), lean silt (ML), highly compressible silt (MH), lean clay (CL), and fat clay (CH). Most of the expansive soil exhibits characteristics of either a CL or CH soil (Rosenbalm, 2013). The location of the different clay minerals is indicated in figure 2.9 adopted from Holtz and Kovacs (1981).

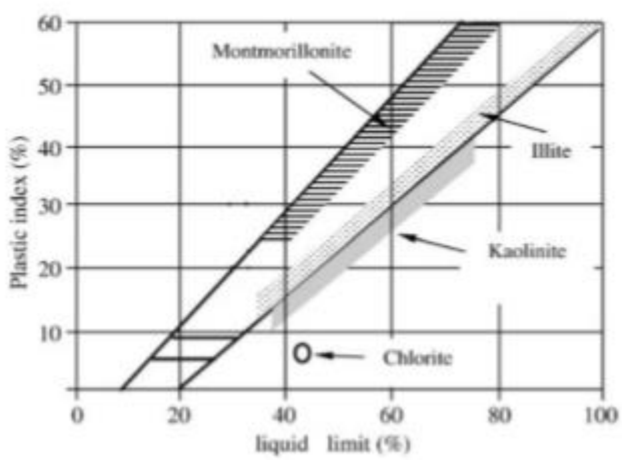

Figure 2.9: Location of clay mineralogy bands on USCS soil classification (adopted from Holtz and Kovacs 1981).

2.3.4 Colloidal Activity

According to Skempton (1953), the activity of a soil is the ratio of the plasticity index, P.I, to percent clay particles smaller than $2\mu m$ as shown in equation 2.1.

$$A = \frac{PI}{\% < 2\mu m} \quad (2.1)$$

The greater the activity, the more important the influence of the clay fraction on properties and the more susceptible their values to changes in such factors as type of exchangeable cations and pore fluid composition (Mitchel and Soga, 2005).

Table 2.3: Activities of different clay minerals (adopted from Mitchel and Soga, 2005).

Clay mineral	Activity
Smectite	1-7
Illite	0.5-1
Kaolinite	0.5
Halloysite	0.5
Attapulgite	0.5-1.2
Allophane	0.5-1.2

2.3.5 Swell Index

Expansive soils have a swelling index greater than 0.2 whereas non-expansive soils have a swelling index less than 0.1 (Mitchel and Soga, 2005). Figure 2.2 below shows the effective stress void ratio curve for a compressive soil. The segment AB is the virgin compression curve, segment BC is the rebound curve, and segment CD is the recompression curve.

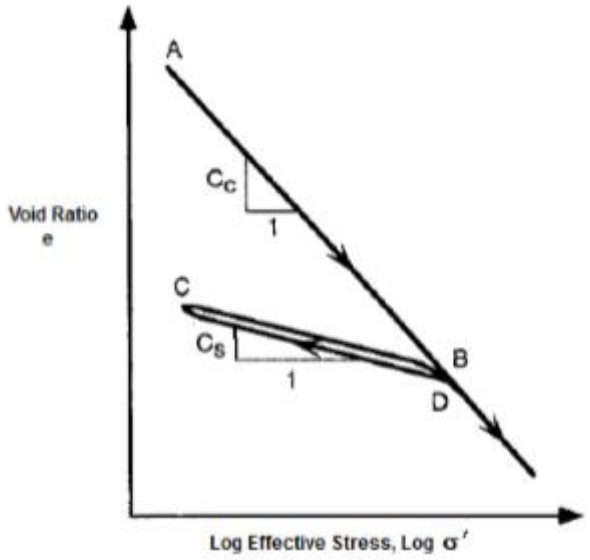

Figure 2.10: Idealized effective stress – void ratio for a compressible soil (Mitchell, J.K. and Soga, K. 2005).

2.3.6 Free Swell and Free Swell Index and Swelling Potential

Holtz and Gibbs (1957) define the degree of swell of soil in accordance with the percentage swell of an air-dry sample in the oedometer under a vertical pressure of 1.0 psi.

$$F.S.I = \frac{V - V_0}{V_0} * 100\% \ldots\ldots\ldots\ldots\ldots\ldots\ldots\ldots\ldots\ldots\ldots\ldots\ldots\ldots\ldots\ldots (2.2)$$

Where F.S.I - free swell index

V - volume after swelling (volume in water)

V_0- volume before swelling (volume in kerosene)

Free swell is the difference between the final height after swelling and the initial height before swelling divided by the initial height before swelling. The token load for the free swell can range from 1 kPa to 5 kPa (20 psf to 100 psf), which the token load is

dependent on the test standard that is used. ASTM D 4546 the token load is 1 kPa and the prescribed token load in Arizona is 5 kPa. ASTM D 4546 states the compactive effort and the moisture content is determined by the laboratory that is running the test, while the Arizona method predetermines the compactive effort and moisture content. The Arizona method requires the moisture content two percent less than the optimum and 90 percent of the maximum dry density (Rosenbalm 2013).

Table 2.4: Relationship between indicative clay properties and degree of swell (Holtz and Gibbs, 1957).

Swell potential	**% Swell in oedometer under 1.0 psi**	**S.L %**	**P.I %**	**Percent smaller than 1μ**	**F.S.I %**
Very high	>30	<10	>32	>27	>100
High	20-30	6-12	23-45	18-37	>100
Medium	10-20	8-18	12-34	12-27	50-100
Low	<10	>13	<20	<17	<50

Swelling pressure is the vertical pressure required to stop the volume change of a soil sample. That is, it is the maximum vertical pressure which the clay can develop for a particular initial moisture content and density placement conditions without any soil movement (Holtz and Gibbs, 1957).

Table 2.5: Relationship between indicative clay properties and degree of swell per USBR 1959.

Swell potential	**% Swell in oedometer under 1.0 psi**	**S.L %**	**P.I %**	**Percent smaller than 1μ**	**F.S.I %**
Very high	>30	<11	>35	>28	>100
High	20-30	7-12	25-41	20-31	>100
Medium	10-20	10-16	15-28	13-23	50-100
Low	<10	>15	<18	<15	<50

In 1955, Altmeyer had major criticisms of USBR method for classifying expansive soils and suggested a new method based on correlations between the linear shrinkage, shrinkage limit and the percent swell. His recommendations are shown in table 2.6 (Rosenbalm 2013).

In 1965, Ranganathan and Satyanarayana used the concept of the shrinkage index (i.e. SI = LL-SL) (Snethen et al. 1977). The correlations between shrinkage index and swell potential are shown in table 2.7.

Table 2.6: Swell Potential Criteria per Altmeyer 1955.

Linear shrinkage	S.L %	Swell	Degree of swell
<5	>12	<0.5	Noncritical
5-8	10-12	0.5-1.5	Marginal
>8	<10	>1.5	Critical

Table 2.7: Swell Potential per Ranganathan and Satyanarayan 1965.

Swell potential	Shrinkage index
Very high	>60
High	30-60
Medium	20-30
Low	<20

As one can tell from the above tables, the ranges for swell potential are different for the different authors. The different guidelines have been used by Geotechnical engineers over the years and sometimes ranges or discrepancies in ranges or the overlaps can cause confusion and arguments. Therefore, it is difficult to come to a conclusion about the swell potential classification but it is safe to note that there is no one single

guideline that is utterly perfect and all the estimates are accepted and used as they are in the literature (Rosenbalm 2013).

2.4 Literature Methods to Measure Volume Change

In practice today, researchers use swell pressure, swell index, and percent heave to estimate swelling of expansive soils. Recognizing the swell potential of an expansive soil helps with improving the design considerations for foundations. The ASTM methods for determining the swelling potential of expansive soils are discussed below (Rosenbalm 2013).

2.4.1 ASTM 4546 standard for determining one-dimensional swell of expansive soils

This standard test method has two versions: one being before 2008 and the other after 2008. Prior to 2008, the standard presented three different methods to analyze swelling. Method A was to determine the percent swell/heave at a token load. Method B determined the swell potential at a specified load/stress and method C determined the swell pressure by increasing the stress to achieve zero volume change. After 2008, all three methods were revised, and changes were made. Method A is now known as "wetting-after-loading test on multiple specimens". The test now requires four or more identical samples to be tested at various loads. Method B is now called "single-point wetting-after-loading on a single specimen". After wetting, the specimen is loaded to a desired stress and the swell strain is calculated from the axial deformation. Method C is now termed as "loading after wetting test" which requires method A/B to be accomplished first (Rosenbalm 2013).

To learn more about other methods used to measure volume change, refer to Rosenbalm (2013) where ASTM D 4829-11 Standard Test Method for Expansion Index of Soils and Arizona Expansion Index are discussed.

2.5 How to Predict Swelling Potential

2.5.1 McDowell's Method (Kassif, Livneh and Wiseman 1969).

This method suggests that it is possible to predict the potential surface heave of a pavement by testing undisturbed samples taken from various depths within the subgrade and measuring the potential volume change for capillary absorption under a confining pressure of 1 psi (Kassif, Livneh and Wiseman 1969).

$$w_i = 0.2 * L.L + 9 \quad \text{.....2.3}$$

$$w_f = 0.47 * L.L + 2 \quad \text{.....2.4}$$

The percent volume change (swelling) is directly related to the P.I (Kassif, Livneh and Wiseman 1969).

$$(\frac{\Delta V}{V})\% = 0.37 * P.I - 3 \quad \text{.....2.5}$$

and the overburden pressure can be expressed as

$$p_o = 0.5 * P.I - 5 \quad \text{.....2.6}$$

2.5.2 Jennings' Method (Kassif, Livneh and Wiseman 1969)

- Determine the depth of the active zone
- Obtain undisturbed samples
- Estimate the pore water suction to be expected throughout the active zone
- Perform swelling tests on the samples
- Integrate the percent swell obtained from the swelling tests with depth

2.6 Volume Change Behavior of Expansive Clays

2.6.1 Swelling/Shrinkage Characteristic Curve, SSCC

Partial shrinkage gives a different structure compared to full shrinkage hence the differences in swelling behavior. The ideal shape associated with wetting and drying cycles has been a topic of discussion among researchers for decades. The volume change behavior associated with wetting and drying cycles was devised as the "Swelling/Shrinkage Characteristic Curve (SSCC)" (Hanafy 1991).

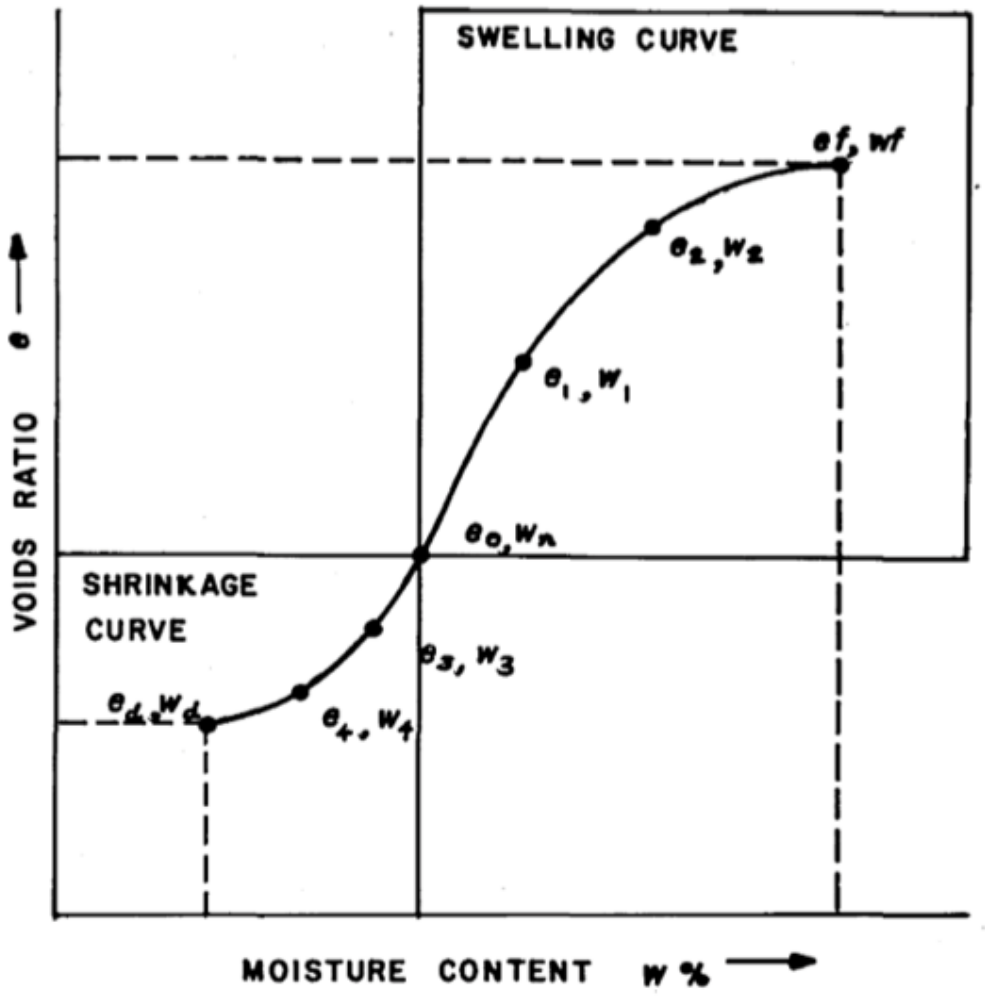

Figure 2.11: Idealized SSCC for expansive soils (Hanafy 1991).

2.6.2 Swelling Strain Changes with Increase in Cycles

The percent strain generally increases with cycles. The swelling strain can be recovered at token loads and is irrecoverable at large stresses. This could be due to changes in the void ratio or dry density during the wetting and drying cycles. With time, the sample reaches a constant swell or shrinkage due to the preconditioning of the normal stress and matric suction i.e., the moisture content changes. Changes in the surrounding environment caused changes in matric suction. On circulating the sample with water, the pores fill causing tension and in turn lowering the matric suction. On drying the sample, there is an increase in matric suction as a result of increasing tension on water. This also caused tension cracks from stresses greater than the tensile strength (Rosenbalm 2013).

2.6.3 Swelling Pressure Changes with Increase in Cycles

The swell pressure decreases with increasing cycles. The swell pressure tends to come to a constant value after about 5-6 wetting and drying cycles. The reduction in swell pressure increases with cycles until an equilibrium is reached (Rosenbalm 2013). On the first cycle, the swell pressure is a function of both the dry density and matric suction. As time goes on, the effect of matric suction is barely noticed and the changes in swell pressure can then be attributed to changes in compacted dry density i.e., moisture content (Rosenbalm 2013).

2.6.4 Moisture Content Changes with Cycles

The moisture content decreases with time during the drying cycles and increases with time during the wetting cycles. The moisture content variation with time during the wetting cycle can best be represented on log scale whereas during the drying cycle, it can best be represented by an exponential function (Rosenbalm 2013).

2.7 Chemical Treatments to Mitigate Expansive Soil Behavior

The following section presents a summary of the chemical treatments currently used in practice to stabilize expansive soils.

2.7.1 Lime Treatment

2.7.1.1 Cation Exchange and Flocculation-Agglomeration

Lime is a source of free calcium and therefore clays display rapid cation exchange and flocculation-agglomeration reactions when treated with lime in presence of water. Multivalent cations replace monovalent cations easily, but adsorption tend to occur according to the lyotropic series Na+<K+<Ca++<Mg++ as cations on the right replace those on the left assuming equal concentration. Herzog and Mitchell () state the aggregation from flocculation and agglomeration is caused by increased electrolyte concentration of the pore water and adsorption of calcium on the clay surface.

2.7.1.2 Soil-Lime Pozzolanic Reactions

Lime, water, soil silica, and alumina react to form various cementitious compounds. Addition of lime increases the pH of soil to approximately 12.4 which is the pH of saturated lime water. At high pH, the solubility of silica and alumina increase drastically. Eades stated that high pH causes the silica from clay to dissolve and combine with Ca++ from calcium hydroxide to form calcium silicate. In general, the precipitates from the reactions are Calcium Silica Hydroxide (CSH) and Calcium Alumina Hydroxide (CAH).

An oversimplified qualitative view of some typical soil-lime reactions is as follows:

$$Ca(OH)_2 \rightarrow Ca^{2+} + 2[OH]^-$$

$$Ca^{2+} + 2[OH]^- + SiO_2(clay\ silica) \rightarrow CSH$$

$$Ca^{2+} + 2[OH]^{-} + Al_2O_3(clay\ alumina) \rightarrow CAH$$

A wide variety of hydrate forms can be obtained depending on reaction conditions (e.g., quantity and lime type, soil characteristics, curing time, and temperature). Typical soil-lime reactions are as follows:

kaolinite + lime →CSH (C/S=0.2-1.0) + CAH + CASH

kaolinite + lime→CASH (prehnite)

montmorillonite + lime →CSH (gel) →CSH (II)

montmorillonite + lime →CSH (gel) + hydrogarnet (C_4AH_{13})

clay + lime →CSH (gel) and/or CSH (I) + C_4AH_{13} + C_3AH_6

where C = CaO, S = SiO_2, A =Al_2O_3, and H = H_2O

2.7.1.3 Properties of Lime-treated soils

2.7.1.3.1 Compaction characteristics

Compaction characteristics are maximum dry density and optimum water content. These factors are vital mainly because density is used for field control and but also because a sufficient level of compaction has to be achieved for good results. On compaction, soil-lime mixtures have a lower maximum dry density than the untreated soil and the maximum dry density decreases with increasing lime content while optimum water content increases with increasing lime content.

2.7.1.3.2 Plasticity and workability

Lime treatment leads to reduced plasticity index and increased shrinkage limit. Highly plastic soils require great amounts of lime to achieve the non-plastic condition if at all it is even achievable. Reduction in plasticity leads to increased workability.

2.7.1.3.3 Volume change behavior

Swelling potential and swelling pressures normally are significantly reduced by treating clay with lime. These reduced swell characteristics are generally attributed to decreased affinity for water of the calcium-saturated clay and the formation of a cementitious matrix that resists volumetric expansion. California bearing ratio (CBR) swell values of lime-treated soils vary, but it is not uncommon to decrease swell to less than 0.1 percent compared to values of 7 to 8 percent for the untreated soil. Shrinkage caused by moisture loss from the stabilized soil is important relative to the problem of shrinkage cracking. Lime treatment improves the shrinkage and swell characteristics of the treated materials.

2.7.1.3.4 Strength

The strength of a soil-lime mixture depends on many variables such as soil type, lime type, lime percentage, curing conditions of time and temperature, and the relationships between these variables are the major factors influencing strength. A distinction must be made with respect to curing. Strength increases with the addition of lime due to flocculation and aggregation. The long-term strength gain is primarily related to the pozzolanic reaction. Therefore, it is necessary to divide the discussion between cured and uncured strength.

2.7.1.3.5 Durability

Durability consideration in soil-lime mixtures is mainly the resistance to cyclic freezing and thawing. In places where freezing temperatures occur, freeze-thaw damage usually happens characterized by an increase in volume and reduction in strength.

2.8 Bio-based treatment of expansive clays

2.8.1 Treatment with silica gel extracted from rice husks

2.8.1.1 Rice ash production

Rice husk is the outermost layer of the rice grains casing and it is the most abundant waste material from the rice industry. The annual production of paddy rice was approximately 400 million metric tons in 2001 (Yalcin and Sevinc, 2001) while the production shot to 740 million metric tons in 2015 (Rivas et al). In 1972, Houston predicted the estimation of the average value of rice husk content in paddy rice to be about 20%. Rice husk is composed of organic and inorganic matter. The organic matter is composed of cellulose, lignin, protein, and vitamins. The inorganic matter is amorphous silica.

Fig 2.12: Rice husks

2.8.1.2 Rice husk ash production

On burning, the silica content of the produced ash may reach over 95% by weight (D.D.Bui, 2001). According to Lanning (1963) and Ibrahim (1980), the silicon present in rice husk is found to be dispersed in the organic material of the husk at the molecular level. This silicon exists in a hydrated amorphous form of silica, probably biogenetic opal or silica gel. Rivas et al. (2016) reported that untreated RHA contained 87.4% of silica

(SiO_2) by weight, with the rest of the material corresponding to metallic impurities such as potassium oxide (K_2O), phosphorus pentoxide (P_2O_5) and calcium oxide, among others. Rivas then treated the rice husk by washing it with one molar of hydrochloric water solution (1M HCl) and then burned at a temperature of 650°C for 3 hours. The treated sample resulted in 96.9% silica (SiO_2) as a weight compound. X-ray diffraction was used to determine whether the silica content in the RHA was amorphous or crystallized.

Several studies were found related to the optimization of time and temperature factors for rice husk combustion. Of interest, Hamed and Khattab (1981) studied the effect of thermal decomposition of rice husk on the amorphous structure of silica ash in the laboratory. They observed that the ash containing amorphous silica formed at comparatively lower temperatures, between 500-600°C. The crystalline forms, cristobalite and trydimite, appeared at higher temperatures of around 800-1200°C. They also compared the state of rice husk ash prepared in a furnace with that of the ash produced in a fixed bed at different air rates. At lower air rates, amorphous silica was formed, whereas, at higher rates, silica crystallization occurred.

Metha (1978) found that amorphous silica can also be obtained at temperatures below 500°C for a prolonged period. Yeoh et al. (1979) found that silica ash can still be amorphous at combustion temperatures up to 900°C, if the combustion time is less than 1 hour, and crystalline silica is obtained at temperatures of 1000°C or higher within 5 minutes or higher. Chopra et al. (1981), using X-ray diffraction, observed that at temperatures of up to 700°C, amorphous silica can still be obtained. Meanwhile, James

and Rao (1986) found that regardless of the burning time, crystallization of silica did not occur at temperatures below 700°C.

In conclusion, several researchers confirmed that amorphous silica is obtained at temperatures under 700°C even if the combustion time is doubled or tripled.

2.8.1.3 Precipitation of Silica from Rice Husk Ash (RHA)

To obtain silica from rice husk ash, three different steps are necessary. Firstly, it is important to perform acid-washing of rice husks; then, the extraction of the silica from the ash followed by the precipitation of the silica (Kamath and Proctor, 1998). The amorphous nature of RHA silica makes it extractable at lower temperature, and hence, it provides a low energy method (Della et al., 2000).

2.8.1.3.1 Acid Washing of Rice Husks

This step is essential to remove small quantities of mineral impurities from rice husks prior to silica extraction, especially to keep the K, Na, Mg, Ca content in silica at a lower concentration (de Luca, 2017).

Fig 2.13: Acid washed rice husks

2.8.1.3.2 Rice Husk Combustion

Rice husks are burnt in a muffle furnace at 600°C for 2 hours (Sayed Mostafa, 2019).

Fig 2.14: Rice husk ash/silica ash

2.8.3.3 Silica Extraction

The following reaction equation represents the extraction of sodium silicate solution (Na_2SiO_3) from the impure silicon dioxide (SiO_2).

$$SiO_2 + 2\text{NaOH} \rightarrow Na_2SiO_3 + H_2O \ldots\ldots\ldots\ldots (3.1)$$

In previous studies performed by de Luca (2017), the silica ash was dissolved in 1N sodium hydroxide (1N NaOH) with constant stirring to dissolve the silica and produce sodium silicate solution. After 1 hour, the solution was filtered through filter paper and the carbon residues were washed with 100 ml of boiling water. The solution was allowed to cool to room temperature (de Luca, 2017).

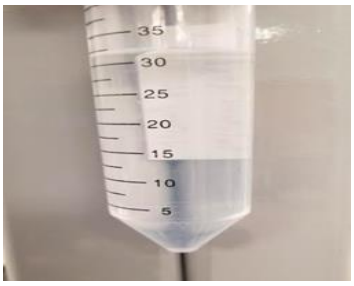

Fig 2.15: Sodium silicate solution

2.8.3.4 Silica Precipitation

In this step, the aim is to precipitate silica gel from the sodium silicate solution. The following equation represents the chemical reaction:

$$Na_2SiO_3 + H_2O + 2HCl \rightarrow Si(OH)_4 + 2NaCl \ldots\ldots\ldots (3.2)$$

The solution is very alkaline (pH 12-13) and hence, hydrochloric acid is used to lower the pH and allow gelation to occur (Rosenbalm, 2013. de Luca, 2017. Sayed Mostafa, 2019). It is worth noting that silica gel forms at two different pH conditions: alkaline condition, at pH between 7 and 10; and acidic condition, at pH between 1.5 and 6 (Rosenbalm, 2013. de Luca, 2017. Sayed Mostafa, 2019). The alkaline silica gel was found to form rather quickly, with fluffy, glassy consistency, and very weak. Hence, it was not useful in improving the mechanical properties of the clay (Rosenbalm, 2013. de Luca, 2017. Sayed Mostafa, 2019). On the other hand, acidic silica gel has proved to be stronger as polymerization is attained at much slower rate (Sayed Mostafa, 2019).

2.8.4 Swell Test

2.8.4.1 Swell Test on Untreated Samples

De Luca (2017) performed the swelling test on two different soils: Soil 1 (90% Anthem Clay and 10% Bentonite Clay) and Soil 2 (70% Anthem Clay and 30% Bentonite Clay). The tests on the untreated samples were important to find out which soil was more expansive. The results on the untreated samples are shown in figure 2.16 below.

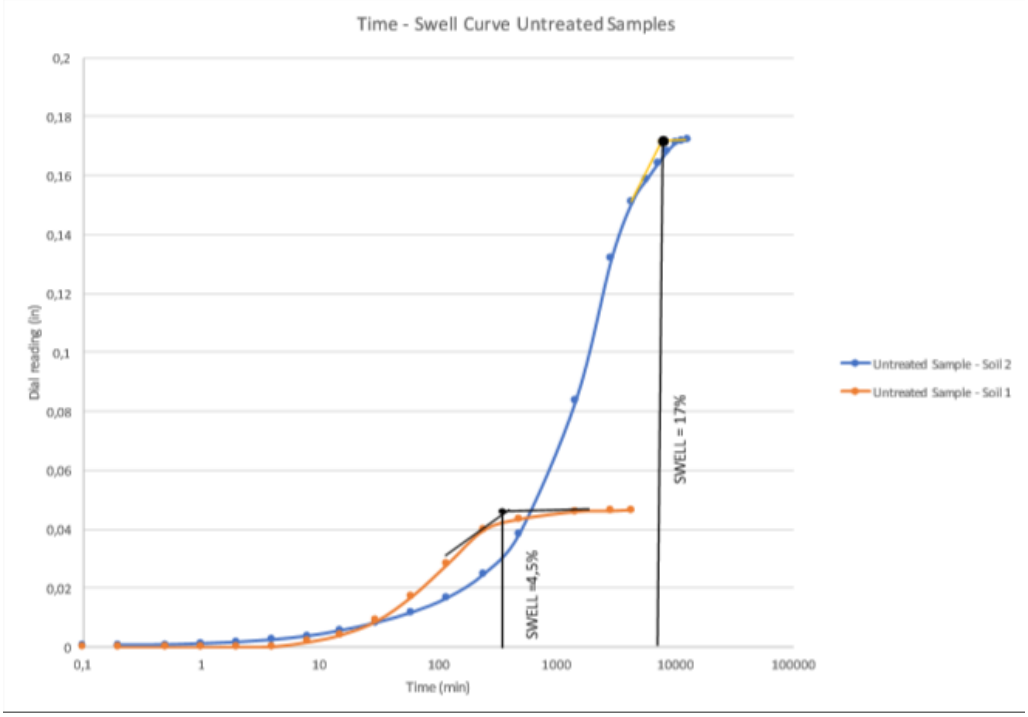

Fig 2.16: Comparison time-swell curve for untreated samples (de Luca, 2017)

As shown in the figure above, the free swell of soil 2 is 17% while that of soil 1 is only 4.5% implying soil 1 is more expansive and responsive to volume change due to wetting and drying cycles (de Luca, 2017).

2.8.4.2 Swell Test of Treated Samples

Going by these results, de Luca (2017) performed treatment on soil 2 only for the reason above and the results are shown in figure 2.17 below.

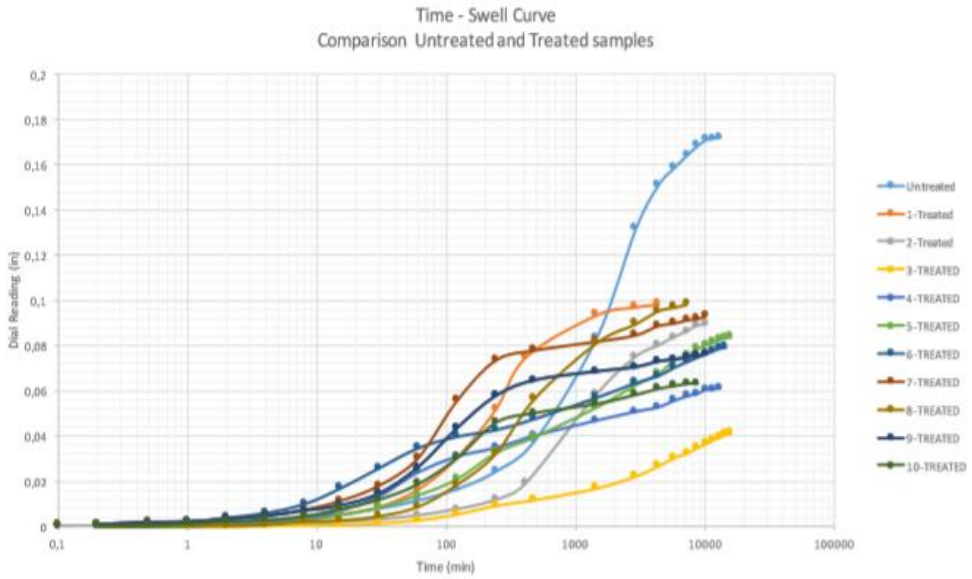

Fig 2.17: Time-Swell Curve for treated samples (de Luca, 2017)

De Luca (2017) treated samples for different gelification times and varying percentages of gel and found that any treatment leads to reduction in swelling as shown in the figure above.

2.8.4.3 Effect of Gelation Time on Swelling

De Luca (2017) investigated the effects gelation time has on swelling as shown in figure 2.18. De Luca (2017) treated three soil 2 samples with 29.3% of gel and left them to cure for 5 days, 10 days, and 15 days and then proceeded to perform swelling test on these samples.

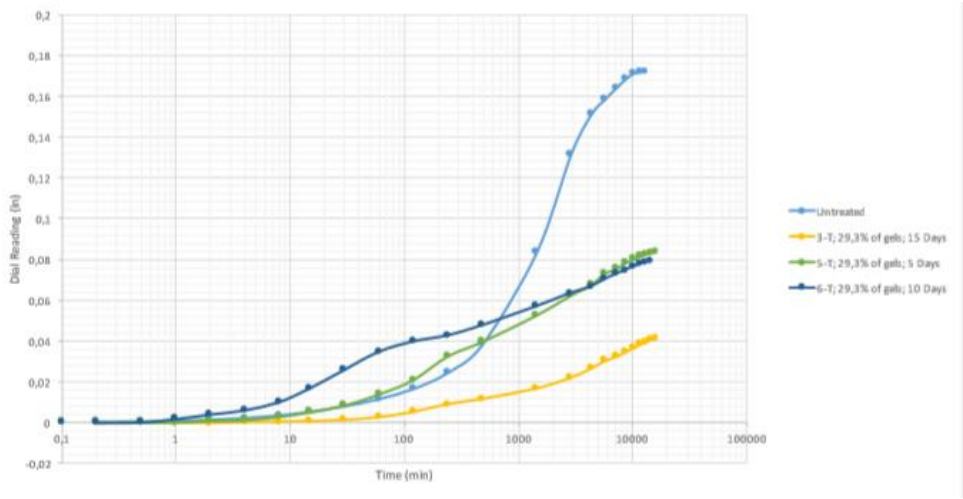

Fig 2.18: Effect of gelation time (de Luca, 2017)

From the figure above, it was clear that the more time taken to cure, the more reduction in swelling was observed.

2.8.2 Treatment with Lignosulfonate

2.8.2.1 Lignosulfonate

Lignosulfonate (LS) is a byproduct of the wood and paper industry (Noorzard & Ta'negonbadi, 2018). It is a polymer made from lignin and contains hydrophilic groups such as sulfonate, phenyl hydroxyl, alcoholic hydroxyl and hydrophobic groups mainly the carbon chain (Noorzard & Ta'negonbadi, 2018). The predominant salt in LS is calcium and therefore LS was characterized as Calcium Lignosulfonate. The caly used was obtained from Amol, Iran.

2.8.2.2 Laboratory Investigation

The Atterberg limits test results of the Amol clay showed that the liquid limit was 56% and the plastic limit was 26% and hence the plastic index determined was 29%. The free swell of the Amol clay was 2.6% at OMC and 95% MDUW. Based on ASTM D-2487, the clay was classified as high plasticity clay (CH). The results of the compaction

test indicated that the OMC was 21.3% and the MDUW was 16.3 $\frac{kN}{m^3}$ and the specific gravity of the soil was found to be 2.70.

2.8.3 Results and Discussion

2.8.3.1 Atterberg Limits

The PL of the clay mixed with LS did not change drastically and almost stayed constant while the LL of the clay fell from 55% to 39% and hence the PI of the treated soil was reduced from 29% to 14% at 0.75% LS addition. The decrease in the PI of the clay changed the soil classification from highly expansive to moderate according to the classification of Gibbs and Holtz as shown in table 2.8(Noorzard & Ta'negonbadi, 2018).

Table 2.8: Atterberg limit results (Noorzard & Ta'negonbadi, 2018)

Sample	LS content (%)	Liquid Limit (LL) (%)	Plastic Limit (PL) (%)	Plastic Index (PI)
Untreated	0	55	26	29
Treated	0.75	39	25	14
Treated	2	41	26	15
Treated	3	43	26	17
Treated	4	44	26	18

2.8.3.2 Compaction test results (Noorzard & Ta'negonbadi, 2018)

Table 2.9 shows the results of the compaction test on the untreated and LS-treated samples. The MDUW of the mixed clay decreased slightly whereas the OMC increased

slightly. The decrease in MDUW can be attributed to the decrease in specific gravity of the soil treated with LS (Noorzard & Ta'negonbadi, 2018).

Table 2.9: Compaction results (Noorzard & Ta'negonbadi, 2018)

Sample	LS content (%)	OMC (%)	MDUW ($\frac{kN}{m^3}$)
Untreated	0	21.3	16.3
Treated	0.5	21.4	16.2
Treated	0.75	21.5	16.2
Treated	1	21.6	16.1
Treated	2	21.9	16.1
Treated	3	22.1	16.0
Treated	4	22.3	15.9

2.8.3.3 UCS Testing

Figure 2.19 shows the relationships between the percentages of LS and UCS of the treated soil versus curing time. The UCS of the treated sample showed a significant increase with an increase incurring time up to 28 days after which it slowed down and became non-significant. This result can be attributed to the neutralization of negative charges on the surfaces of the clay minerals and the decrease in the crystalline size of the minerals due to steady aggregation.

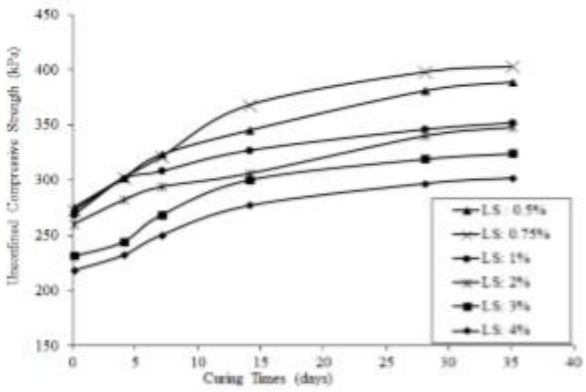

Fig 2.19: UCS vs curing time (Noorzard & Ta'negonbadi, 2018)

The maximum axial stress of expansive soil treated with different contents of LS at a curing time of 28 days is shown in figure 2.20. The UCS test results indicate that the optimum LS content for stabilizing the expansive clay was 0.75% of the dry weight as obtained from the Atterberg limits. A decrease in axial maximum stress with an increase in LS content beyond the optimum is attributed to the repulsive forces caused by additional polymer chains in the admixture (Noorzard & Ta'negonbadi, 2018).

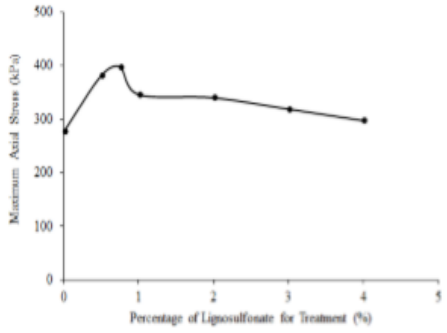

Fig 2.20: Maximum axial stress of treated soil at different LS content for 28 days curing (Noorzard & Ta'negonbadi, 2018)

2.8.3.4 Swelling Behavior

Figure 2.21 shows the swelling behavior of the treated samples and how the treatment affects the swelling percentage and swelling pressure of the soil. At optimum conditions (OMC, MDUW), the swelling percentage decreased from 2.59% to 1.73% due to creation of steady aggregations and the subsequent decrease in specific surface area of the clay particles. The soil PI decreased implying a decrease in clay wettability which led to a decrease in swelling percentage.

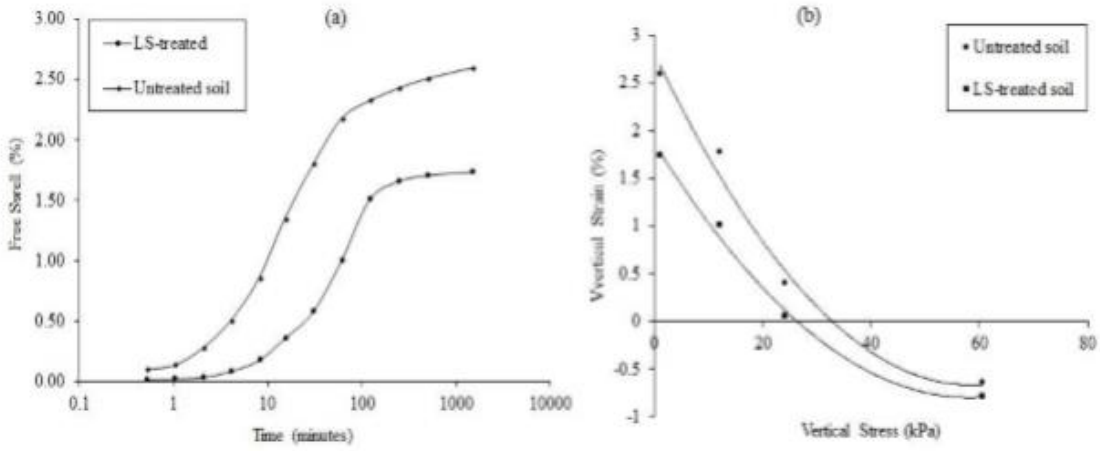

Figure 2.21. Effect of LS-treatment on: a) swell percent and, b) swell pressure of the expansive clay (Noorzard & Ta'negonbadi, 2018)

CHAPTER THREE

CHARACTERIZATION OF BIO-SILICA GEL USED IN THE TREATMENT OF EXPANSIVE CLAYS

3.1 Introduction

When some clays absorb water, they swell and on drying, they shrink, causing deep cracks. Expansive clays cause greater financial loss to property owners than all the other natural disasters combined: **13 billion dollars** of damage annually (Pupalla & Cerato, 2009). Cost of repairs can sometimes exceed the value of property. Swelling soils have been treated historically with lime. Although lime has proven to reduce volume change of problematic soils and increase the strength of these materials, this traditional treatment has **disadvantages** that include carbonation, sulfate attack on concrete and environmental impact (Jawad et al., 2014).

The main goal of this chapter is to study a polymer gel from sodium silicate, which combined with the clay, may improve his volume change properties via ion exchange and blockage of water intake. The polymer gel, elaborated from rice husk extracted silica, is an environmentally friendly solution. It not only allows the recycling of rice husk, which is a waste material, but also its application to the soils leaves no harmful by-products behind. To accomplish the overall goal of this paper, three major studies were pursued: a) the assessment of the chemical differences between ash and silica gels manufactured from rice husk obtained from California (USA) and from India; b) the study of the volume change behavior of stabilized expansive clay materials; and c) the assessment of the behavior of stabilized expansive clay subjected to wetting and drying cycles. This document presents details of the extraction of silica gel from ash,

including the burning process, the silica gelification process and observations made in the laboratory from characterization of ashes obtained from two locations: California rice husk burned at Arizona State University (ASU) laboratory (called ASU ash from here on) and Indian ash. The results from XRF and Fourier Transform Infra-red Spectroscopy (FTIR) analyses are presented. The soil treatment and volume change studies are presented elsewhere.

3.2 Literature Background of Silica Gel Production

This section presents the literature findings on procedures previously used for silica gel production. These procedures provided a framework to find the optimal conditions needed to produce amorphous silica from rice husk combustion in our laboratory.

3.2.1 Rice Husk Production

Rice husk is the outermost layer of the rice grains casing and it is the most abundant waste material from the rice industry (de Luca, 2017). The annual production of paddy rice was approximately 400 million metric tons in 2001 (Yalcin and Sevinc, 2001) while the production propelled to 740 million metric tons in 2015 (Rivas et al. 2015). In 1972, Houston estimated the rice husk content in paddy rice to be 20% in average. Rice husk is composed of organic and inorganic matter. The organic matter is composed of cellulose, lignin, protein and vitamins, while the inorganic matter is mainly amorphous silica.

3.2.2 Silica Ash Production

On burning, the silica content of the produced ash may reach over 95% by weight (D.D.Bui, 2001). According to Lanning (1963) and Ibrahim (1980), the silicon present in

rice husk is found to be dispersed in the organic material of the husk at the molecular level. This silicon exists in a hydrated amorphous form of silica, probably biogenetic opal or silica gel. Rivas et al. (2016) reported that untreated RHA contained 87.4% of silica (SiO_2) by weight, with the rest of the material corresponding to metallic impurities such as potassium oxide (K_2O), phosphorus pentoxide (P_2O_5) and calcium oxide, among others. Rivas then treated the rice husk by washing it with one molar of hydrochloric acid solution (1M HCl) and then burned at a temperature of 650°C for 3 hours. The treated sample resulted in 96.9% silica (SiO_2) as a weight compound. X-ray diffraction was used to determine whether the silica content in the RHA was amorphous or crystallized.

Several studies were found related to the optimization of time and temperature factors for rice husk combustion. Of interest, Hamed and Khattab (1981) studied the effect of thermal decomposition of rice husk on the amorphous structure of silica ash in the laboratory. They observed that the ash containing amorphous silica formed at comparatively lower temperatures, between 500-600°C. The crystalline forms, cristobalite and trydimite, appeared at higher temperatures of around 800-1200°C. They also compared the state of rice husk ash prepared in a furnace with that of the ash produced in a fixed bed at different air rates. At lower air rates, amorphous silica was formed, whereas, at higher rates, silica crystallization occurred.

Metha (1978) found that amorphous silica can also be obtained at temperatures below 500°C for a prolonged burning period. Yeoh et al. (1979) found that silica ash can still be amorphous at combustion temperatures up to 900°C, if the combustion time is less than 1 hour, and crystalline silica is obtained at temperatures of 1000°C or higher within 5 minutes or higher. Chopra et al. (1981), using X-ray diffraction, observed that at

temperatures of up to 700°C, amorphous silica can still be obtained. Meanwhile, James and Rao (1986) found that regardless of the burning time, crystallization of silica did not occur at temperatures below 700°C.

In conclusion, several researchers confirmed that amorphous silica is obtained at temperatures under 700°C even if the combustion time is doubled or tripled.

3.2.3 Precipitation of Silica from Rice Husk Ash (RHA)

To obtain silica from rice husk ash, three different steps are necessary. Firstly, it is important to perform acid-washing of rice husks; then, the extraction of the silica from the ash followed by the precipitation of the silica (Kamath and Proctor, 1998). The amorphous nature of RHA silica makes it extractable at lower temperature, and hence, it provides a low energy method (Della et al., 2000).

3.2.3.1 Acid Washing

This step is essential to remove small quantities of mineral impurities from RH prior to silica extraction, especially to keep the K, Na, Mg, Ca content in silica at a lower concentration (de Luca, 2017).

3.2.3.2 Silica Extraction

The following reaction equation represents the extraction of sodium silicate solution (Na_2SiO_3) from the impure silicon dioxide (SiO_2).

$$SiO_2 + 2\text{NaOH} \rightarrow Na_2SiO_3 + H_2O \ldots\ldots\ldots\ldots (3.1)$$

In previous studies performed by de Luca (2017), the silica ash was dissolved in 1N sodium hydroxide (NaOH) with constant stirring to dissolve the silica and produce sodium silicate solution. After 1 hour, the solution was filtered through filter paper and

the carbon residues were washed with 100 ml of boiling water. The solution was allowed to cool to room temperature (de Luca, 2017).

3.2.3.3 Silica Precipitation

In this step, the aim is to precipitate silica gel from the sodium silicate solution. The following equation represents the chemical reaction:

$$Na_2SiO_3 + H_2O + 2HCl \rightarrow Si(OH)_4 + 2NaCl \ldots\ldots\ldots (3.2)$$

The solution is very alkaline (pH 12-13) and hence, hydrochloric acid is used to lower the pH and allow gelation to occur (de Luca, 2017; Sayed Mostafa, 2019). It is worth noting that silica gel forms at two different pH conditions: alkaline condition, at pH between 7 and 10; and acidic condition, at pH between 1.5 and 6 (de Luca, 2017, Sayed Mostafa, 2019). The alkaline silica gel was found to form rather quickly, with fluffy, glassy consistency, and very weak. Hence, it was not useful in improving the mechanical properties of the clay (de Luca, 2017. Sayed Mostafa, 2019). On the other hand, acidic silica gel has proved to be stronger as polymerization is attained at much slower rate (Sayed Mostafa, 2019).

3.3 Materials and Methodology to Produce Silica Gel

3.3.1 Procedure for Preparing a Sodium Silicate Solution from Rice Husk

The rice husks used in this study to produce the sodium silicate solution were obtained from two different sources. The first source was from California rice fields, used to produce a *white ash* at the ASU laboratories under controlled conditions; while the second source was a *black ash* obtained from India. The Indian ash was obtained by burning rice husks in uncontrolled temperature and time conditions. However, studies of the Indian ash are of interest because the ash burning in a furnace is a high energy

consumption procedure and takes a large amount of time. Both conditions are detrimental to the sustainability of the procedure and increase the carbon emissions footprint.

3.3.1.1 Washing Rice Husk with 1.5 M HCl Solution

The washing procedure was used on the ASU rice husks. Based on concurrent studies at ASU, the best way to wash away impurities from the rice husks is by using of 1.5M hydrochloric acid. Distilled water and 12M hydrochloric acid (HCl) were used to prepare 60ml of 1.5M HCl. The solution was placed on a heater and a magnetic stirrer added. 10 g of RH are immersed in the solution and left to heat at 60°C, stirring at 400 rpm for 20 minutes. The washed rice husks are dried overnight and then transferred to a muffle furnace at 700°C to be burnt. From laboratory experiments and trials of washing rice husks, 10g of RH produces about 3g of silica ash. And therefore, to reduce the workload, the procedure was adjusted to obtain reasonable amounts of ash by washing larger amounts of husks at the same proportions. The ash obtained was then used to extract the silica through dissolution. More details are presented in the next step. This step is essential to remove small quantities of mineral impurities from rice husks prior to silica extraction, especially to keep the K, Na, Mg, Ca content in silica at a lower concentration (de Luca, 2017).

Fig 3.1: Acid washed rice husks

a) Preparing a 1.5 M HCl solution

1.5M HCl is required to wash the rice husks. The lab is installed with an acid storage and hydrochloric acid is in abundance. However, the acid in storage is at large molarity of 12M in stock solution. To prepare 1.5M HCl solution, the molar calculation method was used, as presented in the following equation:

$$M_1 * V_1 = M_2 * V_2 \dots\dots\dots (3.3)$$

Where, M and V are molarity and volume, respectively. 500 ml of deionized (D.I) water are placed in a 1L beaker. 125ml of HCl are added to the beaker from a 12M HCl stock solution obtained from the acid storage. The volume of the solution is adjusted to 1000 ml by adding D.I water until the 1000 ml mark is reached. The beaker is covered with an aluminum foil or any beaker cover provided to avoid evaporation. It is then heated to 60℃ on a hot-plate and a magnetic stir is immersed with stirring adjusted to 200 rpm. The solution is left to heat and stir for 5 minutes to allow uniformity of the 1.5M HCl solution.

b) Washing and Air Drying the Rice Husk

After preparing the 1.5M HCl solution, 50 g of rice husks were immersed in the solution from part a) and stirring was immediately started. The revolution of the magnetic stir was adjusted to 400 rpm to increase chances of uniform mixing and thorough washing. The suspension was left to heat (at 60℃) and stir for 20 minutes. The RHA was then extracted using a filter paper and air dried for 24 hours or left to dry overnight in open space at ambient temperature. The mass of the dry husks was recorded. The procedure was repeated many times and large quantities of dry acid-washed rice husks were obtained.

3.3.1.2 Rice Husk Combustion and Grinding

As explained in the previous section, the rice husks were washed with 1.5M HCl to remove any mineral impurities that might affect the silica content. Then, the muffle furnace was checked for safety measurements and to make sure the switches were working properly, was turned on and set to the desired temperature. The furnace was left to stand for about 2 hours until the temperature reached and stabilized. Washed rice husks were placed in small bowls and a spatula used to place them in the muffle furnace. The furnace was then quickly closed and left to burn the husks for 2 hours. After 1 hour, the ash in the bowls were stirred to allow air to reach the bottom contents and the furnace closed again. After 2 hours, the contents were checked for any unburnt or black ash remaining and if small quantities of black ash existed at the bottom or anywhere, the contents were stirred and left to burn for another hour. At the third hour mark, the contents were removed and allowed to cool at room temperature.

a) **ASU ash** **b) Indian ash**

Fig 3.2: Silica ash

The masses of the silica ash were recorded and finally, the ash was ground in a mortar to obtain fine powder. About 20-30 g of rice husks were placed in each small dish and about 100g in the big dish. The muffle was then opened, and the dishes were quickly and

carefully placed inside. At the same time, the muffle furnace was immediately closed after placing the dishes to avoid disrupting the temperature inside the furnace. It is noted that opening and closing the furnace lowers the temperature reading greatly since cold air flows in. It is therefore important to note that opening and closing the furnace needs to be done with extreme precaution.

To optimize the combustion procedure, the washed and dried rice husks were combusted at different temperatures and different burning times. Four temperatures were used: 500°C, 600°C, 700°C and 800°C, and four burning times: 1, 2, 3 and 4 hours. As shown in Table 3.1 it was found that regardless of combustion time, temperatures below 600°C resulted in black ash, which indicated that complete combustion could not occurred at these temperatures. At 600°C, it took more than 4 hours to obtain complete combustion unless very small amounts were burnt in the furnace. At 700°C, it took between 2 and 3 hours to obtain white ash. Finally, at 800°C, ash turned brown, which might be due to the crystallization of silica. From all the literature work reviewed, the temperature of combustion was between 500 and 800°C and the time between 1 and 3 hours. For this reason, this temperature range was chosen and to avoid prolonged wait times, a maximum time of 4 hours was used.

After several trials, it was found that at a temperature between 600°C and 700°C, the optimum time required to combust the husks thoroughly was 3 hours. It was concluded that the optimal conditions to have complete combustion and obtain pure white silica ash were 3 hours at a temperature of 650°C.

Table 3.1: Setting temperature and time for combustion

Trial	Temperature (^oC)	Time (hours)	Observations
1	500	1	Black ash (incomplete combustion)
2	500	2	Black ash (incomplete combustion)
3	500	3	Black ash (incomplete combustion)
4	500	4	Black ash (incomplete combustion)
5	600	1	Black ash (incomplete combustion)
6	600	2	Black ash (incomplete combustion)
7	600	3	Black ash (incomplete combustion)
8	600	4	Black ash (incomplete combustion)
9	700	1	Black ash (incomplete combustion)
10	700	2	Some black ash (incomplete combustion)
11	**700**	**3**	**White ash (complete combustion)**
12	**700**	**4**	**White ash (complete combustion)**
13	800	1	Brown ash (silica crystallization)
14	800	2	Brown ash (silica crystallization)
15	800	3	Brown ash (silica crystallization)
16	800	4	Brown ash (silica crystallization)

3.3.1.3 Silica Extraction from the Ash

a) Preparing a 1 N Sodium Hydroxide (NaOH) Solution

Sodium hydroxide pellets were obtained from the chemical storage and 2.4 g of the pellets weighed and placed in a 100ml empty clean beaker. 60 ml of D.I water were added to the 100 ml beaker. A magnetic stir was placed into the beaker and this was then covered and placed on a heater/stir balance. The stir option was switched on and initially adjusted to 200 rpm. The heater option is left off at this step. The stirring is left to run for 5-10 minutes until the pellets are completely dissolved.

Fig 3.3: Heaters

b) Dissolution of Ash into NaOH Solution

The heater was switched on and adjusted to 80°C and the solution left to heat for 30 minutes. A known mass of silica ash is added to the solution and stirred at 400 rpm for 1-2 hours. It was found that very large amounts of residue were left after several trials with differing masses of ash and time of heating. After measuring the masses added and the corresponding masses of the residue, it was found that 3.96 g of ash would give the best percent dissolution of silica in 100 ml of sodium hydroxide solution when heating was done for 2 hours.

However, precipitation of silica gel requires large quantities of the silicate solution as gelation occurs at alkaline conditions abruptly. Therefore, the procedure was adjusted to prepare large amounts of silicate solution with corresponding percent dissolution equivalent to that of 3.96 g of ash. It was determined that for 500 ml of NaOH solution, add 33.33 g of silica ash and for 1000 ml of NaOH solution, 66.67 g of rice husk ash is added to the solution for dissolution.

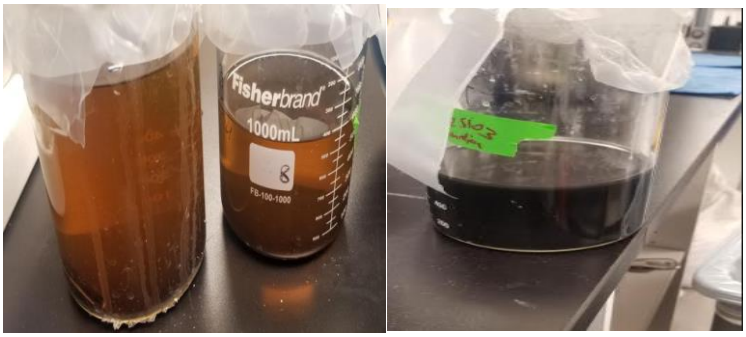

Fig 3.4: Sodium Silicate solution (SSS) a) ASU SSS (left) b) Indian SSS (right)

c) Centrifuging the Solution

The solution is placed in small cylinders of equal volume. The cylinders are then transferred to a centrifuge and balanced out in even numbers. If the number is not even, equal volume of D.I water is added to a cylinder and placed diagonally opposite to the other cylinder. The centrifuge is then closed and set for 10 minutes run at 1500 rpm. The residue settles to the bottom of the cylinder and the sodium silicate is decanted off after centrifuging. The pure sodium silicate solution is placed in its own cylinder and stored for use in the next step. The mass of the residue obtained was recorded. The mass of the dissolved silica was also determined.

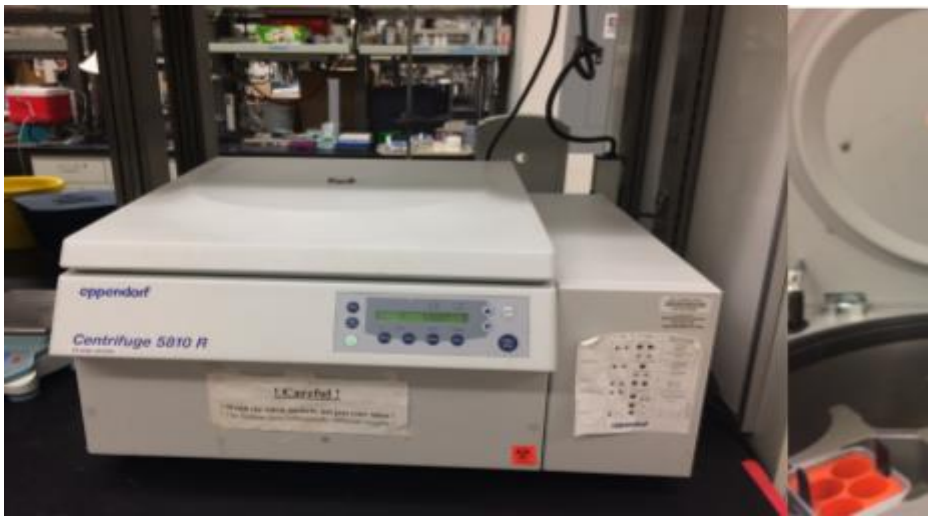

Fig 3.5: Centrifuge

Fig 3.6: SSS after centrifuging a) ASU b) India

d) Precipitation of Silicic Acid

A pH probe calibration method was used to precipitate the silicic acid. Three buffer solutions at pH 4, 7 and 10 are used to calibrate a pH probe. The probe was then placed in D.I water to check pH of D.I water to be used. The pH of the probe storage solution is also checked. The sodium silicate solution was placed in a small beaker. 1M HCl solution was prepared and placed in another small beaker. An empty beaker is obtained, and a small amount of the silicate solution added. The probe was immersed in the silicate solution and the pH of the solution read and recorded. It was usually an

average pH of 12.8. Small amounts of 1M HCl are added quickly to lower the pH of the silicate solution. It is safe to take precaution when adding acid because precipitation of the gel occurs quickly around pH 8-10. These results agree with tests carried out by Sayed Mostafa (2019).

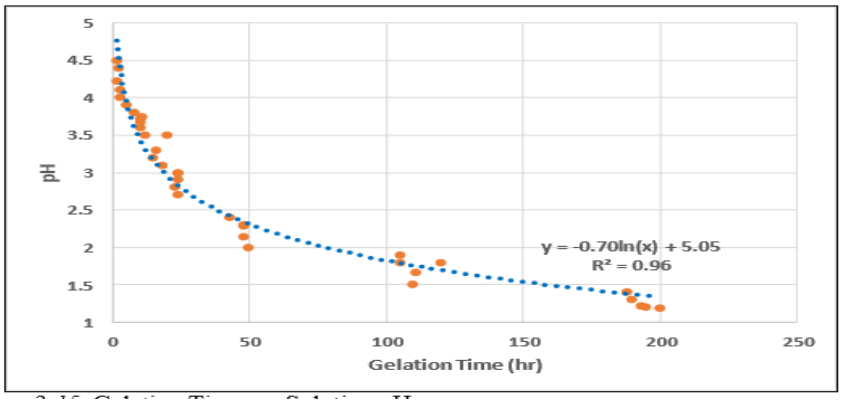

Fig 3.7: pH vs Gelation (Sayed Mostafa, 2019)

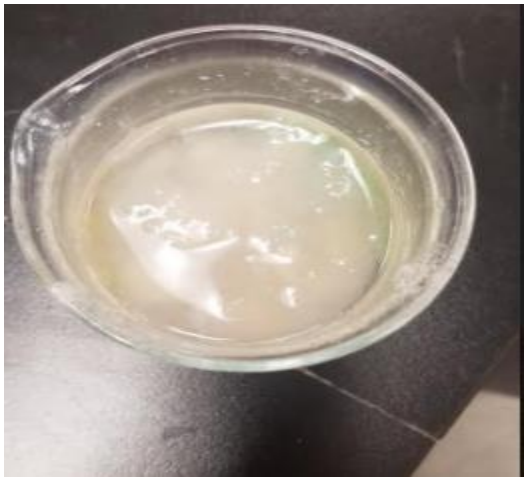

Fig 3.8: Silica gel

Therefore, the amounts of HCl added cannot be drops, it is rather larger amounts of acid compared to the initial amount of the silicate in the beaker being used. The acid is added quickly to skip precipitation at alkaline conditions. The acid added must lower the pH reading quickly to below 1 or even to negative values. Then a small amount of the

silicate is added to increase the pH of the solution. Around pH 1.5, very small amount or just drops of the silicate solution are added to the mixture solution until the pH is 4. The equation for the reaction of precipitation is equation 3.2

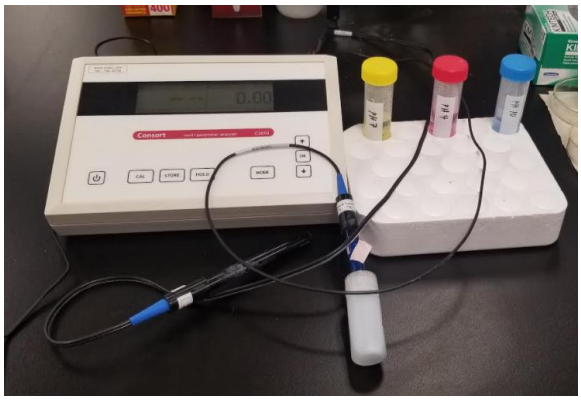

Fig 3.9: pH probe and beakers

3.4 Characterization of Different Ashes Used in the Production of Sodium Silicate

In this section, the comparison between silica ash from California and India is presented. X-ray fluorescence (XRF) procedure was used to determine the silica content from both sources. Subsequently, the chemical composition of both ashes was compared via Fourier Transform Infra-red Spectroscopy (FTIR).

3.4.1 X-ray fluorescence (XRF) of ash to determine silica content

XRF were performed on the ash obtained from India and California. The objective of the XRF testing was to determine the silica content of the ash and identify the significant impurities in the ash. The following results were obtained from the XRF testing.

3.4.1.1 Elemental composition

The results of XRF for the minerals present are presented in figures 3.3 and 3.4 below.

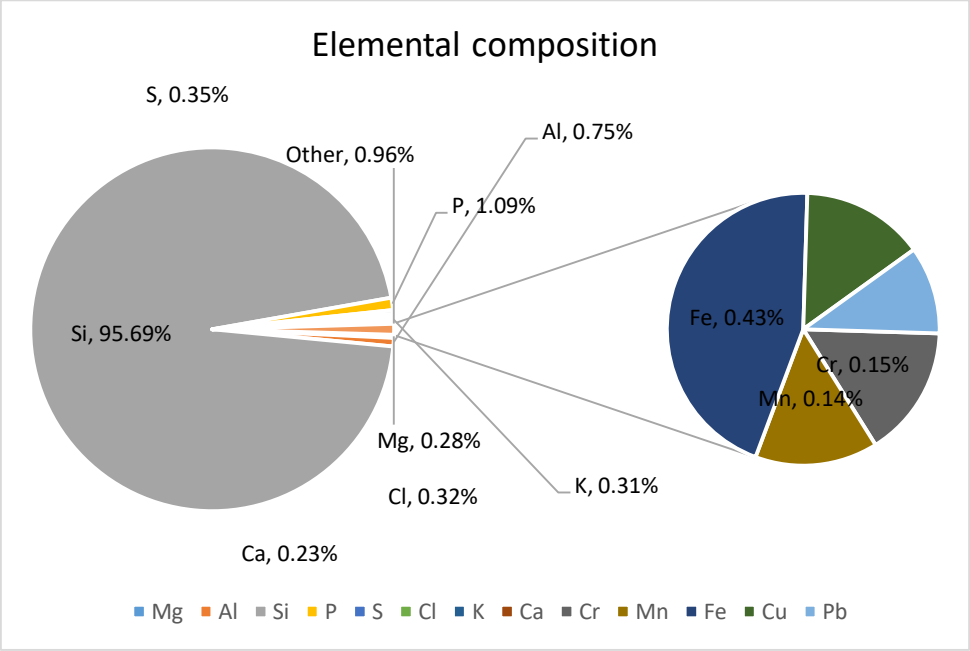

Fig 3.10: ASU ash elemental composition

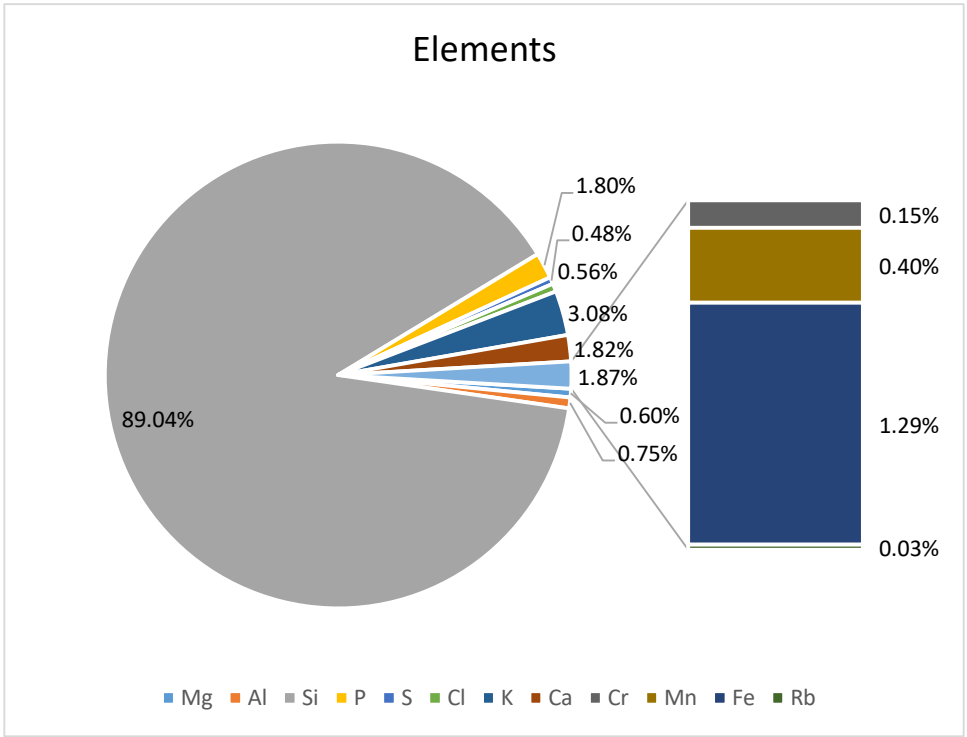

Fig 3.11: India ash elements

The ash produced in the ASU lab contained 96% silicon and other minerals that included phosphorous, magnesium, chlorine, calcium, potassium, and others in small quantities, as shown. The India ash contained just 89% silicon compared to 96% silicon of ASU ash.

3.4.1.2 Ash oxides composition

Figures 3.5 and 3.6 show the chemical composition of the ashes by oxides.

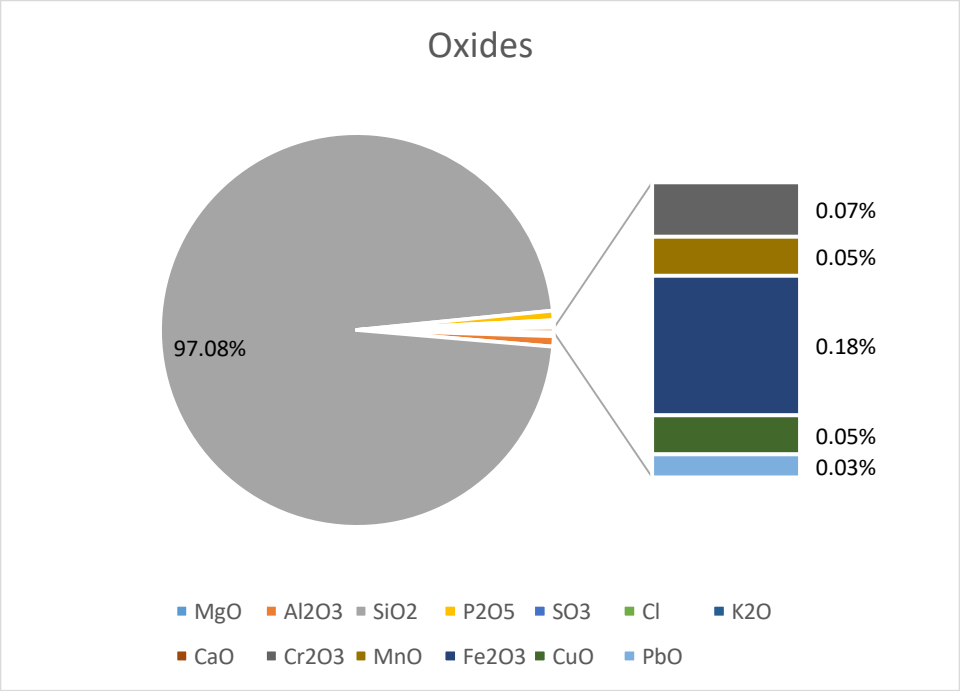

Fig 3.12: ASU ash oxides

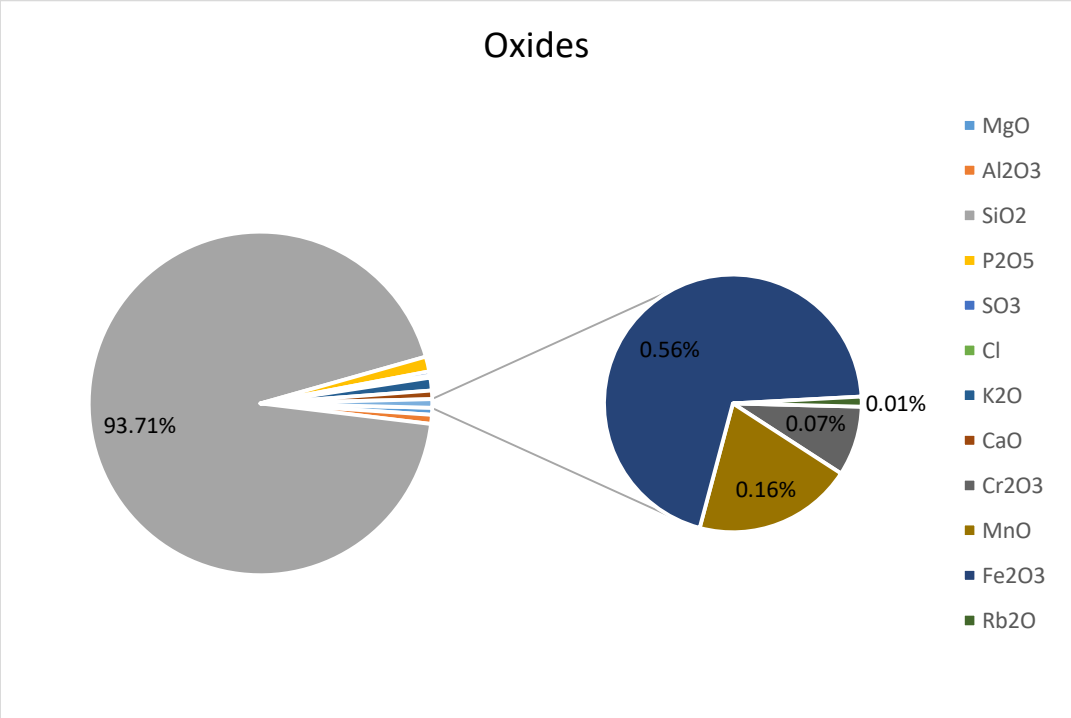

Fig 3.13: India ash oxides

3.4.1.3: Discussion and Conclusions

The ASU ash is by composition 97.1% silica and 3% impurities. The India ash contains 93.7% silica which is very high in comparison to the impurities. Based on the results presented, the ASU ash contains 7% more silicon than the Indian ash and consequently contains almost 3.5% more silica than the Indian ash. These results reflect the effect of the acid washing procedure used on the ASU ash. The acid washing removed some impurities in the rice husks. The Indian ash was obtained from open field combustion which is assumed to generate temperatures above 800°C, at which temperatures, crystallized silica forms, specifically cristobalite. Crystallized silica is insoluble in hydroxide solution. This explains why the India ash left more residue compared to the ASU ash after dissolution.

Table 3.2: ASU Ash Elemental Composition

Elements					
Z	Formula	Concentration	Evaluation Mode	Quantified by	Range Name
12	Mg	0.28%	Stdless	Auto	20 kV, Range 3
13	Al	0.75%	Stdless	Auto	20 kV, Range 3
14	Si	95.69%	Stdless	Auto	20 kV, Range 3
15	P	1.09%	Stdless	Auto	20 kV, Range 3
16	S	0.35%	Stdless	Auto	20 kV, Range 3
17	Cl	0.32%	Stdless	Auto	20 kV, Range 3
19	K	0.31%	Stdless	Auto	20 kV, Range 3
20	Ca	0.23%	Stdless	Auto	20 kV, Range 3
24	Cr	0.15%	Stdless	Auto	20 kV, Range 3
25	Mn	0.14%	Stdless	Auto	20 kV, Range 3
26	Fe	0.43%	Stdless	Auto	20 kV, Range 3
29	Cu	0.14%	Stdless	Auto	20 kV, Range 3
82	Pb	0.10%	Stdless	Auto	40 kV, Range 2

Table 3.3: ASU Composition by Oxides

Oxides					
Z	Formula	Concentration	Evaluation Mode	Quantified by	Range Name
12	MgO	0.31%	Stdless	Auto	20 kV, Range 3
13	Al2O3	0.85%	Stdless	Auto	20 kV, Range 3

14	SiO2	97.08%	Stdless	Auto	20 kV, Range 3
15	P2O5	0.78%	Stdless	Auto	20 kV, Range 3
16	SO3	0.29%	Stdless	Auto	20 kV, Range 3
17	Cl	0.10%	Stdless	Auto	20 kV, Range 3
19	K2O	0.11%	Stdless	Auto	20 kV, Range 3
20	CaO	0.10%	Stdless	Auto	20 kV, Range 3
24	Cr2O3	0.07%	Stdless	Auto	20 kV, Range 3
25	MnO	0.05%	Stdless	Auto	20 kV, Range 3
26	Fe2O3	0.18%	Stdless	Auto	20 kV, Range 3
29	CuO	0.05%	Stdless	Auto	20 kV, Range 3
82	PbO	0.03%	Stdless	Auto	40 kV, Range 2

Table 3.4: Indian Ash Elemental Composition

Elements					
Z	Formula	Concentration	Evaluation Mode	Quantified by	Range Name
12	Mg	0.60%	Stdless	Auto	20 kV, Range 3
13	Al	0.75%	Stdless	Auto	20 kV, Range 3
14	Si	89.04%	Stdless	Auto	20 kV, Range 3
15	P	1.80%	Stdless	Auto	20 kV, Range 3
16	S	0.48%	Stdless	Auto	20 kV, Range 3
17	Cl	0.56%	Stdless	Auto	20 kV, Range 3
19	K	3.08%	Stdless	Auto	20 kV, Range 3

20	Ca	1.82%	Stdless	Auto	20 kV, Range 3
24	Cr	0.15%	Stdless	Auto	20 kV, Range 3
25	Mn	0.40%	Stdless	Auto	20 kV, Range 3
26	Fe	1.29%	Stdless	Auto	20 kV, Range 3
37	Rb	0.03%	Stdless	K	40 kV, Range 2

Table 3.5: Indian Ash Oxide Composition

Oxides					
Z	Formula	Concentration	Evaluation Mode	Quantified by	Range Name
12	MgO	0.66%	Stdless	Auto	20 kV, Range 3
13	Al2O3	0.85%	Stdless	Auto	20 kV, Range 3
14	SiO2	93.71%	Stdless	Auto	20 kV, Range 3
15	P2O5	1.40%	Stdless	Auto	20 kV, Range 3
16	SO3	0.40%	Stdless	Auto	20 kV, Range 3
17	Cl	0.19%	Stdless	Auto	20 kV, Range 3
19	K2O	1.20%	Stdless	Auto	20 kV, Range 3
20	CaO	0.80%	Stdless	Auto	20 kV, Range 3
24	Cr2O3	0.07%	Stdless	Auto	20 kV, Range 3
25	MnO	0.16%	Stdless	Auto	20 kV, Range 3
26	Fe2O3	0.56%	Stdless	Auto	20 kV, Range 3
37	Rb2O	0.01%	Stdless	K	40 kV, Range 2

3.4.2 Fourier Transform Infra-red Spectroscopy (FTIR) of Sodium Silicate and Silica Gel

This test was performed to identify the chemical nature of the gel formed and make assumptions on how it could affect the structure of the clay materials. In order to verify the presence of the various types of sodium silicate compounds from plant-based ashes, FT-IR spectroscopy was performed on the sodium silicate, gel formed and treated samples from the two different ash sources.

3.4.2.1 Background

FTIR is a technique used to obtain an infra-red spectrum of absorption or transmission of a substance. A spectrophotometer collects high resolution data over a wide range of wavelength. FTIR is used to identify compounds by determination of their functional groups. Sodium silicate is a generic name for compounds with the chemical formula, $(Na_2O)_x.(SiO_2)_y$. This compound is sometimes referred to as water glass. Sodium silica is used in the production of silica gel on a commercial scale. When silica reacts with sodium hydroxide, the reaction is:

$$2xNaOH + ySiO_2 \rightarrow (Na_2O)_x.(SiO_2)_y + xH_2O \ldots\ldots\ldots\ldots\ldots (3.4)$$

If the value of x is equal to 1 and the value of y is equal to 1, then the compound formed is called sodium metasilicate. In metasilicate formation, the sodium hydroxide and silicon dioxide react in a ratio of 2:1. If the value is different, the compound will be different kind of sodium silicate as elaborated in the following paragraph.

The common method of production is fusion of silicon dioxide with silica.

$$xNa_2O + ySiO_2 \rightarrow (Na_2O)_x.(SiO_2)_y \ldots\ldots\ldots (3.5)$$

The value of x and y determine which kind of sodium silicate we have. If x =1 and y=1, sodium metasilicate is formed. If x=2 and y=1, sodium orthosilicate is formed. If x=3 and y=2, sodium pyrosilicate is formed. However, in the lab we used sodium hydroxide to produce sodium silicate. Therefore, we must find how many moles of Na_2O the solution of NaOH produces and relate them to the moles of SiO_2 that reacted (ash that dissolved) to determine the amount of ash to be dissolved. The chemical equation for reaction of NaOH with Silica is presented in equation 3.6:

$$2xNaOH + ySiO_2 \rightarrow (Na_2O)_x.(SiO_2)_y + xH_2O \ldots\ldots\ldots (3.6)$$

3.4.2.2 Procedure for FTIR

The FT-IR spectroscopy is done in 3 steps.

- ✓ Purging nitrogen/air
- ✓ Installing the smart orbit
- ✓ Opening the OMNIC software and running background and then run the sample

Once the experiment is done, the system is shut down in reverse order.

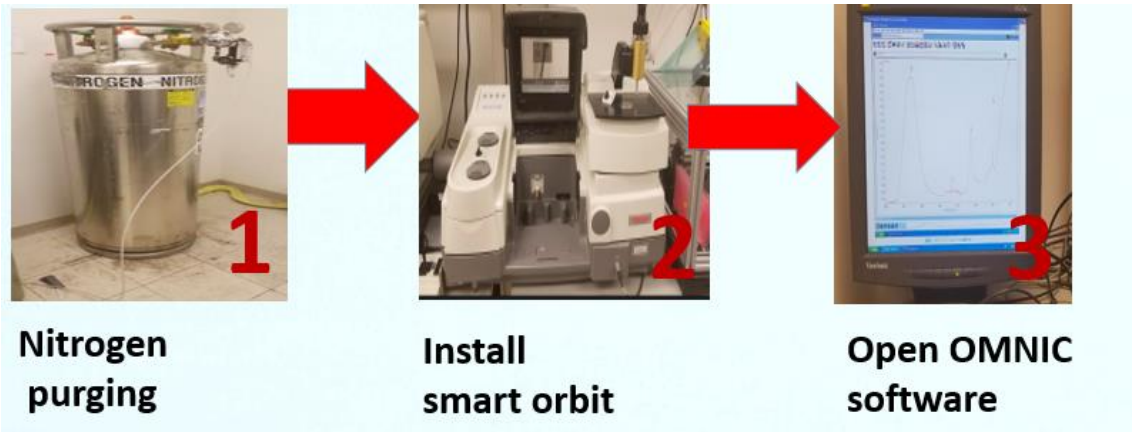

Fig 3.14: FTIR apparatus

Figures 3.15 through 3.17 show the FTIR spectra of the samples and that of commercial SSS used as a control.

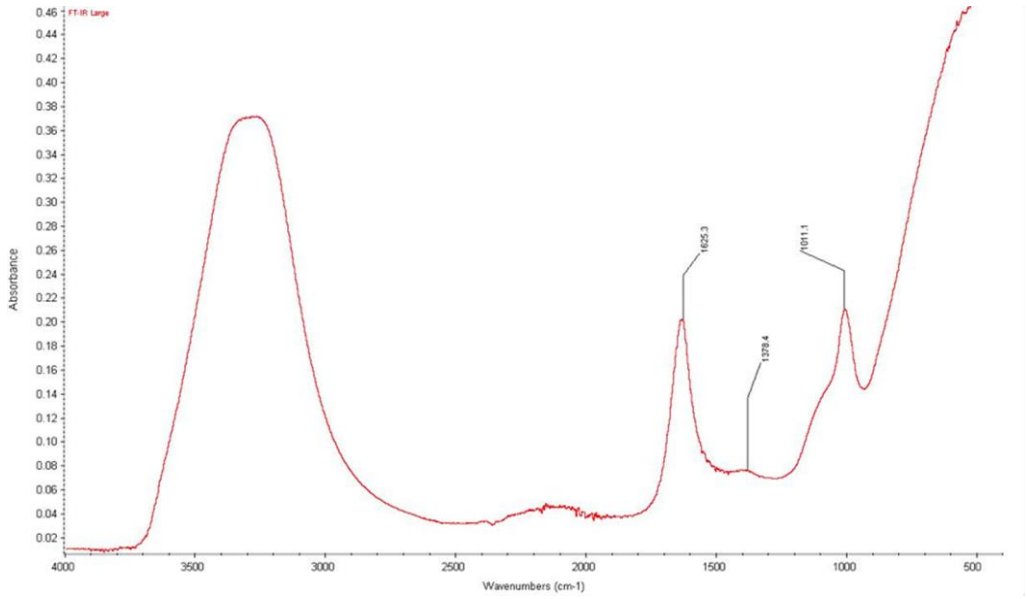

Fig 3.15: FTIR of ASU sodium silicate/gel

Figure 3.15 shows FTIR spectrum of ASU SSS. The unlabeled broad band at 3300 cm^{-1} usually represents OH presence. It is explained in the discussion.

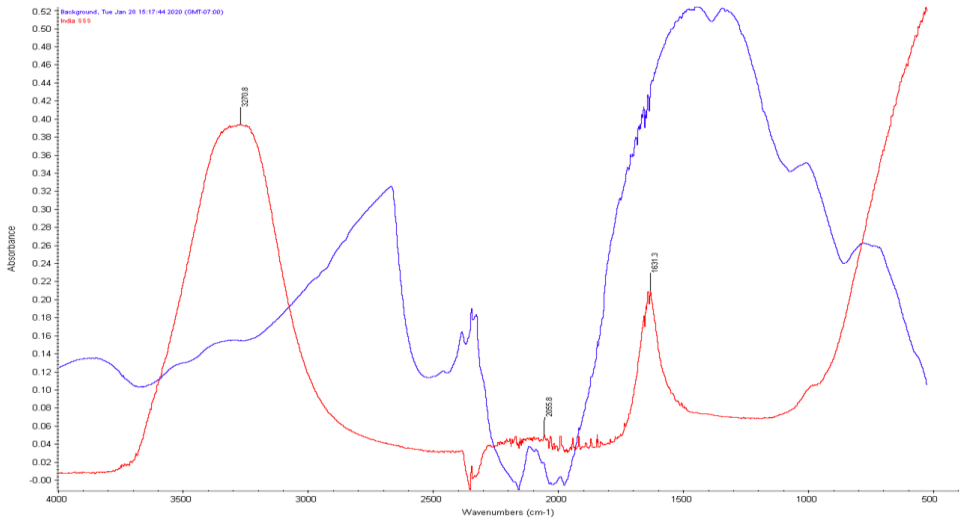

Fig 3.16: FTIR of India Sodium silicate solution/gel

The figure above shows the FTIR of India SSS. The blue spectrum is for the background and the red spectrum is for the Indian SSS. The background is ran each time a sample is to be analyzed through FTIR.

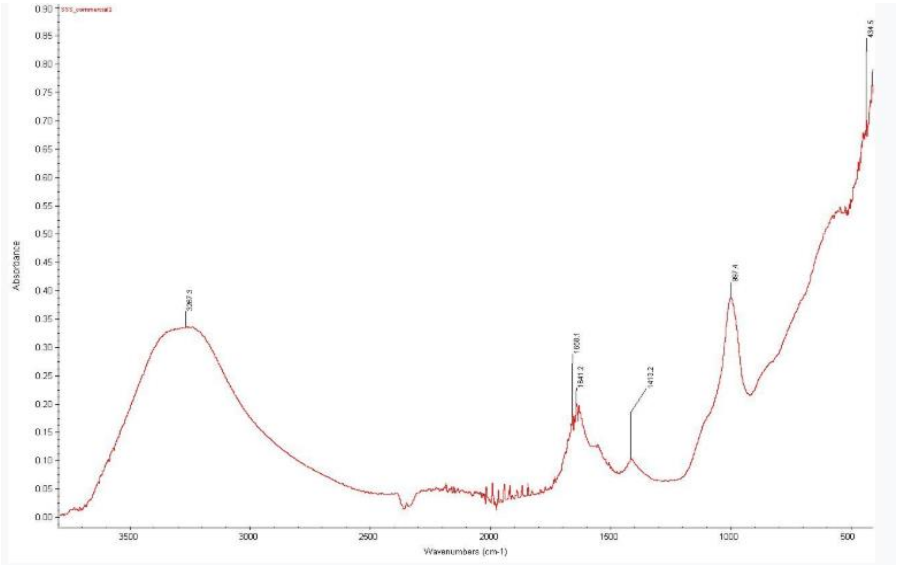

Fig 3.17: FTIR of Commercial sodium silicate solution

Figure 3.17 shows FTIR of SSS from commercial sodium hydroxide pellets. A commercial solution of sodium silicate was made to act as a control experiment for the FTIR analysis to help in making deductions.

3.4.2.3 Discussion of the results

The bands with maxima at 1008 – 1138 cm^{-1} confirm the **presence of silica structure bound** by O – Si – O. A **film of water** was created on the surface (surface felt greasy). This is indicated by the strong band in the spectrum with a maximum at 3260 cm^{-1} and the band with a peak at 1640 cm^{-1}.The band with a maximum at 1032 cm^{-1} is difficult to unambiguously identify, since it could be due to both stretching vibrations of the atoms in the Si – O bond in $Na_2O.2SiO_2$ or asymmetric vibrations of the Si – O bond in silicates from $2Na_2O.SiO_2$ to $3Na_2O.SiO_2$. The unclear peak around 850 cm^{-1}

represents the Si-OH functional group that appears due to formation of silicic acid which is responsible for gelling. The values of the peaks are presented in table 3.5 below.

Table 3.5: Functional groups of sodium silicate obtained from FTIR spectroscopy

Wavenumber (cm^{-1})	Functional Group	Literature range (cm^{-1})	Reference
3260	-OH(hydroxyl group)	3200-3500	(Noorzard & Ta'negonbadi, 2018)
1019	O-Si-O(silica presence)	1008-1138	(Noorzard & Ta'negonbadi, 2018)
1630	Si-O (vibrations)	1008-1138	(Noorzard & Ta'negonbadi, 2018)
850	Si-OH (silicic acid)	810-900	(Noorzard & Ta'negonbadi, 2018)

3.4.2.3 Conclusions

The ASU and India sodium silicate solutions give identical spectra and hence it is safe to conclude that the two ashes produce the same compound when dissolved in sodium hydroxide. These spectra are also identical to the spectrum of commercial sodium silicate solution produced from sodium silicate pellets and hence it is already known that commercial sodium silicate has the molecular formula of sodium metasilicate. Therefore, it is concluded that the compound produced from the ash is sodium metasilicate or sodium silicate.

CHAPTER FOUR

STABILIZATION OF EXPANSIVE SOILS USING THE SILICA GEL

4.1 Introduction

This section presents details of the technique used for stabilization and improvement of the volume change properties of expansive clay materials using silica gel. The rice husks used in this study to produce the sodium silicate solution were obtained from two different sources. The first source was obtained from California rice fields. On burning at the ASU laboratories under controlled conditions, these husks produced a *white ash*; while the second source was a *black ash* obtained from India. The Indian ash was obtained by burning rice husks in uncontrolled fire pit and under unknown time conditions. Studies of the Indian ash are of interest because the ash burning in a furnace is a high energy consumption procedure and takes a large amount of time. Both conditions are detrimental to the sustainability of the procedure and increase the carbon emissions footprint.

4.2 Background on Stabilization

Chemical or permeation grouting is the most common way of introducing chemicals into the soil. Silica is mostly introduced via colloidal silica grouting. Grouting is the injection of specially formulated cement of stable suspension into subsurface rock. Low viscosity non-particulate chemical is injected into pores of a granular soil to create a "cement" (Karol, 2003). In the past, colloidal silica has been investigated and more recently adopted as a low viscosity grouting (Pedrotti et al. 2017). The potential of colloidal silica as a favorable grouting material exists due to: its initial low viscosity; its low hydraulic conductivity after gelling; the very low injection pressures required; its

controllable set/gel times; the fact it is environmental friendly; its small particle size and its cost-effectiveness (Pedrotti et al. 2017). Despite the success of colloidal silica in soil improvement, little to no research has led to use in the industry and the reason for this is that there is no predictive model for grout gelling which controls grout penetration (Pedrotti et al. 2017).

4.3 Materials and Methodology to Stabilize Expansive Soils

4.3.1 Soil Used in the Study and Characterization Methods Performed

The soil used for this study was a low to intermediate expansive material found in Anthem, Arizona. In order to increase plasticity and expansivity, the Anthem clay was mixed with bentonite clay in a ratio of 7:3. Bentonite consists mainly of smectite minerals predominantly montmorillonite. The natural clay also contains other minerals such as quartz, feldspar, mica and illite. The following preliminary tests were performed on the untreated and treated samples for classification and characterization.

- ✓ Wet sieve analysis and hydrometer analysis for grain size distribution
- ✓ Atterberg limits for liquid limit, plastic limit and plastic index of the soil
- ✓ Standard proctor compaction test

4.3.1.1 Wet Sieve Analysis

The wet sieve analysis was carried out based on the standards ASTM C92-95, ASTM C136 and ASTM D2216-10 standard test methods for sieve analysis and determination of water content. The soil sample was placed in a container and water added allowed to settle. After 1 hour, more could be added if necessary. The test sample was then transferred to a No. 200 sieve and is washed with water until the water passing contains only traces of the soil. The residue was put in an oven at 105 ℃ and dried

overnight for 24 hours. The procedure was repeated for various other sieves and the percent passing and retained determined as shown in the table below 4.1. The sieves were arranged in descending order and the test sample introduced to the top No. 4 sieve. Residues on each sieve were collected and dried in an oven and the dry mass recorded. The percentage of the soil retained and the soil passing each sieve were calculated as shown in the table 4.1 below.

Table 4.1: Wet sieve analysis for percent finer

Sieve #	Diameter (mm)	Retained (g)	% Retained	Cumulative Retained %	% Passing
4	4.75	0.1	0.17	0.17	99.83
10	2.00	1.51	2.52	2.68	97.32
30	0.85	3.83	6.38	9.07	90.93
60	0.43	4.28	7.13	16.20	83.80
100	0.25	2.95	4.92	21.12	78.88
200	0.075	4.12	6.87	27.98	72.02
pan		43.21	72.02	100.00	0.00

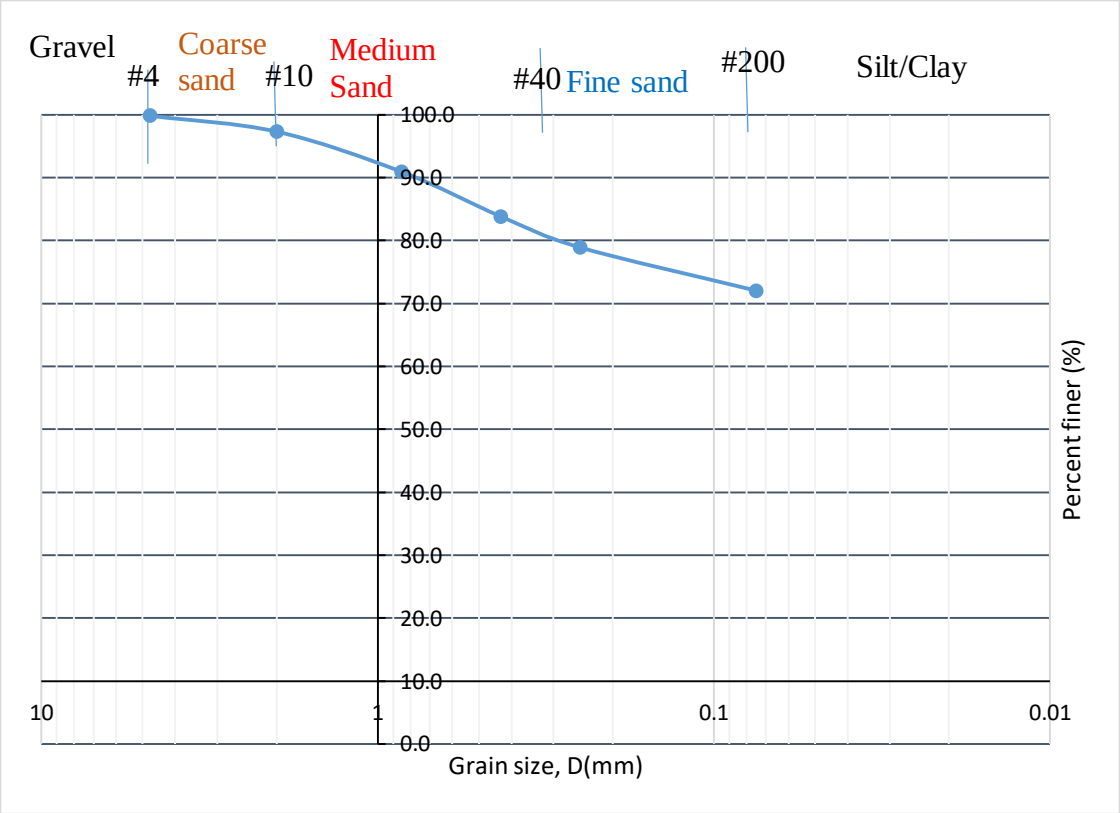

Fig 4.1: Wet sieve analysis

4.3.1.2 Hydrometer Analysis

This analysis was used to determine the particle size distribution for particles finer than sieve No. 200 (0.075 mm) but larger than 0.001 mm. The standard used for reference was ASTM D7928-17. The assumption is that the soil particles behave like spheres when immersed in water and therefore Stoke's law applied to calculate the velocity (de Luca, 2017).

$$v = \frac{\gamma_s - \gamma_w}{18\eta} D^2 \ldots\ldots\ldots\ldots\ldots\ldots\ldots\ldots (4.1)$$

Where, $v = velocity\ of\ a\ soil\ particle, \frac{cm}{s}$

$$\gamma_s = specific\ weight\ of\ soil\ solids, \frac{g}{cm^3}$$

$$\gamma_w = unit\ weight\ of\ water, \frac{g}{cm^3}$$

$$\eta = viscosity\ of\ water, \frac{g.s}{cm^2}$$

$$D = diamter\ of\ soil\ particle, mm$$

A hydrometer is suspended in water and the effective depth, L, is measured from the readings. The hydrometer measures the specific gravity of the suspension at the depth, l. At any given time, the particles that settled have a diameter, D, expressed as (A is a function of specific gravity of soil and temperature of the water);

$$D\ (mm) = A\sqrt{\frac{l\ (cm)}{t\ (min)}} \ldots\ldots\ldots\ldots\ldots\ldots\ldots\ldots\ldots\ldots (4.2)$$

The effective depth at different times is calculated as shown in the table 4.2 below. The following corrections to the hydrometer reading were applied; F_z the zero correction (the deflocculating agent added might change the zero reading of the suspension), F_m, the meniscus correction (usually the upper level of the meniscus is taken for readings), F_T, the temperature correction if the room temperature varies but this is usually ignored as was in this case. 60 g of oven dry soil was used in this test.

Table 4.2: Hydrometer analysis results

Time (mins)	Reading	L1	Effective depth, L (cm)	Composite correction	Corrected reading, Rcp	Percent finer (%)	diameter (mm)
0.25	21.5	7.6	11.607	21.60	19.10	40.15	0.0879
0.5	21.5	7.6	11.607	21.60	19.10	40.15	0.0622
1	21.5	7.6	11.607	21.60	19.10	40.15	0.0439
2	21	7.6	11.675	21.10	18.60	39.10	0.0312
4	21	7.6	11.675	21.10	18.60	39.10	0.0220
8	20.5	7.7	11.743	20.60	18.10	38.04	0.0156
15	20	7.8	11.812	20.10	17.60	36.99	0.0114
30	19.5	7.8	11.88	19.60	17.10	35.94	0.0081
60	19	7.9	11.948	19.10	16.60	34.89	0.0058
120	18.5	8	12.017	18.60	16.10	33.84	0.0041
240	17.5	8.1	12.153	17.60	15.10	31.74	0.0029
480	17	8.2	12.222	17.10	14.60	30.69	0.0021
1440	16	8.3	12.358	16.10	13.60	28.59	0.0012
2880	15.5	8.4	12.427	15.60	13.10	27.54	0.0008

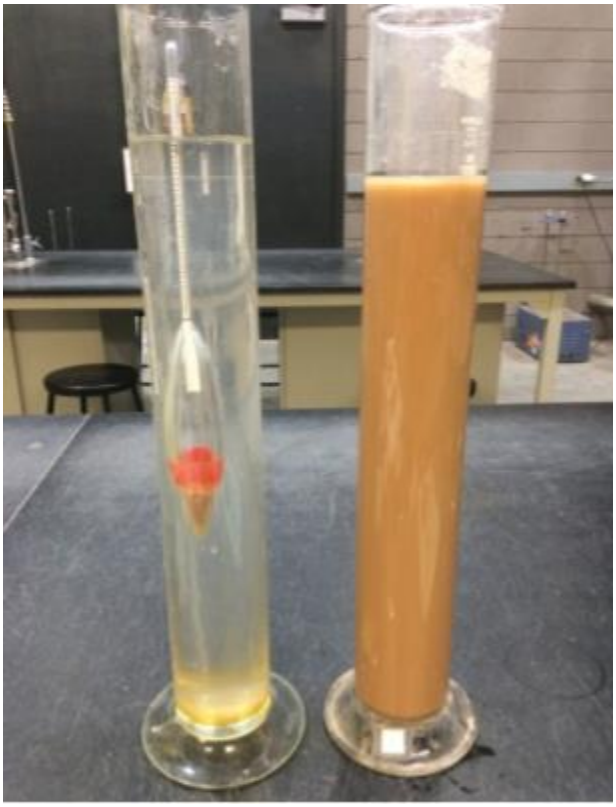

Fig 4.2: Hydrometer analysis experiment

The results of this analysis are shown in figure 4.3 below.

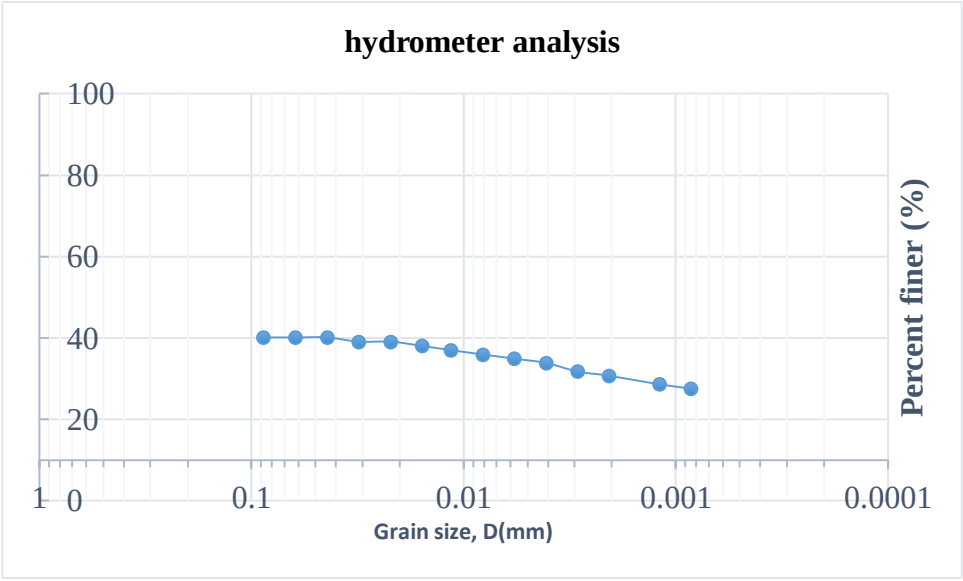

Fig 4.3: Hydrometer analysis results

Combining the two plots gives the grain size distribution curve shown in figure 4.4 below.

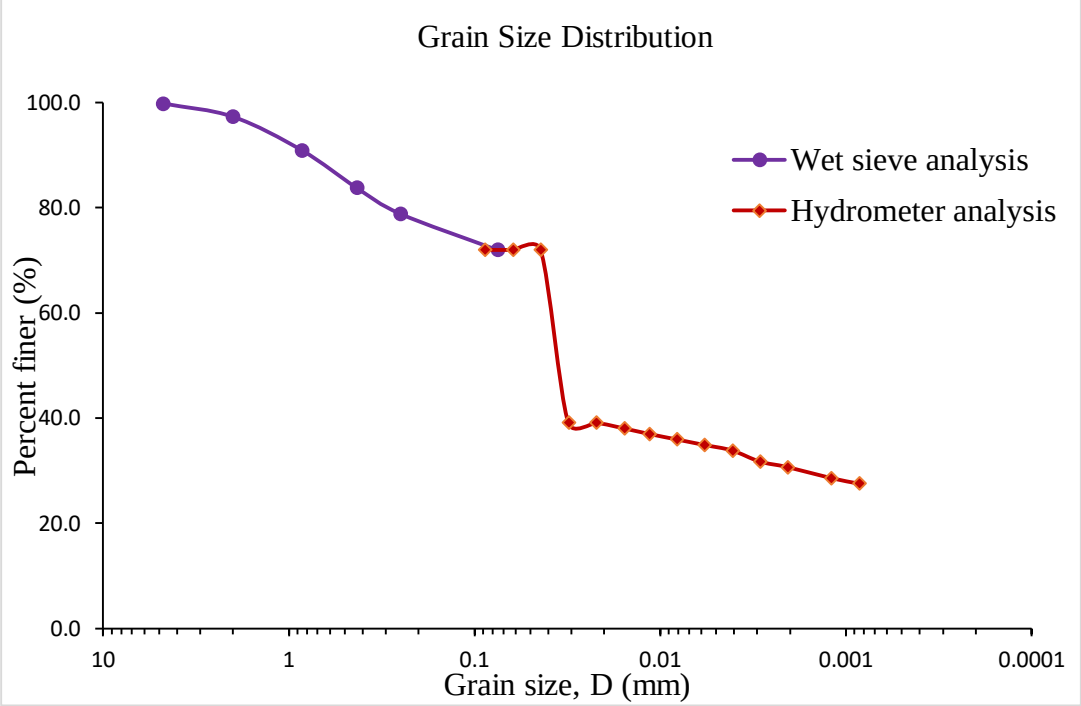

Fig 4.4: Grain size distribution curve

4.3.1.3 Atterberg Limits

Atterberg limits are liquid limit (SL), plastic limit (PL), shrinkage limit (SL) and plasticity index (PI). These tests are used to classify the mechanical properties of the soil. To do this, the critical water contents of a fine-grained soil need to be known. The liquid limit of the soil is the water content at which the soil passes from plastic state to liquid state. The plastic limit is the water content at which the soil changes from plastic to semi-solid state or vice versa. The Casagrande method was used to determine the liquid limit. The materials used in this test are brass cup, a spatula, groove, water bottle, mixing bowl, scale, and cans as shown in figure 4.4.

Fig 4.4: Casagrande apparatus

To perform the test, about 300g of soil is needed, after crushing it to remove any crumps. Add water to the sample until it is uniform. The Casagrande apparatus was calibrated by placing the grooving tool underneath the cup and rotating the apparatus till cup just touches the cup. A soil paste was added to the cup and the grooving tool used to make a groove. The handle was then rotated at 120 revolutions per minute and 2 cycles per second and the number of blows to close the 13mm gap in the groove counted and noted. The procedure was repeated 3 times and each time a soil sample was taken, and moisture content determined. A plot of water content vs logarithm of number of blows was produced and the liquid limit was calculated as the water content at 25 blows.

For the plastic limit, a glass plate to roll out 3mm soil sample, 3mm rod to gauge, spatula to spread and dry out the soil. The plastic limit is the average of the water content when the soil starts to crumble when it is rolled into a 3mm thread. About 20g of soil

were wetted and spread out onto the glass plate. The soil was then rolled into 3mm threads between the palms of the fingers. Once the soil crumbled at 3mm, samples of the threads were collected and used to determine the water content. The procedure was repeated several times and the average water content is taken as the plastic limit. The plastic index is the difference between the liquid limit and plastic limit (i.e., upper plastic limit and lower plastic limit)

$$PI = LL - PL \ldots\ldots\ldots\ldots (4.3)$$

The PI of the soil was determined to be 61.7%. This is a very high PI implying the soil is highly plastic.

4.3.1.4 Conclusion

The Atterberg limit values are summarized in tables 4.3 and 4.4 below.

Table 4.3: Liquid limit results

Weight of can	# of blows	Weight of wet soil + can	Weight of dry soil + can	Weight of wet soil	Weight of dry soil	Water content (%)
15.80	16.00	26.80	21.10	11.00	5.30	107.55
15.90	21.00	37.20	26.70	21.30	10.80	97.22
14.70	29.00	40.50	28.10	25.80	13.40	92.54
14.90	35.00	34.50	25.20	19.60	10.30	90.29
						LL=97%

The liquid limit of the used soil was found to be 97%

Table 4.4: Plastic limit results

Weight of can	Weight of wet soil + can	Weight of dry soil + can	Weight of wet soil	Weight of dry soil	Water content (%)
15.00	31.90	27.50	16.90	12.50	35.20
14.60	30.70	26.50	16.10	11.90	35.29
					PL=35%

The plastic limit of the soil was determined to be 35%

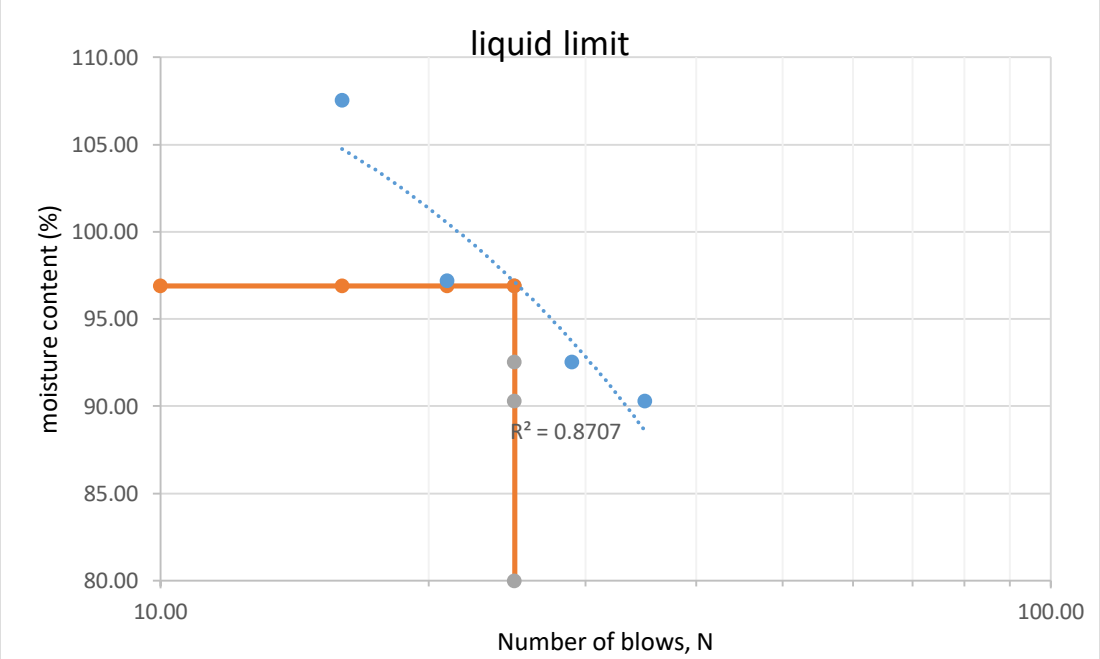

Fig 4.5: Liquid limit

From the grain size distribution curve (GSD) and using the Unified Soil Classification System (USCS), the soil was classified as shown in table 4.5 below.

Table 4.5: USCS classification for soil used

Soil Type	% content
% Gravel	0.00
% Sand	28.00
% Silty & Clay	72.00

From the Atterberg results, the soil can be classified as inorganic fat clay (CH) of high plasticity consisting mainly of illite or montmorillonite according to the USCS (refer to figure 2.9 adopted from Holtz and Kovacs, 1981).

4.3.1.5 Proctor Compaction Test

4.3.1.5.1 Objective

The main aim of this test is to determine the optimal moisture content and maximum dry density of untreated soil sample and the treated clay samples.

4.3.1.5.2 Materials:

- Compaction mold
- No. 4 U.S sieve
- Trowel and Jack
- Standard proctor hammer
- Balance
- Mixing pan
- Drying oven
- Moisture cans
- Plastic squeeze water bottle

Procedure

This test procedure covers laboratory compaction procedures used to determine the relationship between water content and dry unit weight of soils compacted in a 4 or 6 in. diameter mold with a 5.5 lb. hammer dropped from a height of 12 in., producing a compactive effort of 12,400 ft-lb/ft3. A soil at a selected water content is placed in three layers into a mold of the given dimensions, with each layer compacted by 25 blows of the hammer. The resulting dry unit weight is then determined. This procedure is repeated for enough water contents to establish a relationship between the dry unit weight and the water content of the soil. The following steps were followed during the testing process:

1. Obtain a sample of soil, break up clumps and pass through #4 sieve. Discard granular component retained on sieve.
2. Assemble and secure the mold to the base plate.
3. Weigh the empty mold and base plate without collar and record.
4. Place the mold on a level surface and use a scoop to place 1 layer of soil. The mold will be filled by 3 layers.
5. Compact each layer with 25 blows from the hammer. Distribute the blows over the entire surface. The hammer should freefall 12” onto the soil surface.
6. On the 3rd layer, the collar must be secured to top of mold to compact layer.
7. After the layer is placed and compacted, remove the collar gently so as not to disturb the sample.
8. Use the straightedge to trim soil even with the top of the mold. Fill any holes on the surface with trimmings.
9. Weigh the mold and compacted sample and record.

10. Remove the material from the mold and slice vertically through the center. Take a representative sample of the material from one of the cut faces and determine the moisture content.

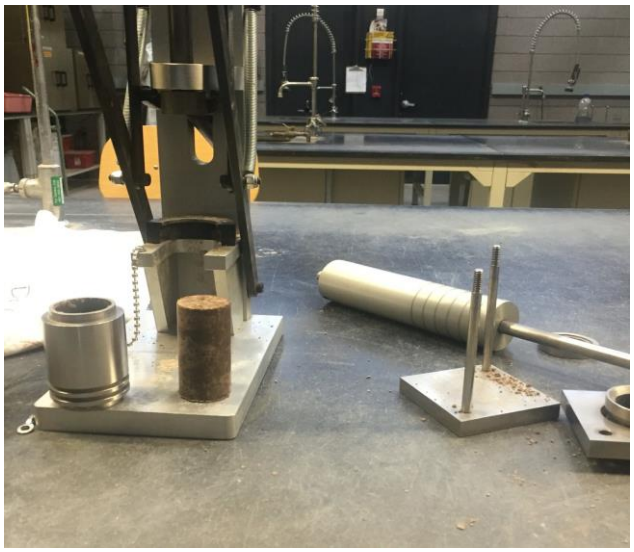

Fig 4.6: Standard Proctor Compaction Apparatus

Figures 4.7-4.9 show the results for the compaction test for untreated sample, ASU-treated and Indian-treated soil-silica gel mixture samples. All samples were compacted at 90% maximum dry unit weight (MDUW). The MDUW of the treated samples decreased slightly and the optimum moisture content (OMC) increased slightly with an increase in silica gel content. The reduction in MDUW can be attributed to a reduction in specific gravity. According the Soil Mechanics Laboratory Manual published by Braja Das (2002), the maximum theoretical dry unit weight of a compacted soil at any given moisture content will occur when there is no air left in the voids. This is called the zero-air-void unit weight. The saturation curve (ZAV) was calculated using the following formula (Das, 2002):

$$\gamma_{d(theory-max)} = \gamma_{zav} = \frac{\gamma_w}{(\frac{w(\%)}{100} G_s + \frac{1}{G_s})} \ldots\ldots\ldots\ldots\ldots\ldots\ldots\ldots\ldots\ldots (4.4)$$

Where $\gamma_{zav} = zero - air - void\ unit\ weight$

$\gamma_w = unit\ weight\ of\ water$

$w = moisture\ content$

$G_s = Specific\ gravity\ of\ the\ soil\ solid$

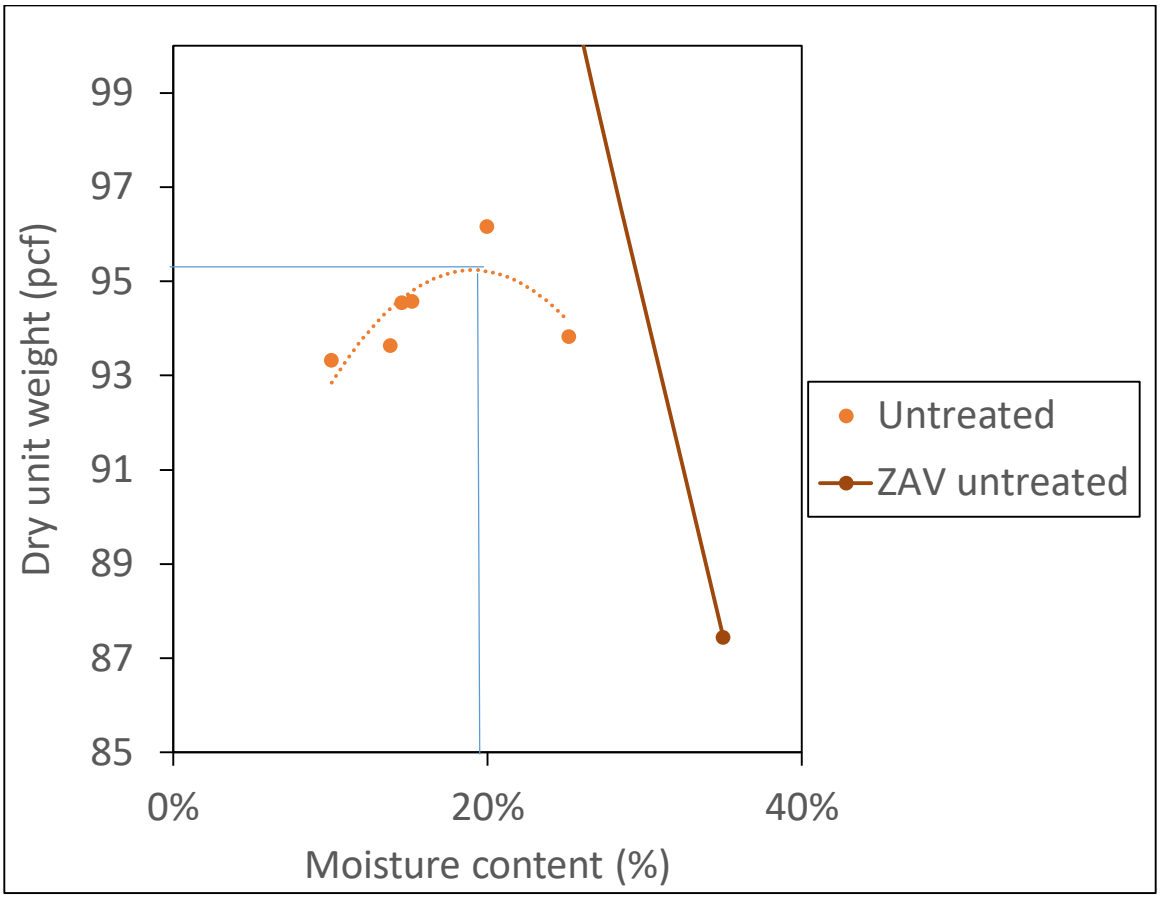

Fig 4.7: Compaction curve for untreated sample

The MDUW of the untreated sample was determined to be 95.3 pcf (14.98kN/m^3) and the optimum water content (OWC) was 19.9%.

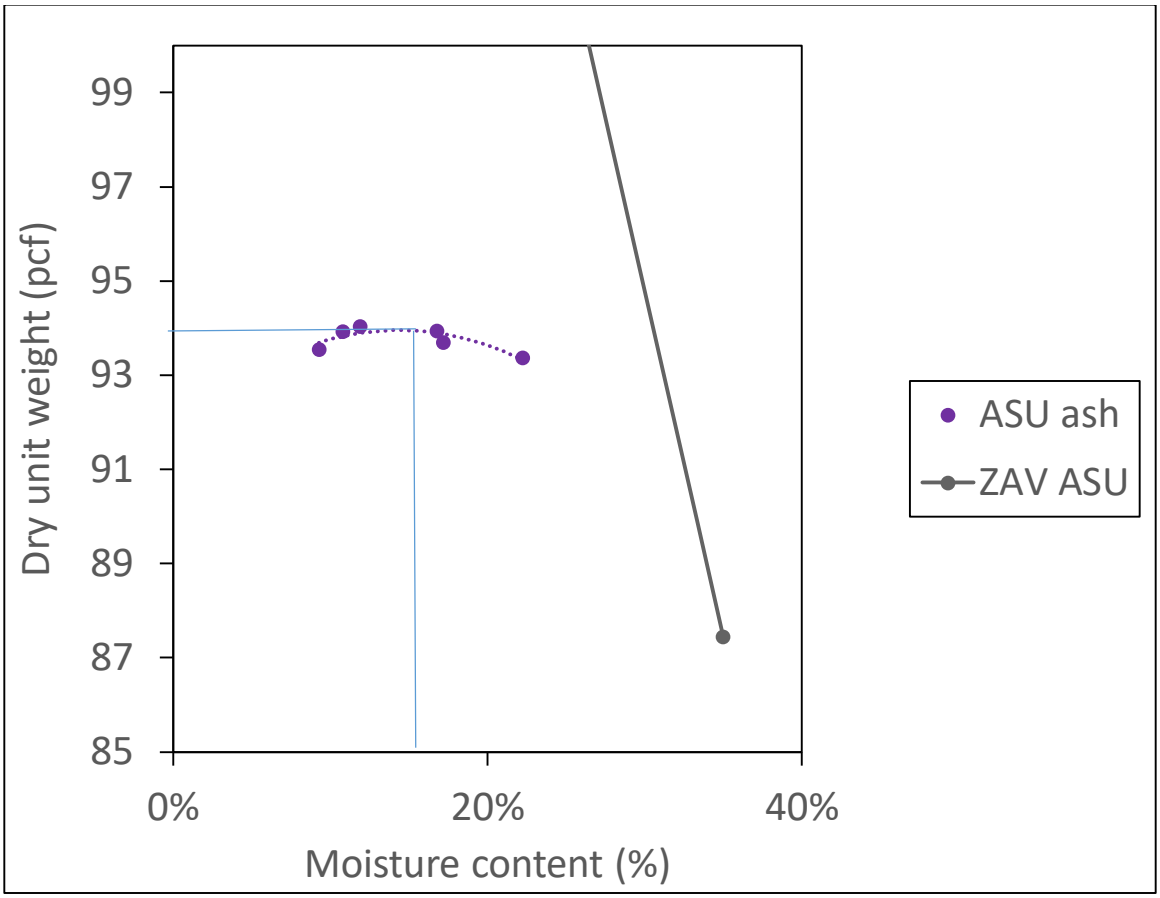

Fig 4.8: Compaction curve for ASU gel treated sample

The MDUW of the ASU treated sample was 93.9 pcf (14.75 kN/m^3) and the OMC was 16.0%.

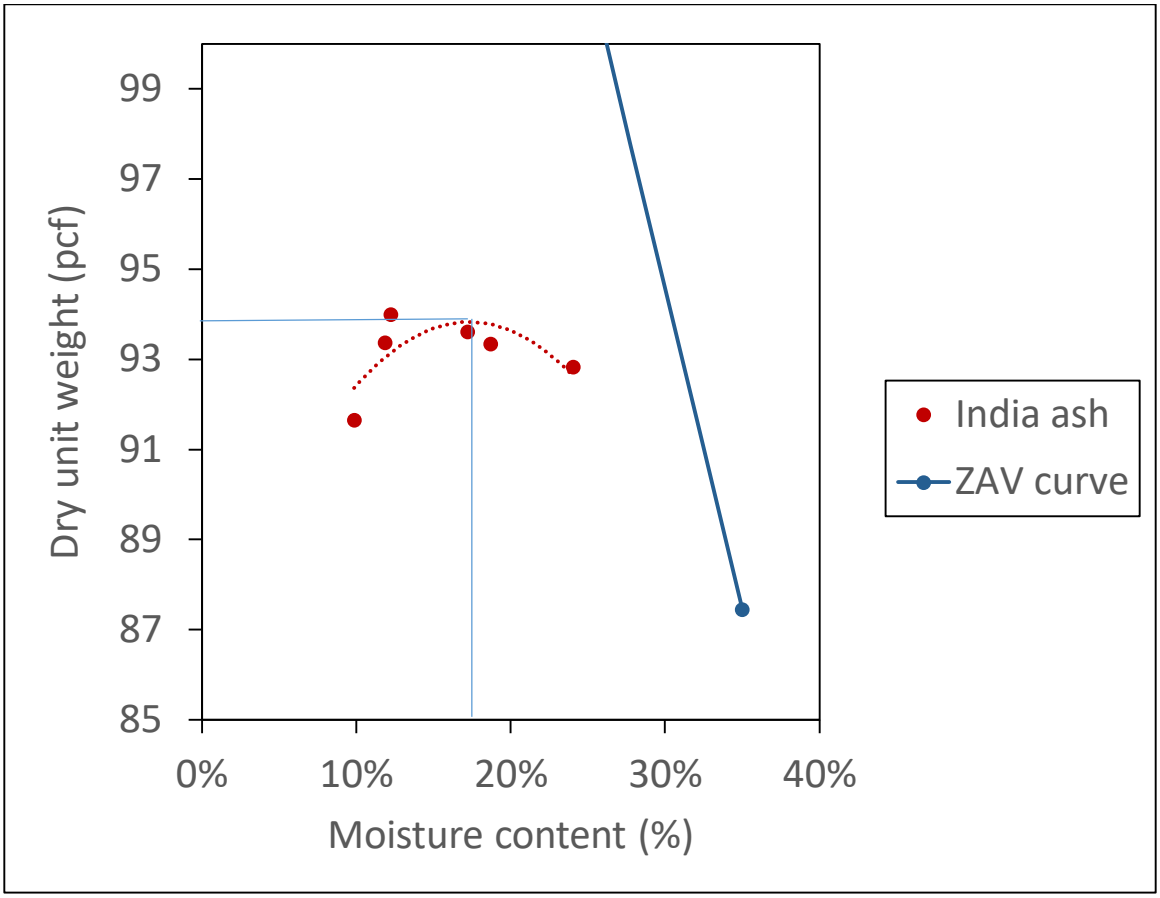

Fig 4.9: Compaction curve for India gel treated sample

The MDUW of the India treated sample was 93.8pcf (14.73kN/m^3) and the OMC was 17.5%.

4.4 Soil Treatment Methods with Silica Gel

4.4.1 Percolation

In this method, the soil was placed in a dish and a known volume of silica gel was added. The mixture was left to stand for the solution to percolate to the bottom of the soil sample. After percolation, the soil would be left to cure for 14 days. The observation made was that fine soils are very difficult to percolate. The soil did not percolate even

after being left to stand for hours or days. The gel formed on the top surface of the clay and split to glassy solids. This was not an effective method of treatment as the gel could not get to the bottom and spread through the soil structure. This method does not work with clay soils because their low conductivity but could work with sands as they have quick water drainage.

4.4.2 Adding Soil to Gel

In this method, silica gel solution was placed in a dish and the clay mixture was added slowly. This method seemed like the inversion of the percolation and acted as a control experiment. However, the two methods seemed to have similar problems and results were not different. Adding soil to the gel did not allow mixing of the two contents unless mixing was done manually. This in conclusion led to the third method, which was mixing the contents but instead of adding soil to the gel, the gel was added to the soil and mixed.

4.4.3 Adding Gel to Soil and Mixing

This was found to be the easiest way possible to work with fine soils. The silica gel was made, and 170 g of clay was placed in a Ziploc bag. A target water (solution) content was chosen and the mass of the solution to be added was calculated. The initial water content of the untreated clay was 6.48% and it was used in determining the mass of silica gel solution to be added and finding the optimum percentage of gel to be added. The initial mass of moisture present is 10.3 g (from 6.48% water content). Fig 4.11 below shows treated samples in Ziploc bags curing for 14 days.

Fig 4.10: Anthem-bentonite clay after mixing

Fig 4.11: Treated samples left to cure

Table 4.6: Mass of silica gel to be added

Target moisture content (%)	Target (total) mass of solution present in soil after addition	Mass of silica gel to be added (g)
11	17.6	7.3
14	22.4	12.1
17	27.1	16.8
21	33.5	23.2
26	41.5	31.2
30	47.9	37.6

The compaction tests carried out determined the optimum moisture contents of the untreated and treated samples. The optimum moisture content of the untreated sample was 21.0%. The OMC of the ASU gel sample was 13.7% and that of the Indian gel sample was 14.5%. A plot of moisture content of sample versus mass of solution added was used to determine the masses of the solutions added at the optimum moisture contents. Figure 4.12 below shows moisture content versus mass of solution added for the different samples.

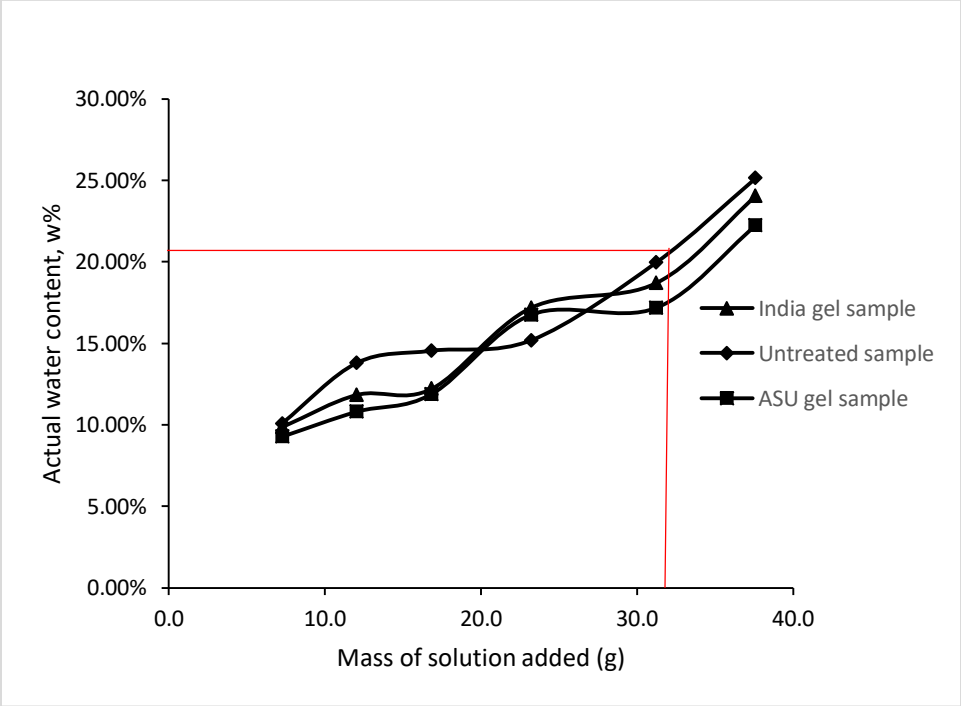

Fig 4.12: Moisture content vs mass of solution

The optimum mass of water to be added to the untreated sample to achieve a water content of 21.0% was found to be 32 g which is about 20% of the dry mass of the soil. The optimum percentage of ASU gel to be added was determined to be 11.3% of the dry soil mass and that of the Indian gel solution was 12.2% of the dry soil mass.

4.5 Chemical Characterization of Treated Clay

4.5.1 Fourier Transform Infra-Red Spectroscopy (FTIR) of Treated Samples

4.5.1.1 FTIR of Untreated Sample

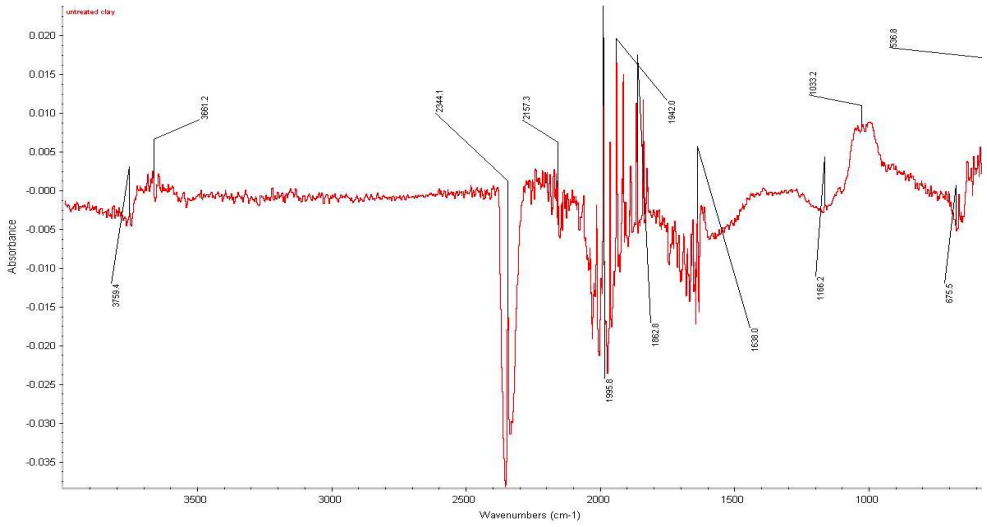

Fig 4.13: FTIR of untreated clay sample

Figure 4.13 shows the spectrum of an untreated clay sample. In the spectra, the clay minerals show Si-O stretching and bending at range of 1300-400 cm^{-1} as well as OH bending absorptions at about 2344 cm^{-1}.

4.5.1.2 FTIR of treated samples before and after gelation

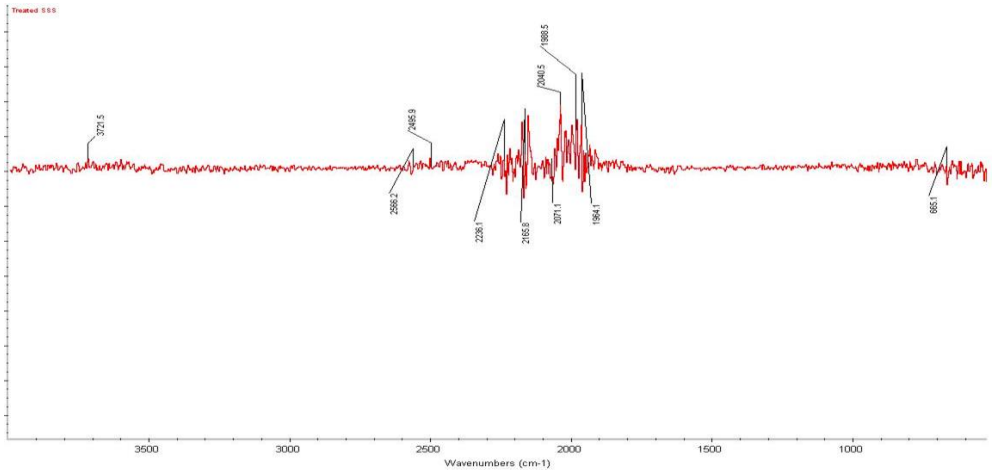

Fig 4.14: FTIR of treated sample before gelling occurred

Figure 4.14 shows the spectra of a treated sample during gelation.

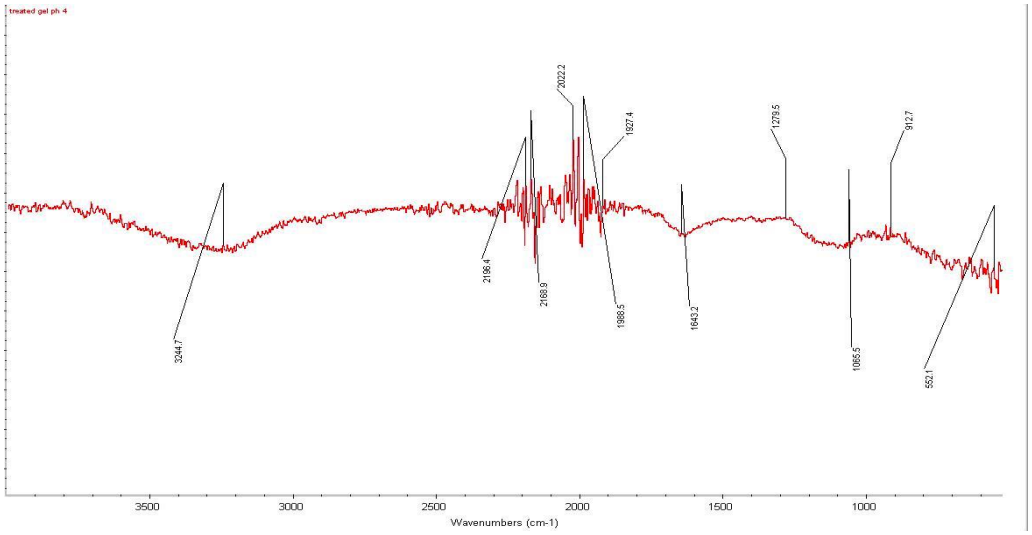

Fig 4.15: FTIR of treated sample after gelling occurred

Figure 4.15 shows FTIR spectra of a treated sample after gelation occurred. It can be seen from figures 4.14 and 4.15, that the Si-O and OH functional groups are not present as the case is in the untreated sample. This implies that reaction took place and gel formed. Therefore, FTIR could be used to distinguish different clay minerals and provide information on their chemical composition.

4.5.2 Scanning Electron Microscopy (SEM) and Energy Dispersive X-ray Spectroscopy (EDS) Analysis of Samples

Figure 4.16 shows an EDS analysis of the untreated sample. The minerals present are shown in the figure above on their energy level and shell.

Table 4.7a shows the concentration of the elements in terms of weight % or atomic %.

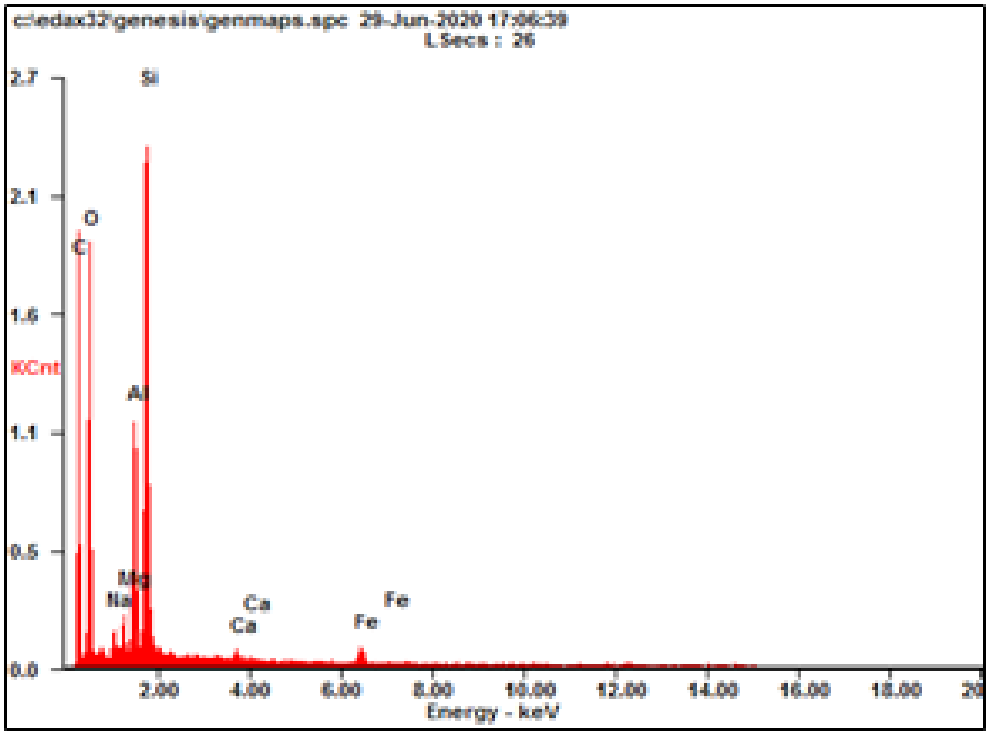

Fig 4.16: EDS of an untreated sample

Table 4.7a: Energy dispersive detector results of untreated sample

Element	Wt%	At%
CK	52.05	61.98
OK	35.17	31.44
NaK	00.79	00.49
MgK	00.76	00.45
AlK	03.67	01.94
SiK	06.88	03.50
CaK	00.18	00.06
FeK	00.51	00.13
Matrix	Correction	ZAF

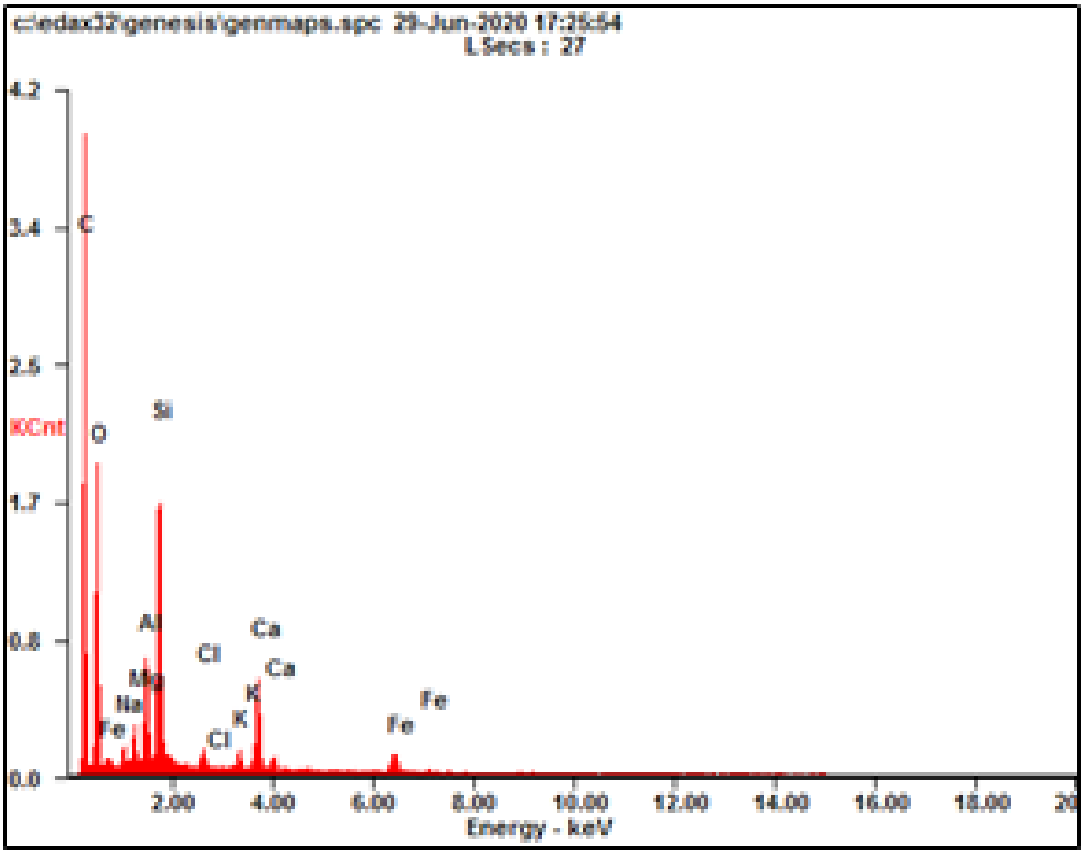

Fig 4.17: EDS of ASU treated sample

Figure 4.17 shows the EDS analysis of the ASU treated sample. The minerals present are shown in the figure above on their energy level and shell. Table 4.7b shows the concentration of the elements of ASU treated sample in terms of weight % or atomic %.

Figure 4.18 shows an EDS of India treated sample. The minerals present are shown in the figure above on their energy level and shell.

Table 4.8 shows the concentration of the elements of India treated sample in terms of weight % or atomic %.

Table 4.7b: EDS results of ASU treated sample

Element	Wt%	At%
CK	62.32	71.18
OK	28.99	24.85
NaK	00.46	00.27
MgK	00.63	00.36
AlK	01.67	00.85
SiK	03.50	01.71
ClK	00.23	00.09
KK	00.26	00.09
CaK	01.26	00.43
FeK	00.69	00.17
Matrix	Correction	ZAF

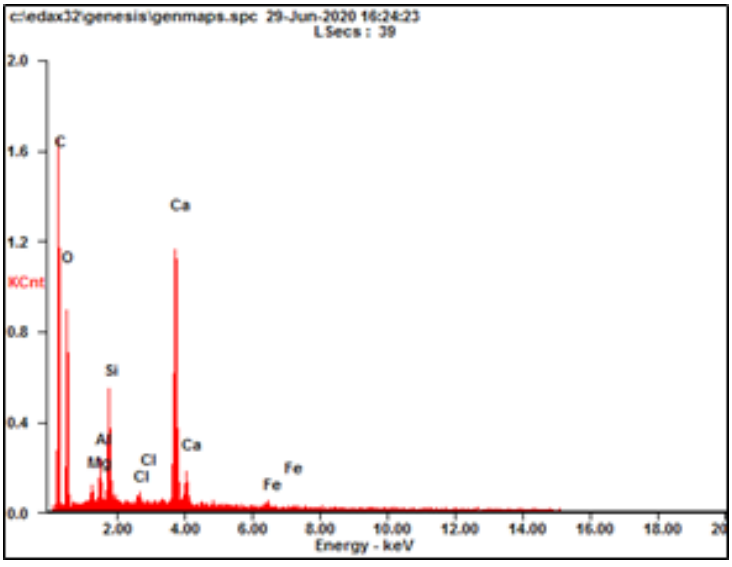

Fig 4.18: EDS of Indian treated sample

Table 4.8: EDS of Indian treated sample

Element	Wt%	At%
CK	56.77	66.62
OK	33.23	29.27
MgK	00.60	00.35
AlK	00.90	00.47
SiK	02.14	01.07
ClK	00.19	00.08
CaK	05.85	02.06
FeK	00.33	00.08
Matrix	Correction	ZAF

The following conclusions can be made from the EDS analysis of the samples:

- All elements are emitted from the same energy level shell (K) in all the three samples
- The treated samples show a decrease in the intensity of Si and O indicating that the **silicon and oxygen already present in the clay adds to the gelation of the samples**
- There is an increase in carbon meaning more bands are created in the clay thus, **more polymerization**
- The increase in calcium in the Indian sample signifies **more insoluble calcium compounds formed from the impurities** in the Indian ash.

The SEM images of the samples are shown below.

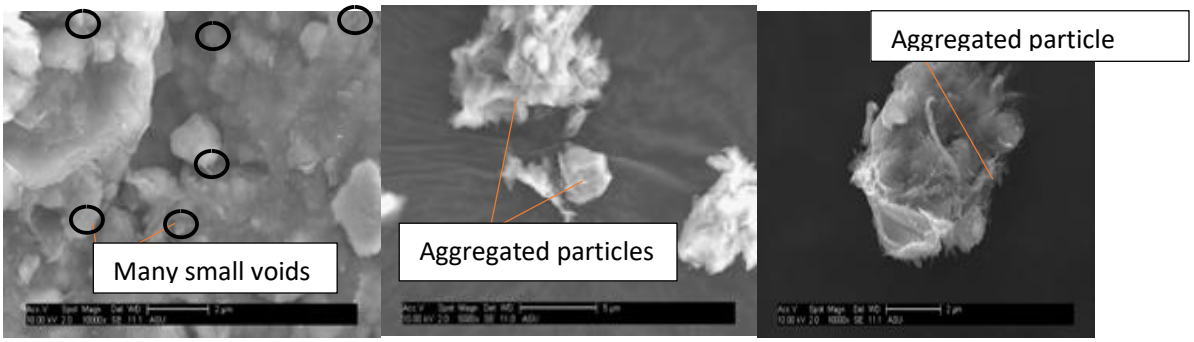

a) Untreated **b) ASU Treated (5K)** **c) Indian Treated**

Fig 4.19: SEM image of untreated and treated samples at 10K Resolution (2 mm)

a) Untreated **b) ASU Treated** **c) Indian Treated**

Fig 4.120:50K Resolution (500 nm)

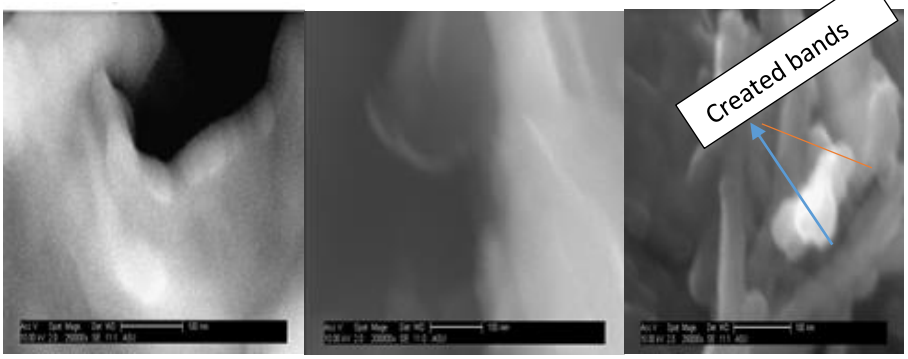

a**)** **Untreated** **b) ASU Treated (200k)** **c) Indian Treated**

Fig 4.21: 250K Resolution

The SEM images of the untreated and treated samples were taken at different resolutions and used to examine the effect of silica gel on the microstructure of the clay.

The structure of the untreated clay was discontinuous, flaky and without aggregates. Pores were visible throughout the microstructure due to a lack of cementation of the particles. The SEM image of the treated samples cured for 14 days revealed important changes in the microstructure of the clay. There were lesser but larger voids, new bands were created, and aggregation occurred in both samples treated with ASU gel and Indian gel. These changes are attributed to the process of gelation and interactions between the clay particles and the gel formed.

There was electrostatic reaction between the clay particles and the water-gel mixture which led to steady aggregation over time. The formation of larger pores decreased the number of inter-aggregate pores; thus, the attraction of water into soil structure was limited and this in turn led to reduced swelling.

4.5.3 X-Ray Diffraction (XRD) of Silica Gel Treated Clay Samples

X-ray diffraction is used for phase identification and composition, crystal structure, crystal quality, orientation, strain state, crystal chemistry and defect density, surface quality, film thickness and sample texture (Mitchell & Soga, 2005). The typical samples are thin films (both single crystal and polycrystalline) (Mitchell & Soga, 2005). X-Ray diffraction analysis was carried out using a Philips X-ray diffractometer. The ground samples were analyzed by 2θ $K_{\alpha 1}$ Cu radiation with a wavelength, λ of 1.54Å.

4.5.3.1 Objective

The goal of this technique was to find the d-spacing of the samples and attempt to assess the effect of treatment on the clay diffused double layer.

4.5.3.2 Methodology

Three samples were compared: an untreated sample of Anthem clay mixed with bentonite, a sample treated with silica gel from ash produced at ASU, and a sample treated with silica gel from ash produced in India. The soil samples were put in small containers and silica solution at pH = 1.5 was added immediately to soak up and mixed thoroughly. The samples were then left *to cure* for 7 days in Ziploc bags, when the gel was allowed to be formed inside the clay. It is worth noting that *curing* is a term used frequently in the concrete industry. During curing, the water reacts with the cement and the concrete becomes stronger. It is important to clarify that the term cure is used in here to indicate the time allowed the gel to form inside the soil.

After curing, the samples were transferred to an X-ray diffractometer and the analysis was carried out. The results showing the differences and the similarities between the treated samples are presented below.

4.5.3.3 Results

The results of the XRD on the samples are shown in figures 4.22 to 4.24. Each peak and angle indicate the presence of a clay mineral. Tables 4.9 to 4.11 summarize the minerals present in the clay at their respective d-spacing, according to Mitchell and Soga (2005).

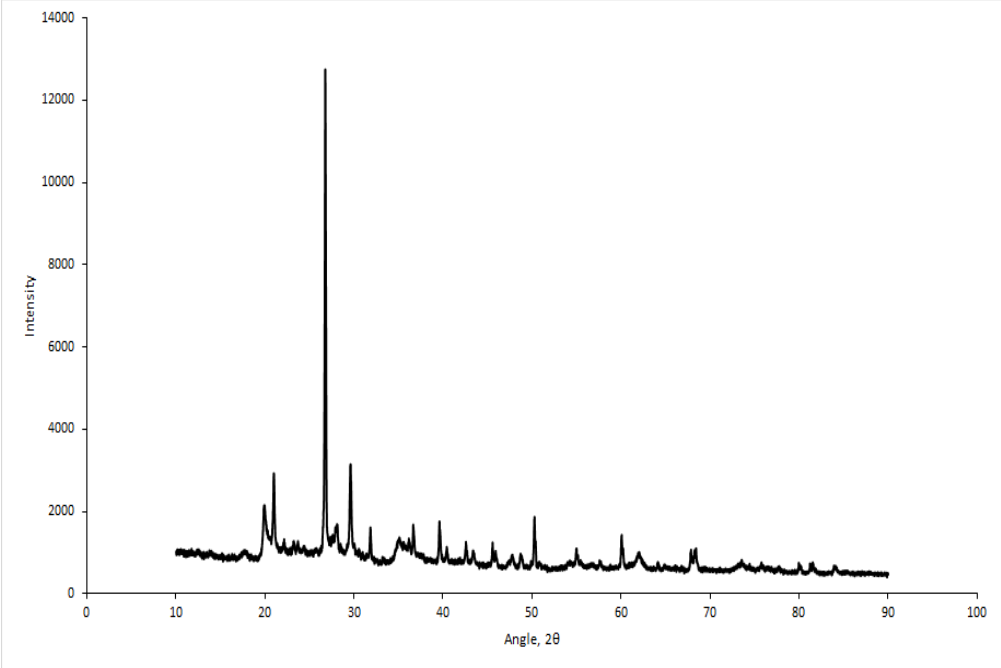

Fig 4.22: XRD results of the India gel treated sample

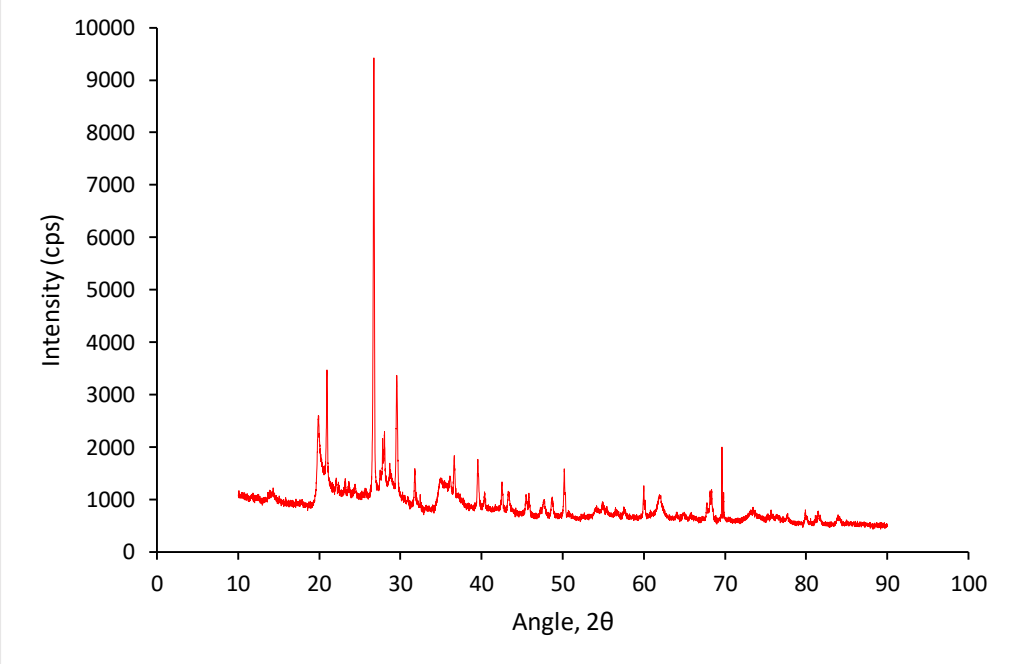

Fig 4.23: ASU gel treated sample XRD

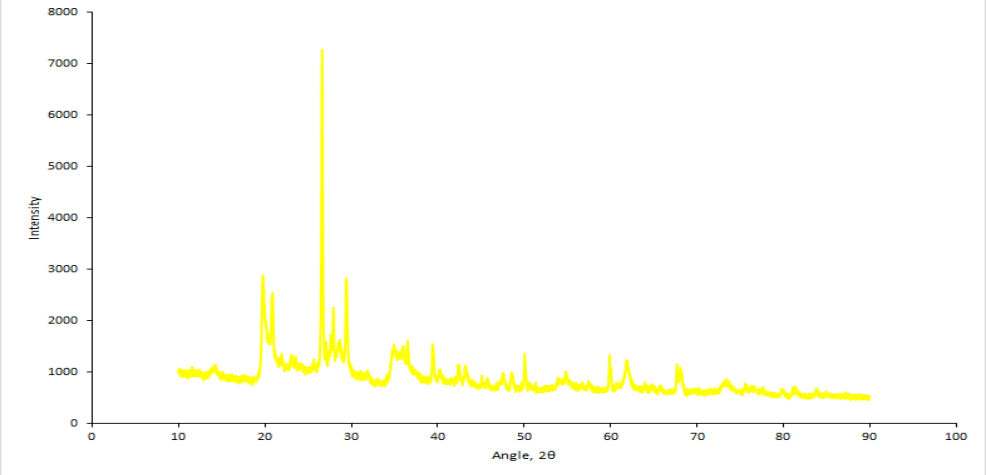

Fig 4.24: Untreated sample XRD

Table 4.9: ASU sample

peak #	2θ	d (Å)	I (cps)	I/Imax	Mineral
1	20.949	4.237	3472	36.8	Quartz
2	26.73	3.332	9429	100.0	Illite
3	29.555	3.020	3272	34.7	Feldspar
4	36.64	2.451	1836	19.5	Chlorite
5	39.541	2.277	1764	18.7	Quartz, Sepiolite
6	43.29	2.088	1156	12.3	Kaolite
7	50.191	1.816	1583	16.8	Quartz
8	59.992	1.541	1263	13.4	Verm. (S), Illite
9	62.089	1.494	1074	11.4	Kaol. (VS), Mont.
10	69.631	1.349	1998	21.2	Kaol. (B)

Table 4.10: India sample

peak #	2θ	d (Å)	I (cps)	I/Imax	Mineral
1	20.982	4.231	2938	**23.1**	Quartz
2	26.762	**3.329**	12734	100.0	**Illite**
3	29.599	3.016	3156	**24.8**	Feldspar
4	36.64	**2.451**	1691	**13.3**	**Chlorite**
5	39.585	2.275	1768	13.9	Quartz, Sepiolite
6	42.595	2.121	1199	9.4	Quartz, Mica
7	50.266	1.814	1878	14.7	Quartz
8	60.068	**1.539**	1442	11.3	**Verm. (S), Illite**
9	62.0567	**1.494**	1011	7.9	**Kaol. (VS), Mont.**
10	68.414	**1.370**	1114	**8.7**	**Kaolinite**

4.5.3.4 Discussions and Conclusions

From the results presented, it can be found the d-spacing for illite in the untreated sample is 4.47 Angstroms (Å) and it decreases to 3.33Å in treated samples, while the d-spacing for the quartz decreased from 4.47 Å in the untreated to 4.237 Å in the treated samples. This occurs because the double layer might get depleted on treatment and the gel coats the illite particles. Illite being the main peak means it is the clay type that is mainly responsible for the expansion and when the d-spacing decreases, the clay sample loses its ability to expand.

Table 4.11: Untreated sample

peak #	2θ	d (Å)	I (cps)	I/Imax	Mineral
1	19.84	**4.471**	2871	**39.5**	**Illite, Sepiolite**
2	26.665	3.340	7266	100.0	Quartz
3	29.457	3.030	2834	39.0	Feldspar
4	36.553	**2.456**	1626	**22.4**	**Chlorite**
5	39.465	2.281	1494	20.6	Quartz, Sepiolite
6	42.508	2.125	1152	15.9	Quartz, Mica
7	50.104	1.819	1365	18.8	Quartz
8	61.85	**1.499**	1239	**17.1**	**Kaolinite, Mont**
9	62.046	**1.495**	1146	**15.8**	**Kaol. (VS), Mont.**
10	67.707	**1.383**	1160	**16.0**	**Kaolinite**

The second way the swell potential seems to be reduced is through the coating of the illite particles. When the illite particles are coated, there is no room for interaction between the clay mineral and the water and hence, there is a reduction of swell potential on wetting the sample. It is also noted that the ASU treatment gives better coating of the illite particles. This is deduced from the intensities of the illite (highest peak) in treated samples. It is to be noted that the intensity is a measure of the crystallinity of the sample. Higher intensity indicates more crystalline structure, more order and arrangement, while lower intensity indicates more amorphous structure.

The intensity of the illite in the ASU sample is 9429 counts per second (cps) whereas that in the India sample is very high at 12734 cps implying that on treatment, the ASU gel coats illite particles more efficiently hence less intensity was noted in the XRD results. However, both intensities are much higher than illite intensity in an untreated sample. On treatment, most of the quartz is converted to gel leaving illite to be the highest peak. The peak intensity increases on treatment means the treated samples are more crystalline than the untreated sample, and the India sample is the most crystalline as it has the highest peak intensity. The ASU ash has a higher concentration of silica and therefore, it provides better coating and less time for gelation.

4.6 Response to Wetting and Drying Cycles

4.6.1 Introduction/Overview

The volume change behavior of problematic soils is commonly studied through testing undisturbed or remolded samples for swelling potential based on the ASTM D4546-08 standard (Rosenbalm, 2013). To assess the heave and swelling potential of an untreated sample, the sample was first loaded to a predetermined net normal stress and inundated with water. The change in volume of the sample that occurs during the test was recorded with the LabVIEW software program installed in the ASU laboratories to automatically read the oedometer results. The extent to which the sample expands is proportional to the initial moisture content and net normal stress (Rosenbalm, 2013). The magnitude of swell under known vertical or axial pressure is what was called the percent swell and the vertical pressure required to maintain no volume change of the specimen loaded axially was termed as the swell pressure (de Luca, 2017).

4.6.2 Net Normal Stress Selection

For the response to wetting test, two net normal stresses were selected to work with and determine the percent swell and shrinkage of the samples used. The two normal stresses used were the light token load (2.24 kPa) and a working normal stress of 49.4 kPa to compare with the token to determine the effect of net normal stress on swelling.

4.6.3 Number of Cycle Selection

For this experiment, three full cycles (wetting and drying) were chosen with each half cycle running for 7 days. From experimental trials, it was shown that after 4-5 days, the swelling or shrinkage becomes constant. From literature, it was estimated that after 4-5 full cycles, the swelling becomes asymptotic and the swell pressure begins to stabilize to a constant value (Tripathy et al., 2002). However, after working with multiple cycles, I found that after 3 cycles, the swelling becomes asymptotic as shown in figure 4.10 below. This finding was in line with Rosenbalm (2013) findings. Therefore, the goal was to complete three wetting and three drying cycles for each specimen at the two chosen normal stresses.

4.6.4 Testing Procedure

After mixing the soil with gel, the admixture was left in a Ziploc bag and left to cure for 7 days. After curing, the mass of the soil-gel admixture to be consolidated was calculated from the volume of the ring as shown in table 4.12. A consolidation ring was obtained, and the diameter measured at three different angles and the average diameter recorded. The height of the ring was measured and recorded. The mass of the soil to be added at 90% MDUW and OMC was for the different samples was calculated as shown in table 4.13.

Table 4.12: Calculation of mass of soil to be compacted using 0.8-inch ring height and India gel OWC and 90% MDUW

Maximum dry unit weight (kN/m^3)	13.3560
OWC (%)	14.5000
Ring radius (m)	0.0317
Ring Height (m)	0.0203
Area of the ring (m^2)	0.0031
Volume of the ring (m^3)	0.0001
Wet mass of the soil (kN)	0.0010
Wet mass of the soil (N)	0.9785
Wet mass of the soil (kg)	0.0997
Wet mass of the soil (g)	99.7489
Dry mass of the soil (g)	87.1170
Wet mass of the soil (6.5% OWC initial)	92.7360
Mass of water/solution to be added (g)	7.0129
Clay mass (g)	27.8208
Anthem mass (g)	64.9152

Table 4.13: Mass of soil to be added

Ring height (inches)	Mass of soil to be added (90%MDUW, OWC) (g)		
	Untreated	ASU sample	Indian sample
0.8	94.4		92.7
1.0		115.6	

A porous stone was placed at the bottom of the ring and the mass of the soil added and compacted evenly to ensure uniform distribution as shown in figure 4.25.

Fig 4.25: Compacted sample in ring

The ring was then transferred to a consolidometer and another porous stone was added to the top as indicated in figure 4.26. The consolidometer was then transported to the odometer apparatus and a cap added to hold the Linear Variable Displacement transducer (LVDT) in place which itself was clamped to a stand. This is shown in figure 4.27.

Fig 4.26: Ring with soil and porous stone

Fig 4.27: Odometer apparatus with LVDT and ring.

4.6.5 Moisture Content Determination

The assessment of moisture content variation during cycles is presented here. A total of three samples were used for this purpose. To achieve this goal, samples were unloaded at the end of each cycle and the sample was weighed and the mass recorded. After which the sample was reloaded and subjected to the same conditions as before and the LabVIEW program continued to record data during both the unloading and reloading. The unloading and reloading led to discontinuities in the data collection (Rosenbalm,

2013). Once all the same conditions were applied to the specimen, the LVDT capture in the LabVIEW program was re-zeroed to allow for easy repair when the discontinuities were removed from the data (Rosenbalm, 2013). Table 4.14 shows the moisture contents of the samples during the wetting and drying cycles.

Table 4.14: Moisture content calculations during cycles

Untreated sample 2.2 kPa 7 days							
Cycle	Water content, w %	Volume of ring, V (m^3)	Mass of sample Mt (g)	Mass of solids, Ms	Mass of solution Mw	Wet density (kPa)	Dry density (kPa)
Initial	21.13	6.399E-05	107.32	88.6	18.72	16.45	13.58
Swell 1	54.85	7.188E-05	137.2	88.6	48.6	18.72	12.09
Shrink 1	13.54	6.316E-05	100.6	88.6	12	15.62	13.76
Swell 2	54.40	6.319E-05	136.8	88.6	48.2	21.24	13.75
Shrink 2	12.19	6.260E-05	99.4	88.6	10.8	15.58	13.88
Swell 3	42.66	6.269E-05	126.4	88.6	37.8	19.78	13.86
Shrink 3	3.27	4.159E-05	91.5	88.6	2.9	21.58	20.90

ASU sample 49.4 kPa 7 days							
Initial	14.44	6.399E-05	98.65	86.2	12.45	15.12	13.22
Swell 1	51.04	6.809E-05	130.2	86.2	44	18.76	12.42
Shrink 1	9.28	6.579E-05	94.2	86.2	8	14.05	12.85
Swell 2	47.91	6.584E-05	127.5	86.2	41.3	19.00	12.84
Shrink 2	3.71	6.364E-05	89.4	86.2	3.2	13.78	13.29
Swell 3	46.75	6.579E-05	126.5	86.2	40.3	18.86	12.85
Shrink 3	1.97	6.266E-05	87.9	86.2	1.7	13.76	13.5
India sample 49.4 kPa 7 days							
Initial	15.16	8.008E-05	124.83	108.4	16.43	15.29	13.28
Swell 1	47.32	8.741E-05	159.7	108.4	51.3	17.92	12.17
Shrink 1	17.71	8.012E-05	127.6	108.4	19.2	15.62	13.27

Swell 2	52.68	8.979E-05	165.5	108.4	57.1	18.08	11.84
Shrink 2	3.04	7.487E-05	111.7	108.4	3.3	14.64	14.2
Swell 3	42.16	8.243E-05	154.1	108.4	45.7	18.34	12.9
Shrink 3	1.01	5.836E-05	109.5	108.4	1.1	18.41	18.22

4.6.6 Effect of Wetting and Drying Cycles and Net Normal Stress on Volume Change of the Sample

4.6.6.1 Free Swell at Token Load

Fig 4.28 below shows how the behavior of the untreated sample and treated samples during the first wetting cycle at the token load varies.

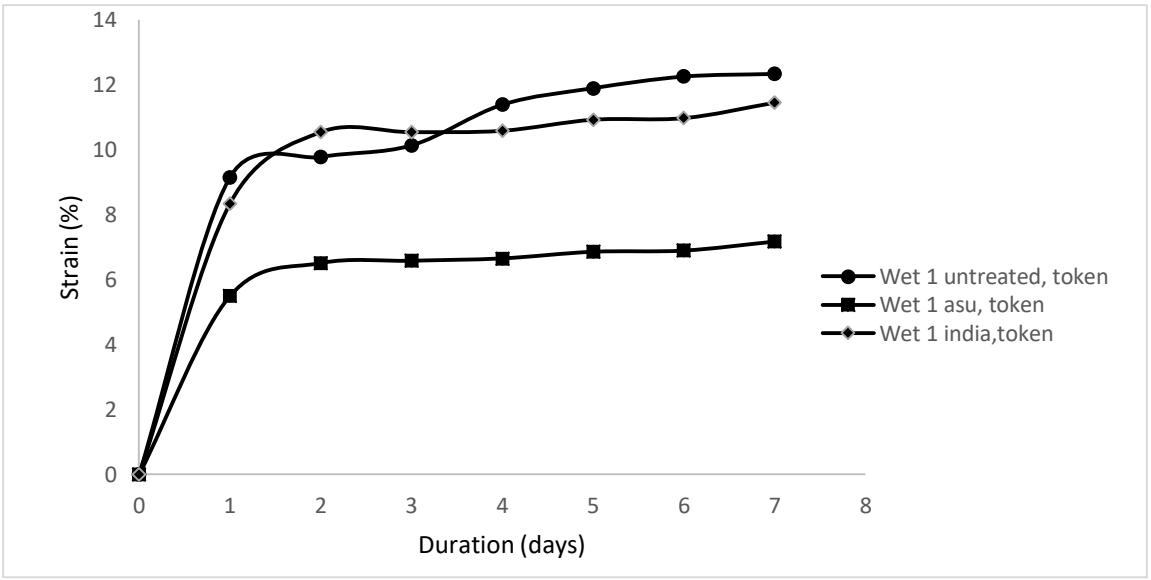

Fig 4.28: Wetting cycle 1 at 2.24 kPa

The free swell of the untreated sample is 12.3% strain and the free swell of the treated samples are 10.9% for the Indian gel treated sample and 7.2% for the ASU gel treated sample. Fig 4.29 below shows how the behavior of the untreated sample and treated samples varies during the first drying cycle at the token load.

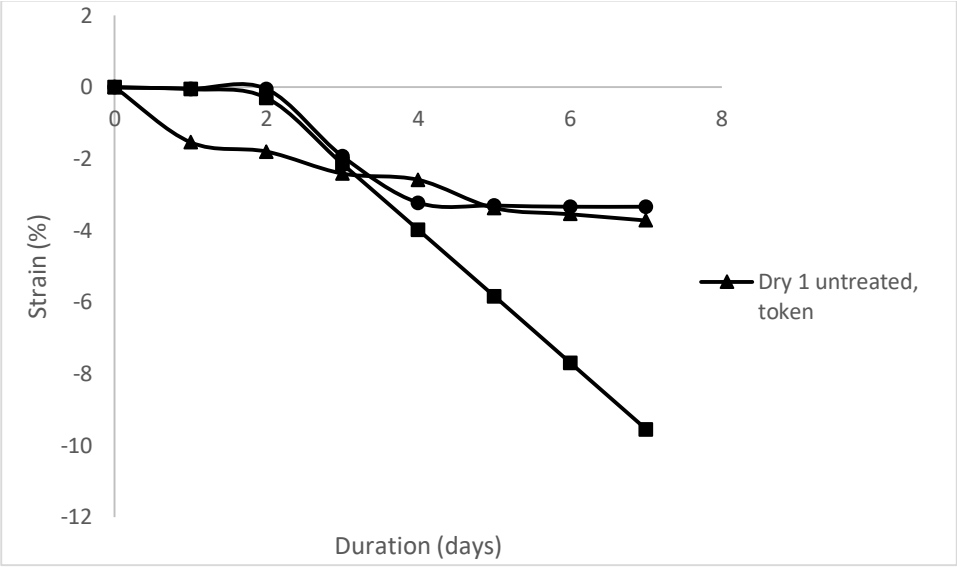

Fig 4.29: Drying cycle 1 at 2.24 kPa

4.6.6.2 Net Normal Stress of 49.4 kPa

Figures 4.30 and 4.31 below show the behavior of the untreated sample and treated samples during the first drying cycle at a net normal stress of 49.4 kPa.

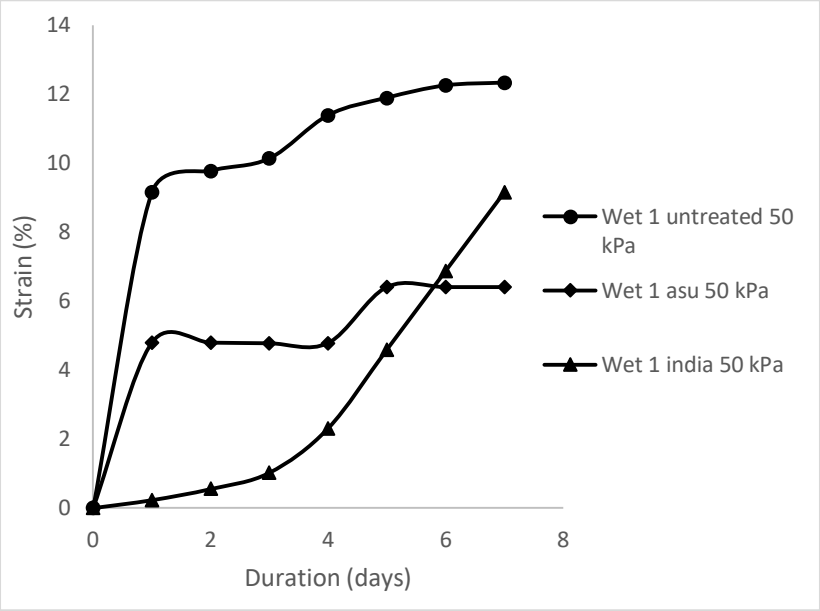

Fig 4.30: Wetting cycle 1, 50 kPa

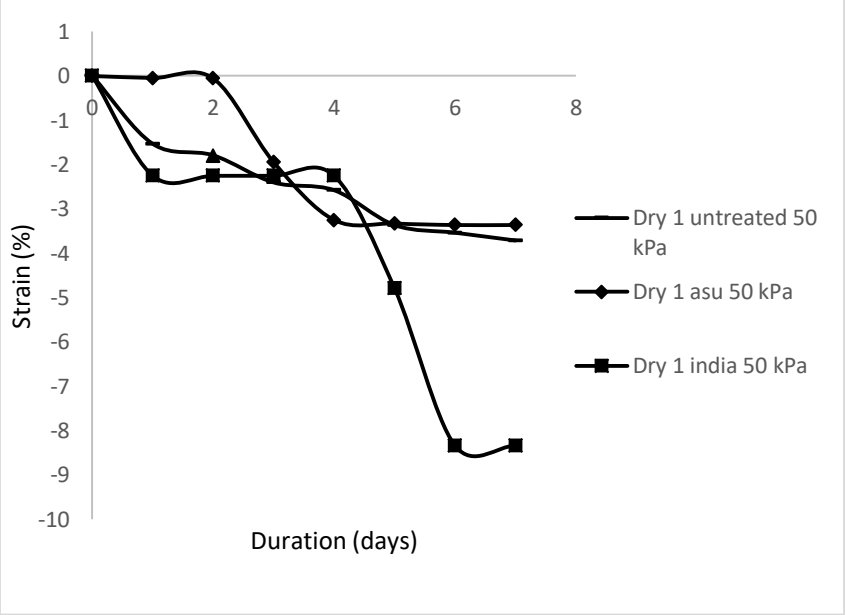

Fig 4.31: Drying cycle 1, 50 kPa

It is indicated from these results that the net normal stress affects the swelling of the samples. As stress is applied, the vertical strain of the sample decreases and this leads to lower swelling percentage.

A plot of net normal stress versus maximum swelling during the first wetting cycle was generated and extrapolated to determine the swelling pressures of the samples as shown in figure 4.32.

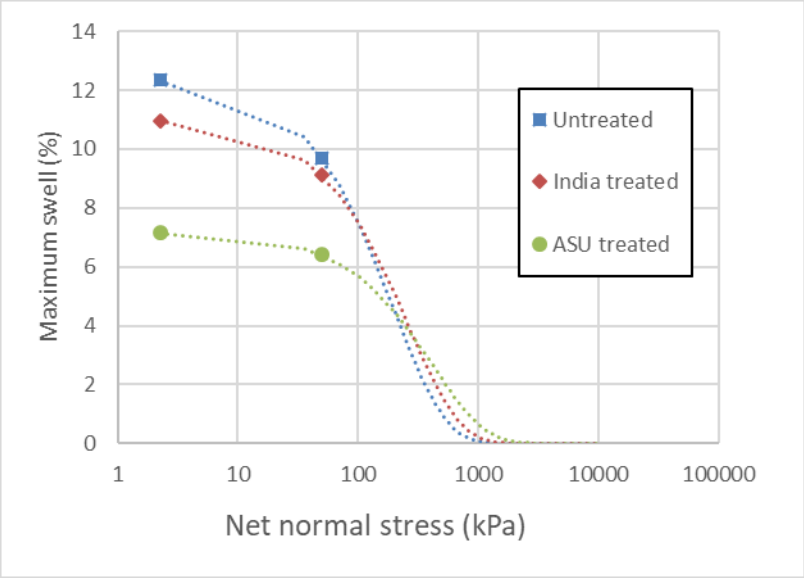

Fig 4.32: Swelling pressure determination

An attempt to measure the swelling pressure is presented in Figure 4.32. As shown, two points is not enough to truly define a relationship between net normal stress and maximum swell. However, it appears the treatment with both, India and ASU ashes, tends to increase the swell pressure, when compared to the untreated sample results. More data at higher net normal stresses need to be obtained in order to have a better estimate of the swelling pressure.

4.6.6.3 Effects of Wetting and Drying Cycles

The following figures show the effects of wetting and drying cycles on the untreated sample and the treated samples. The response of the samples to the wetting and

drying cycles is expressed in vertical strain (%) which implies swelling of the sample or shrinkage on drying.

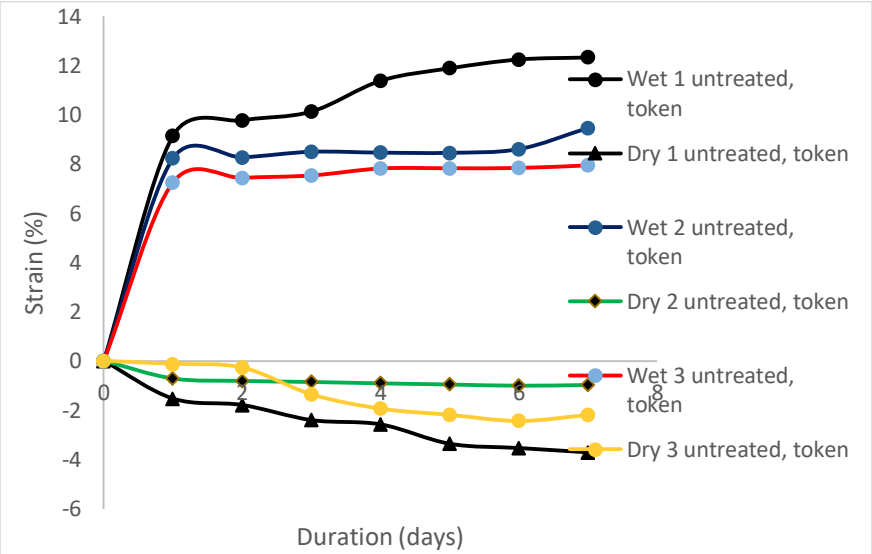

Fig 4.33: Effect of cycles on untreated sample at token load

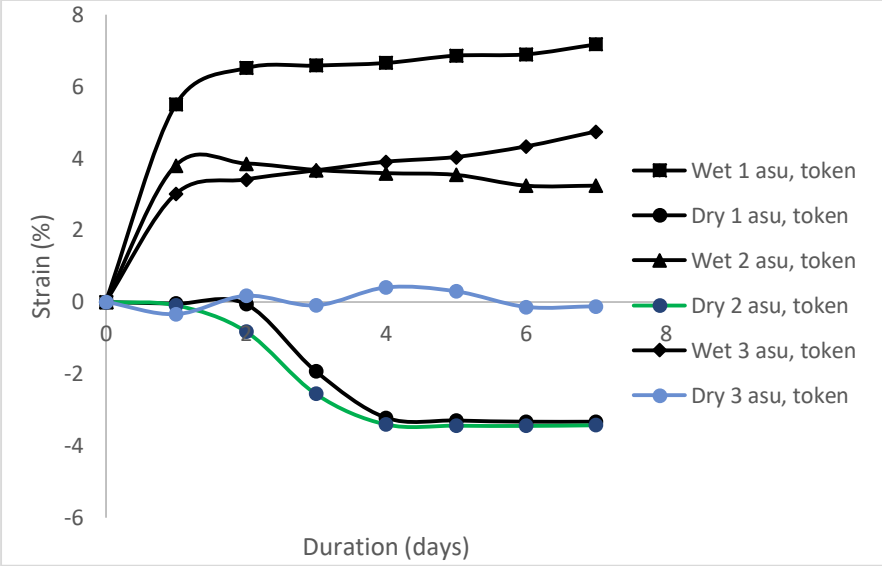

Fig 4.34: Effect of cycles on ASU sample at token load

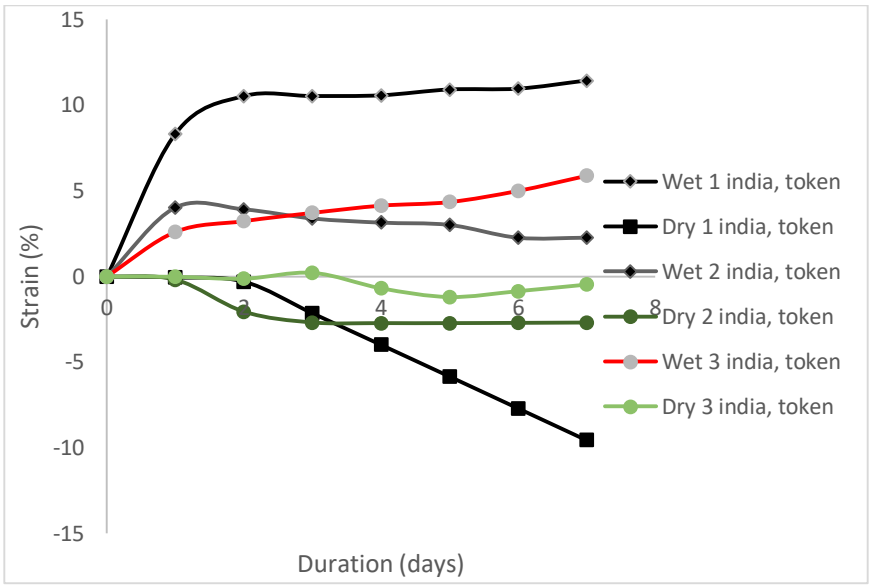

Fig 4.35: Effect of cycles on India sample at token load

The Untreated sample has the highest free swell percentage. The ASU sample shows a decrease in the strain after cycle 1 implying the method works. This means that gelation occurred in the ASU sample after 7 days of curing. This was not the case for the Indian sample.

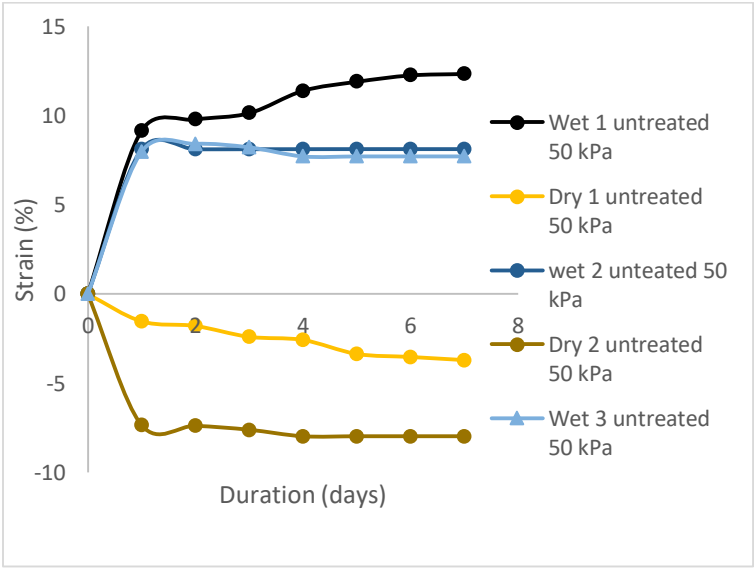

Fig 4.36: Effect of cycles on untreated sample at 50 kPa

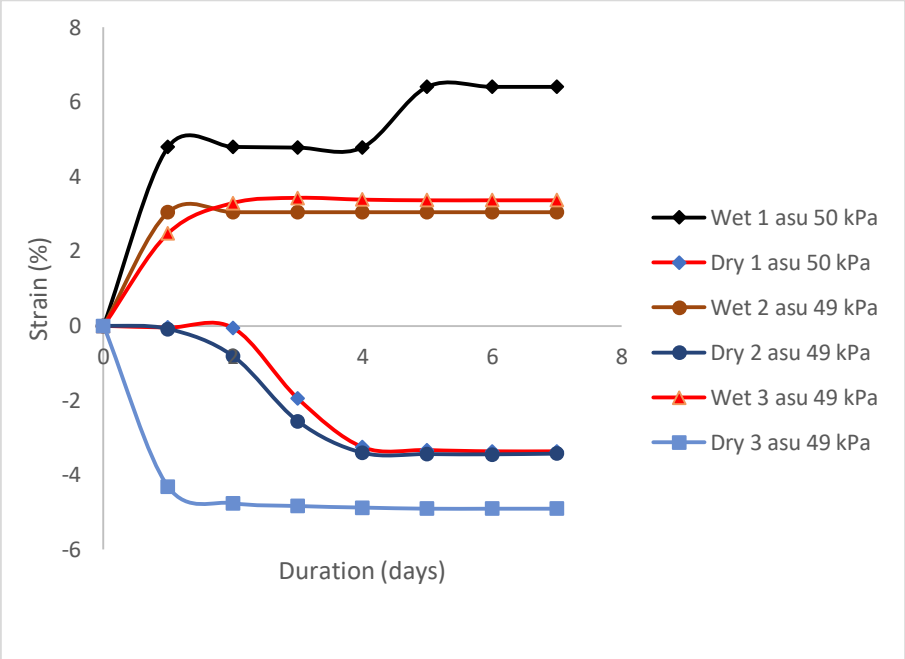

Fig 4.37: Effect of cycles on ASU sample at 50 kPa

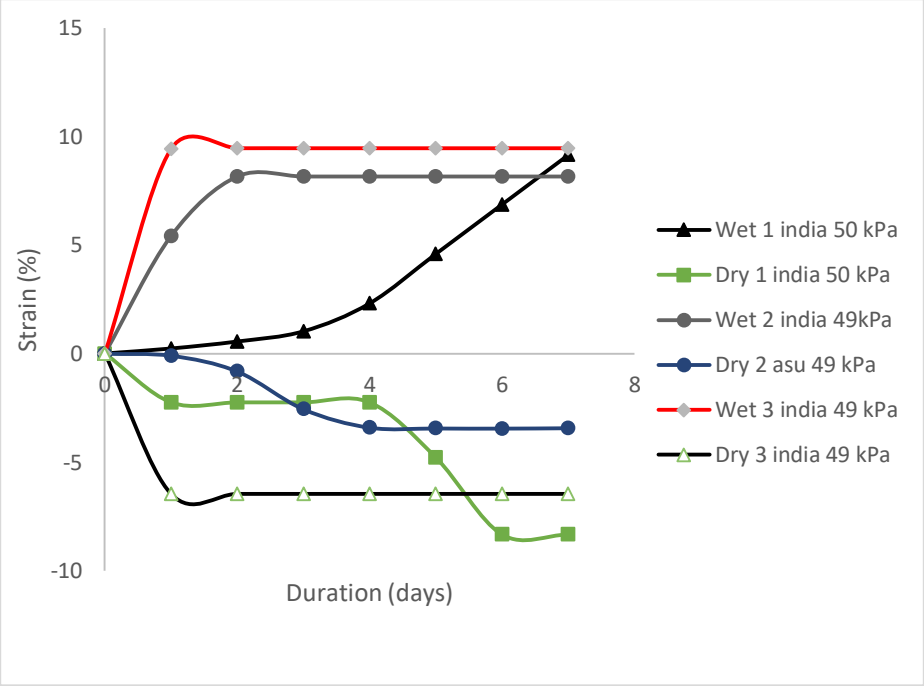

Fig 4.38: Effect of cycles on India sample at 50 kPa

The Indian sample shows more swelling ability than the ASU sample. The swelling percentage at cycle 1 wetting is very high implying gelling had not occurred

after 7 days of curing the Indian sample. The Indian gel is less efficient than the ASU gel. At wetting cycle 2, the Indian gel shows about the same capacity to mitigate volume change behavior of the clay. The following figures show how the number of cycles affects the swelling behavior of the samples.

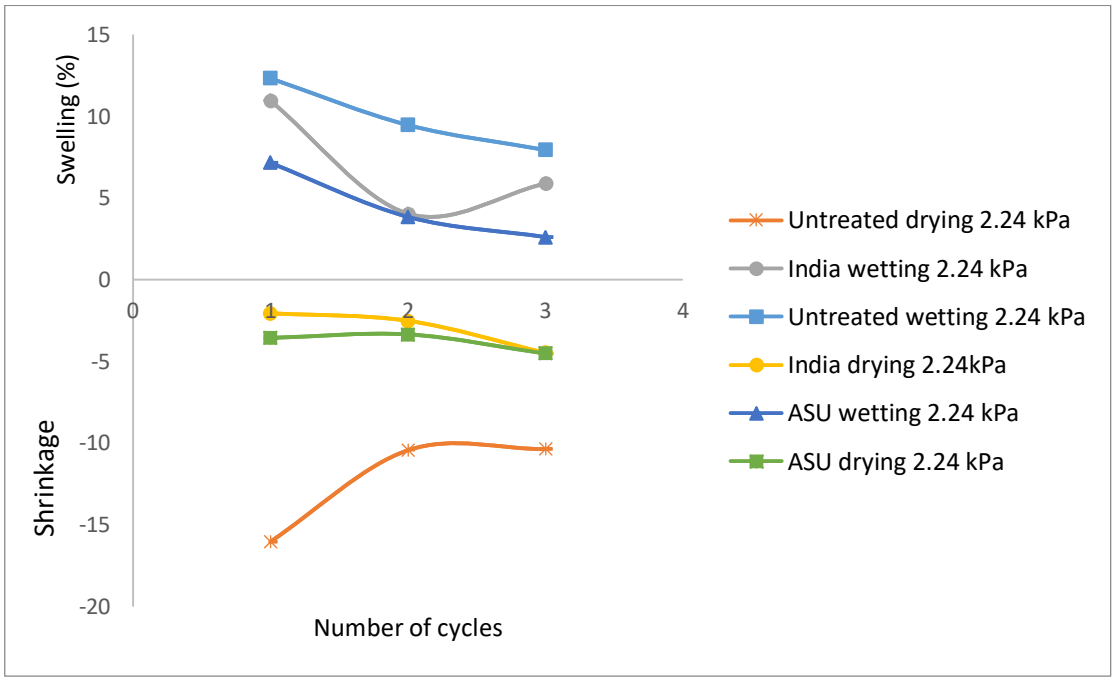

Fig 4.40: vertical strain vs number of cycles at token load

The vertical strain decreases with increasing number of cycles. As the wetting and drying cycles increase, there is a decrease in the wettability of the sample.

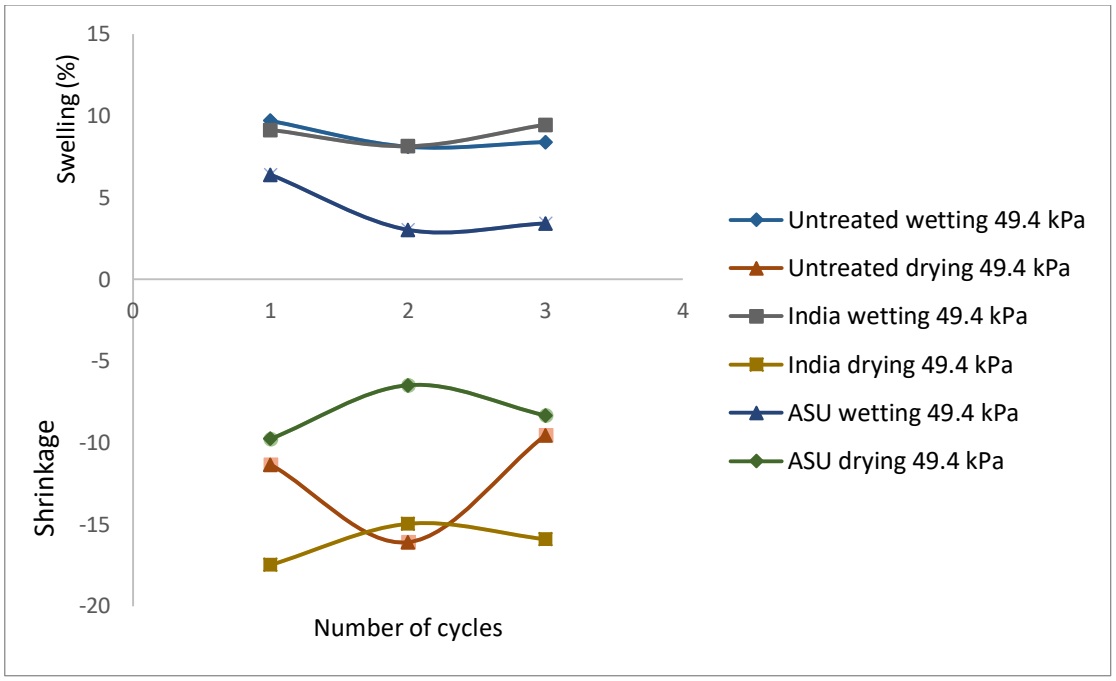

Fig 4.41: Vertical strain vs number of cycles at 50 kPa

From figures 4.40 and 4.41 above, it can be deduced that the swelling percentage generally decreases with number of cycles. However, cycle 3 usually had more swelling than cycle 2 due to reasons relating to more pores opening up after drying cycle 2. After some wetting and drying cycles, the small pores in the clay start to open up leading to more swelling in the next cycle. There could also be some moisture left in the sample after drying and so on wetting again, it could show more swelling. The plots of the drying cycles take a similar trend for similar reasons and due to moisture content of the sample left after drying.

CHAPTER FIVE

CONCLUSIONS AND RECOMMENDATIONS

5.1 General Conclusions about this Study

In this research, the effect of the silica gel on the volume change behavior of expansive clays was investigated and the most important results were summarized as follows:

1. With the addition of silica gel, the MDUW did not change much and almost remained constant whereas the OMC changed drastically that is decreased with addition of silica gel. The OMC of the ASU sample was 13.7% and that of the Indian sample was 14.5%, both of which are much smaller than that of the untreated sample (21.0% OMC). The decrease in moisture content altered the category of the soil from highly expansive to intermediate. This means that the PI of the soil decreased as expected. The plastic limit was expected to stay the same but the liquid limit was expected to reduce significantly which lead to a decrease in the PI of the soil. The results met the expectations.
2. The treatment of the soil with silica gel at an amount equivalent to the optimum water content led to a decrease in swell percentage as indicated by the strain (%) for the untreated and treated samples. The free swell of the clay decreased from 12.3% (untreated sample) to 7.2% (ASU sample) and 11.4% (Indian sample). This can be attributed to a decrease in clay wettability which leads to a decrease in swelling percentage.
3. The effect of the wet and dry cycles on the swelling and consolidation characteristics of the untreated clay was more apparent during the first wet and dry cycle,

after which its effect decreased considerably. However, with the treated samples, the effect of wetting and drying became more pronounced with increase in cycles.

4. The SEM images showed that the structure of the untreated clay was discontinuous, flaky and without aggregations. The clack of cementation increased the number of pores which were larger. In the treated samples, new bands were created, and the particles were aggregated due to reaction with the silica gel.

5. The XRD results showed that the main mineral responsible for expansive behavior of the clay studied was illite. The d-spacing of the illite decreased from 4.47Å in the untreated clay to 3.33Å in the treated clay. The double layer of the clay was depleted as the d-spacing decreased and the silica gel coated the particles, subsequently leading to a reduce in the swelling potential.

6. The FTIR test indicated the main functional group of the gel was O-Si-O, which represents the silica; while the hydroxyl group was representative of an acid, which is the silicic acid. Therefore, the gel formed was a polymer of silicic acid. The tests on the sodium silicate solution revealed that the sodium silicate formed was sodium metasilicate and not the other forms of the compound.

7. The XRF results showed that the ASU ash contained more amorphous silica than the Indian ash. The ASU rice husks were washed with acid before combustion removing some impurities and then burned in a furnace at 650°C whereas the Indian rice husks were not washed and were burned in an open space at very high temperatures. The ASU ash contained more silicon (95.6%) and hence more amorphous silica (SiO_2) at 97.1% compared to Indian ash silicon (89.0%) and amorphous silica (93.7%). The high

temperatures of combustion of Indian rice husks led to crystallization of silica. Not washing the Indian rice husks led to a high percentage of impurities.

5.2 Final Considerations

This research project serves as a basis for future studies and exploration of the advantages of using bio-based silica gel as a stabilizer in comparison to the most common method of Portland cement or lime. First and foremost, the silica gel is environmentally inert, and it is best the rice husks do not go to waste. The adverse effects of using lime were listed in this paper and can be explored for further research.

The process of manufacturing silica gel is rigorous and requires patience. The most important things to put in mind are the steps that affect the amount of amorphous silica formed. The combustion process was studied thoroughly to calibrate and optimize the temperature of combustion. The optimized temperature was 650℃ and many researchers stated that very high temperatures lead to crystallization of silica. Washing the rice husks was found to increase the percentage of silica in the ash.

The precipitation of silica has two important parameters to be considered: pH and gelation time. Acidic conditions were found to have benefits to this research and proved to be the best fit for the gel. Acidic gel took longer time to form and was much stronger than the alkaline gel that formed instantly. The optimized pH for gel in this research was 4 and the curing time for the treated samples was 7 days. Different tests were done to decide a pH suitable for this research and the gelation time was between a few hours and a few days depending on the pH and amount of the solution. After many tests, pH 4 and curing time of 7 days were chosen to allow complete gelation.

The swelling tests were performed in a basement at room temperature of 72F during the wetting cycles and 143F during the drying cycles. The heater temperature was placed to 143F to facilitate drying of the samples and save time during the research as drying at room temperature took several weeks to dry the sample.

5.3 Recommendations for Future Research Work

The following future studies are recommended to explore and improve this research for better results applicable to geotechnical engineering:

- Use this method on different types of clay and determine the similarities and differences between results.
- Perform durability tests using the UCS tests to estimate the strength of the treated clay samples.
- Find the liquid limit and plastic limit of the treated samples and determine the PI of the treated clay.
- Determine the compression index and swell index of the consolidation tests by using higher levels of net normal stress (higher than 50 kPa)
- Produce silica gel at different pH values (acidic) and compare their gelation times and strengths.
- Perform silica grouting in a field and determine the effectiveness of this method in real life. Estimate the depth of treatment and how long the treatment stays in the soil.

5.4 Acknowledgements

This research project is based upon work primarily supported by the Engineering Research Center Program of the National Science Foundation in cooperation with the Center for Bio-mediated and Bio-Inspired Geotechnics at Arizona State University.

REFERENCES

De Luca, M. (2017). Rice Husk Based Silica Gelification for Stability of Expansive Soils in Road Construction. Master's Thesis, Polytechnic University of Turin, Turin, Italy.

Mostafa, A. S. (2019). Properties of Sand Stabilized with Bio-Based Sodium Silicate Solution. Master's Thesis, Arizona State University, Tempe, Arizona

Rosenbalm, D. C. (2013). Volume Change Behavior of Expansive Soils due to Wetting and Drying Cycles. PhD Dissertation, Arizona State University, Tempe, Arizona.

Mitchell, J. K., & Soga, K. (2005). *Fundamentals of Soil Behavior* [3rd edition].

Noorzad, R., & Ta'negonbadi, B. (2018). Volume Change Behavior of Stabilized Expansive Clay with Lignosulfonate.

ASTM Standard D4546-96. (1996). Standard Test Methods for One-Dimensional Swell or Collapse of Cohesive Soils. ASTM International, West Conshohocken, PA. DOI: 10.1520/D4546-03. www.astm.org.

ASTM Standard D4546-03. (2003). Standard Test Methods for One-Dimensional Swell or Collapse of Cohesive Soils. ASTM International, West Conshohocken, PA. DOI: 10.1520/D4546-03. www.astm.org.

ASTM International - Standards Worldwide. (2019). Retrieved October 25, 2020, from http://www.astm.org/. ASTM C136 / C136M-19. Standard Test Method for Sieve Analysis of Fine and Coarse Aggregates, ASTM International, West Conshohocken, PA, www.astm.org.

ASTM International Designation: C92-95. (2015). Standard Test Method for Sieve Analysis and Water Content of Refractory Materials.

ASTM International Designation: D4318 - 10. Standard Test Method for Liquid Limit, Plastic Limit, and Plasticity Index of Soils.

ASTM Standard D4546-08. (2008). Standard Test Methods for One-Dimensional Swell or Collapse of Cohesive Soils. ASTM International, West Conshohocken, PA. DOI: 10.1520/D4546-08. www.astm.org.

ASTM Standard D4829. (2011). Standard Test Method for Expansion Index of Soils. ASTM International, West Conshohocken, PA. DOI: 10.1520/D4829-11. www.astm.org.

ASTM Standard D4943. (2008). Standard Test Method for Shrinkage Factors of Soils by Wax Method. ASTM International, West Conshohocken, PA. DOI: 10.1520/D4943-08. www.astm.org.

ASTM Standard D698. (2000). Standard Test Methods for Laboratory Compaction Characteristics of Soil Using Standard Effort (12,400 ft-lbf/ft3). ASTM International, West Conshohocken, PA. DOI: 10.1520/D698-00a. www.astm.org.

ASTM Standard D6836. (2002). Standard Test Methods for Determination of the Soil Water Characteristic Curve for Desorption Using Hanging Column, Pressure Extractor, Chilled Mirror Hygrometer, or Centrifuge. ASTM International, West Conshohocken, PA. DOI: 10.1520/D6836-02R08E02. www.astm.org.

ASTM Standard D854. (2006). Standard Test Methods for Specific Gravity of Soil Solids by Water Pycnometer. ASTM International, West Conshohocken, PA. DOI: 10.1520/D854-06. www.astm.org.

ASTM D968-17. (2017). Standard Test Methods for Abrasion Resistance of Organic Coatings by Falling Abrasive, ASTM International, West Conshohocken, PA, www.astm.org.

Altmeyer, W.T. (1955). Discussion of Engineering Properties of Expansive Clays. Journal of the Soil Mechanics and Foundations Division 81(658): 17 – 19.

Al-Shamrani, M.A. (2004). Influence of lateral restraint on the swelling behavior of expansive soils. Journal of the Southeast Asian Geotechnical Society, December 2004: 101 – 111.

Al-Shamrani, M.A. and A.I. Al-Mhaidib. (1999). Prediction of potential vertical swell of expansive soils using a triaxial stress path cell. Quarterly Journal of Engineering Geology (32): 45 – 54.

Al-Shayea, N.A. (2001). The Combined Effect of Clay and Moisture Content on the Behavior f Remolded Unsaturated Soils. Engineering Geology (62): 319 – 342.

ASTM Standard D2487. (2000). Standard Practice for Classification of Soils for Engineering Purposes (Unified Soil Classification System). ASTM International, West Conshohocken, PA. DOI: 10.1520/D2487-00. www.astm.org.

Bergna, H., Roberts, W. (2005). Colloidal silica: fundamentals and applications.

Chakraverty, A., Shaik, K. (1991). Conversion of rice husk into amorphous silica and combustible gas. Energy Conversion and Management.

Cheng, L., A. Shahin, M., Cord-Ruwisch, R., Addis, M., Hartanto, T., Elms, C. (2014). Soil stabilization by microbial-induced calcite precipitation (MICP): Investigation into some physical and environmental aspects.

Cheung, K., Venkitachalam, T. (2000). Improving phosphate removal of sand infiltration system using alkaline fly ash. Chemosphere.

Chungsangunsit, T., Gheewala, S., and Patumsawad, S. (2005). Environmental assessment of electricity production from rice husk: A case study in Thailand. International Energy Journal.

Clough, G. W., Kuck, W. M., Kasali, G. (1979). Silicate-stabilized sands. Journal of Geotechnical and Geoenvironmental engineering.

Air Quality - National Summary. (2020, September 02). Retrieved October 25, 2020, from https://www.epa.gov/air-trends/air-quality-national-summary.

Della, V. P., Kuhn, I., & Hotza, D. (2002, December). Rice husk ash as an alternate source for active silica production. Retrieved from https://www.sciencedirect.com/science/article/abs/pii/S0167577X02008790?via%3Dihub

Holtz, R. D., Kovacs, W. D., & Sheahan, T. C. (1981). An introduction to geotechnical engineering.

Bui, D. D. (2001). Rice husk ash as a mineral admixture for high performance concrete.

Yalcin, N. and Sevinc, V. (2001). Studies on Silica Obtained from Rice Husk. Ceramics International, 27, 219-224. http://dx.doi.org/10.1016/S0272-8842(00)00068-7

Hanle L.J. (2004). CO2 Emission Profile of the U.S.Cement Industry, U.S. Environmental Protection Agency, Washington.

Ibrahim D.M., El-Hemaly S.A., & Abdel-Kerim F.M. (1980). Study of rice husk ash silica by infrared spectroscopy.

Lanning F. C. (1963). Silicon in Rice, Journal of Agriculture and Food Chemistry, Vol. 11.

Puppala, A.J. and Cerato, A. (2009). Heave distress problems in chemically-treated sulfate-laden materials. Geo-Strata 10(2): 28 – 32.

Raman, V. (1967). Identification of Expansive Soils from the Plasticity Index and the Shrinkage Index Data. The Indian Engineer 11(1): 17 – 22.

Ranganathan, B.V. and Satyanarayana, B. (1965). A Rational Method of Predicting Swelling Potential for Compacted Expansive Clays. Proceedings of the 6th International Congress of Soil Mechanics and Foundation Engineering. Montreal, Canada (1): 92 – 96.

Gallagher, P., Conlee, C., Rollins, K. (2007a). Full-scale field testing of colloidal silica grouting for mitigation of liquefaction risk. Journal of Geotechnical and Geoenvironmental Engineering.

Gallagher, P., Pamuk, A., Abdoun, T. (2007b). Stabilization of liquefiable soils using colloidal silica grout. Journal of Materials in Civil Engineering.

Real, C., M.D, Alcalá., Criado, J. (1996). Preparation of silica from rice husks.

Rivas, A., Vera, G., Palacios, V., Rigail, A., Cornejo, M. (2016). Characterization of rice husk and the crystallization process of amorphous silica from rice husk ash.

Zamani, M. K., Bin Hashem, R., Suhatril, M., Motamedi, S. (2015). Review of chemical grouting by various types of materials.

Zhao, Q., Li, L., Li, C., Li, M., Amini, F., Zhang, H. (2014). Factors affecting improvement of engineering properties of MICP-treated soil catalyzed by bacteria and urease. Journal of Materials in Civil Engineering.

Shen, Y., Zhao, P., Shao, Q. (2014). Porous silica and carbon derived materials from rice husk pyrolysis char. Microporous and Mesoporous Materials.